TRIBHUVAN UNIVERSITY

INSTITUTE OF ENGINEERING

PULCHOWK CAMPUS

THESIS NO. 079/MSCCD/010

Evaluating the Impact of Climate Change on Hydrological Extremes Using Deep Learning Method

by

Pramesh Karki

A THESIS

SUBMITTED TO THE DEPARTMENT OF APPLIED SCIENCES AND CHEMICAL ENGINEERING IN PARTIAL FULFILLMENT OF THE REQUIREMENTS FOR THE DEGREE OF MASTER IN CLIMATE CHANGE AND DEVELOPMENT

DEPARTMENT OF APPLIED SCIENCES AND CHEMICAL ENGINEERING

LALITPUR, NEPAL

MAY, 2025

COPYRIGHT

TRIBHUVAN UNIVERSITY

INSTITUTE OF ENGINEERING

PULCHOWK CAMPUS

DEPARTMENT OF APPLIED SCIENCES AND CHEMICAL ENGINEERING

The thesis titled "Evaluating the Impact of Climate Change on Hydrological Extremes Using Deep Learning Method" prepared and submitted by Pramesh Karki in partial fulfilment of the requirements for the degree of Master of Science (M. Sc.) in Climate Change and Development has been examined by us and is accepted for the award of M. Sc. in Climate Change and Development by Tribhuvan University.

The undersigned certify that they have read, and recommended to the Institute of Engineering for acceptance, a thesis report entitled "Evaluating the Impact of Climate Change on Hydrological Extremes Using Deep Learning Method " submitted by Pramesh Karki in partial fulfillment of the requirements for the degree of Master in Master in Climate Change and Development

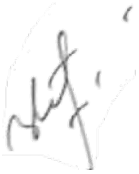

Supervisor:

Prof. Vishnu Prasad Pandey, PhD
Professor
Department of Civil Engineering
Pulchowk Campus

External Examiner:

Saurav KC, PhD
Center of Research for Environment Energy and Water
Deputy Executive Director

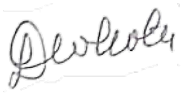

Co-supervisor

Laxmi Prasad Devkota, PhD
Academician
Nepal Academy of Science and Technology (NAST)

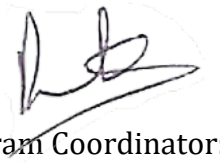

Program Coordinator:

Prof. Rinita Rajbhandari, PhD
Professor
Department of Applied Sciences and Chemical Engineering

Date: 6th May, 2025

DECLARATION

I hereby declare that this study titled "**Evaluating the Impact of Climate Change on Hydrological Extremes Using Deep Learning Method**" is based on my original research work. Related works on the topic by other researchers have been duly acknowledged. I owe all the liabilities relating to the accuracy and authenticity of the data and any other information included hereunder.

Pramesh Karki

079MSCCD010

MSc in Climate Change and Development

Date: 6th May, 2025

ACKNOWLEDGEMENTS

This research would not have been possible without the support and guidance of many individuals and institutions. First and foremost, I express my deepest gratitude to my supervisors, Prof. Dr. Vishnu Prasad Pandey and Academician Dr. Laxmi Prasad Devkota. Their expert guidance, critical feedback, and unwavering support were instrumental in shaping this research and helping me navigate challenges along the way.

My sincere appreciation extends to Tribhuvan University, Institute of Engineering, Pulchowk Campus, for providing an academic platform that has nurtured my research. My thanks extend to my friends, particularly Aashutosh Paudel and Apechhya Aryal, for engaging discussions and for constant encouragement.

Furthermore, I want to thank my friends including Koshish Raj Maharjan and Nishan Hamal, whose insightful input and enthusiastic support were greatly valued. Their skills and unique viewpoints were highly valuable and a source of motivation.

PRAMESH KARKI

079/MSCCS/010

ABSTRACT

The study aims to evaluate the impact of climate change on hydrological extremes using the deep learning method. Climate change has substantial impacts on hydrological regimes, with the most impacted extreme events being those that occur in vulnerable areas such as the Himalayas. Traditional hydrological models tend to be limited in high complexity and limited-data regimes. The study uses a Bidirectional Long Short-Term Memory (BiLSTM) network to simulate the daily streamflow of nine heterogeneous watersheds in the Koshi River Basin in Nepal. The model uses downscaled future climate projections from CMIP6 global climate models (GCMs) under Shared Socioeconomic Pathways (SSP) SSP245 and SSP585 scenarios to predict future discharge. The study further seeks to explain hydrological extremes based on the trained model and future climate data simulations. The use of BiLSTM, a deep learning method, improves extreme flow estimation and provides more precise predictions for sustainable water resource management.

The multi-basin BiLSTM was developed using diverse dynamic meteorological forcings and watershed attributes to address heterogeneity across watersheds. It demonstrated satisfactory performance in simulating daily streamflow for most of the nine heterogeneous Himalayan watersheds, achieving good performance on test sets, indicating its ability to predict unseen data effectively.

Daily streamflow simulations for the period 2026–2055 were conducted using a validated BiLSTM model driven by CMIP6 climate projections under SSP245 and SSP585 scenarios. The analysis reveals a consistent pattern of increased mean annual streamflow across most watersheds and scenarios, with significant increases anticipated during the monsoon and pre-monsoon seasons. The increase in flow, with different temporal patterns, is consistent with the projected strong future warming, although considerable uncertainty remains regarding the direction and magnitude of future precipitation changes among different GCMs.

The BiLSTM simulations, driven by future climate scenarios, consistently projected increases in both low and high flow conditions when historical and future periods are compared using flow percentiles. Low flow percentiles showed mostly positive and relatively small changes, while high flow percentiles indicated substantial intensification, suggesting increased flood risks. These results highlight a dual water management challenge for the region and underscore the need for adaptive strategies that consider both increased flood risks and shifting water availability patterns amid high climate projection uncertainty.

Keywords: LSTM, BiLSTM, Deep Learning, Hydrological Modeling, Climate Projections, Hydrological Extremes, Koshi River Basin

TABLE OF CONTENTS

LIST OF FIGURES

LIST OF TABLES

ABBREVIATIONS AND ACRONYMS

AI	Aridity Index
ALO	Ant Lion Optimizer
APHRODITE	Adaptation Pathways and High-Resolution Observations for Development of Innovative Technologies and Evaluations
ASTER	Advanced Spaceborne Thermal Emission and Reflection Radiometer
BiLSTM	Bidirectional Long Short-Term Memory
CDF	Cumulative Distribution Function
CDO	Climate Data Operators
CMIP6	Coupled Model Intercomparison Project Phase 6
CRS	Coordinate Reference System
DEM	Digital Elevation Model
DHM	Department of Hydrology and Meteorology (Nepal)
DSMW	Digital Soil Map of the World
ECMWF	European Centre for Medium-Range Weather Forecasts
EQM	Empirical Quantile Mapping
ERA5	ECMWF Reanalysis 5th Generation
ESGF	Earth System Grid Federation
FAO	Food and Agriculture Organization
FDC	Flow Duration Curve
GCM	General Circulation Model (or Global Climate Model)
GEE	Google Earth Engine
GEV	Generalized Extreme Value distribution
GIS	Geographic Information System
GLEAM	Global Land Evaporation Amsterdam Model
GLOF	Glacial Lake Outburst Flood

HAR2	High-Resolution Atmospheric Reanalysis, version 2
HMA	High Mountain Asia
HWSD	Harmonized World Soil Database
IGBP	International Geosphere-Biosphere Programme
IPCC	Intergovernmental Panel on Climate Change
KGE	Kling-Gupta Efficiency
LAI	Leaf Area Index
LOOCV	Leave-One-Out Cross-Validation
LR	Learning Rate
LSTM	Long Short-Term Memory
MAE	Mean Absolute Error
MAP	Mean Annual Precipitation
ML	Machine Learning
MODIS	Moderate Resolution Imaging Spectroradiometer
MPI-ESM1-2-LR	Max Planck Institute - Earth System Model 1.2 - Low Resolution
MSWEP	Multi-Source Weighted-Ensemble Precipitation
NAST	Nepal Academy of Science and Technology
NCEP-CFSR	National Centers for Environmental Prediction - Climate Forecast System Reanalysis
NESM3	Nanjing University of Information Science and Technology Earth System Model version 3
NEX-GDDP-CMIP6	NASA Earth Exchange Global Daily Downscaled Climate Projections for CMIP6
NOAA	National Oceanic and Atmospheric Administration
NSE	Nash-Sutcliffe Efficiency
PBIAS	Percent Bias
PERSIANN-CDR	Precipitation Estimation from Remotely Sensed Information using Artificial Neural Networks - Climate Data Record

PET	Potential Evapotranspiration
POT	Peaks-Over-Threshold
PUB	Prediction in Ungauged Basins
Q_5, Q_{10}	5^{th} and 10^{th} percentile flows
Q_{90}, Q_{95}	90^{th} and 95^{th} percentile flows
R^2	Coefficient of Determination
RMSE	Root Mean Square Error
RNN	Recurrent Neural Network
RSR	RMSE-observations standard deviation ratio
SMAP	Soil Moisture Active Passive
SMU	Soil Mapping Unit
SRI	Standardized Runoff Index
SRTM	Shuttle Radar Topography Mission
SSI	Standardized Streamflow Index
SSP	Shared Socioeconomic Pathway
SSP245	Shared Socioeconomic Pathway 2 - 4.5 W/m^2 forcing
SSP585	Shared Socioeconomic Pathway 5 - 8.5 W/m^2 forcing
SWAT	Soil & Water Assessment Tool
USGS	United States Geological Survey
WCRP	World Climate Research Programme
WRF	Weather Research and Forecasting model
XAI	Explainable Artificial Intelligence

1 INTRODUCTION

1.1 Background

Climate change is a global topic that causes considerable concern in today's society. Warming during the past century has led to several changes in Earth's system like increased evaporation, increased atmospheric water vapor content, and altered precipitation patterns and intensities. Such changes often involve complex alterations, e.g., rainfall frequency and intensity changes, leading to disruptions in water cycle patterns. These changes are closely linked to the occurrence of extreme hydrological events such as floods and drought which can be concerning in the regions like the Himalayan river basins (Singh et al., 2021).

The phenomena caused by the rise in global temperatures, such as heatwaves, an increase in the number of hot days, a decrease in the number of cold days, and dramatic shifts in climatic zones, have become more visible and intense with each passing decade or year. (Kim & Bae, 2021; Perkins-Kirkpatrick & Lewis, 2020). Similarly, there is also a change in precipitation patterns due to global warming. The intensity of extreme precipitation has been increasing, which is causing frequent flooding events. Consequently, the amount of seasonal and regional availability of water resources is also impacted by these events (Tabari, 2020).

The Higher Himalayan region contributes to freshwater downstream, which impacts millions of people's lives. Climate change has a severe impact on this region, such as a decrease in freshwater storage, retreat of glaciers, glacial lake outburst flood (GLOF) events, etc. (Bajracharya et al., 2006). Increased melt from glaciers and snowpack can temporarily enhance river flows, but this trend ultimately jeopardizes the long-term reliability of water resources obtained from these vital frozen storage systems. If we look into socio-economic aspects, the environment, people's lives, and the economy are all impacted by these issues, which are made worse in the Himalayan river basins (Neupane et al., 2022). These concerns highlight the need for more effective strategies for water management and disaster risk reduction (Wahid et al., 2017). These extremes can be accessed using a hydrological model and ensemble climate data, which helps with efficient water resource management (Kay et al., 2024).

1.2 Research Gaps and Problem Statement

Traditional process-driven models, which rely on physical formulas, often struggle to represent the stochastic variability of medium- and long-term runoff patterns, making them less effective for predicting hydrological extremes (Yuan et al.,

2018). The challenge is further amplified in regions where observational data is scarce or incomplete. To improve hydrological forecasting and reduce uncertainties, advancements in data availability and modeling techniques are necessary.

Extreme hydrological events such as floods and low-flow conditions pose serious socio-economic and environmental risks, making accurate streamflow forecasting essential for irrigation, hydropower management, and disaster preparedness (Ghimire et al., 2020). However, predicting these events remains challenging due to complex climate dynamics and the limited availability of detailed meteorological data. This issue is particularly pronounced in mountainous regions, where the lack of continuous and systematic meteorological records is further complicated by difficult terrain, remoteness, and frequent data gaps caused by weather station failures and infrequent maintenance (Khadka et al., 2022). The need for high-resolution, small-scale data is crucial for river-basin-level planning, yet uncertainties persist due to the limitations of conventional hydrological models in capturing extreme events with high precision (Banda et al., 2022).

Given these challenges with traditional models, data-driven alternatives like Long Short-Term Memory (LSTM) networks offer a promising approach. LSTM models have demonstrated the ability to capture long-term dependencies in hydrological systems, enabling improved streamflow predictions even in data-limited mountainous regions. Variants such as Bidirectional LSTMs (BiLSTMs) further enhance this by processing information in both forward and backward directions Moreover, LSTM models can transfer learning from well-monitored catchments to data-scarce basins, enhancing hydrological forecasting where traditional methods fall short (Xu et al., 2020). By integrating LSTM-based learning with existing hydrological models, it is possible to improve extreme flow estimation and provide more reliable forecasts for sustainable water resource management.

1.3 Objectives

The general objective of this research is to develop, implement, and evaluate a multi-basin Bidirectional Long Short-Term Memory (BiLSTM) modeling framework for daily streamflow simulation across nine diverse Himalayan watersheds within the Koshi River Basin system of Nepal. The specific objectives of the study include

- To develop a multi-basin BiLSTM model for predicting streamflow across diverse Himalayan river basins.

- To simulate future streamflow under different climate change scenarios using the BiLSTM model.
- To apply the developed multi-basin BiLSTM framework to evaluate hydrological extremes.

1.4 Scope and Limitations

The following are the study's scopes to achieve its goals:

- The study aims at nine watersheds of the Koshi River Basin and applies a BiLSTM model to simulate daily streamflow.
- The model predicts future streamflow for 2026–2055 by driving the BiLSTM model with preprocessed CMIP6 climate projections of three GCMs and compares them with a historical baseline (1985–2014).
- The model accepts both static catchment properties such as topography, soil, vegetation, and land cover, and time-varying meteorological inputs.
- The impacts of climate change are assessed by calculating the percentage change in extreme flow percentiles in low flows (Q_5 and Q_{10}) and high flows (Q_{90} and Q_{95}) between the future periods and the historical period.

The limitations of this study include:

- The "black-box" nature of the LSTM model restricts the comprehension of the learned hydrological processes, hindering diagnostic analysis as compared to physically-based models.
- Much uncertainty arises from the spatial resolution and accuracy limitations of the meteorological forcing data sets, particularly in the topographically complex mountain terrain.
- Inaccuracies may result from inherent data gaps or quality issues of the historical observed streamflow data for model training and testing.
- Basin averaging of the climate inputs smooths potentially important sub-basin scale variability, especially for heterogeneous topography areas.
- Limiting extreme analysis to one or more detached percentiles of flow might miss significant alteration in extreme event seasonality, frequency, or duration.

2 LITERATURE REVIEW

2.1 Hydrological Modeling

There are two types of models for runoff prediction: process-driven models and data-driven models. Both have been used with varying degrees of success. Data-driven methods can be further categorized into statistical techniques and machine learning (ML) models. They are also capable of model simulation without watershed internal physical processes modeling (Adamowski & Sun, 2010).

Steep slope affects temperature lapse rates, wind patterns, orographic precipitation augmentation, and incoming solar radiation. These fine-scale fluctuations are poorly represented in models because they require more processing cost to capture and include in hydrological modeling (Lundquist & Cayan, 2007; Winstral et al., 2002). The remoteness of weather stations further limits the accuracy of hydrological modeling in regions with high elevations. Because the stations are usually found at lower elevations, they are unable to capture spatial variability, especially when modeling basins at higher elevations when the hydrological flow is already negligible (Evin et al., 2024).

2.1.1 Hydrological modeling approaches

Process-driven models are constrained by our understanding of natural processes and computational limitations. Conversely, data-driven models can often provide accurate predictions (Nourani, 2017; Tanty & Desmukh, 2015). One prominent type of data-driven model is the artificial neural network (ANN), known for its robust non-linear fitting capabilities. Since ANNs were first applied in streamflow modeling (Daniell, 1991), their use in hydrological studies has expanded significantly (ASCE, 2000). Other various artificial neural network (ANN) techniques have been employed to model the rainfall-runoff relationship, including fuzzy neural models (Nayak et al., 2004), wavelet-integrated neural networks (W. Wang & Ding, 2003), and Bayesian-based neural networks (Bateni et al., 2007)

Deep learning has made tremendous advancement in the field of machine learning and data science in recent years (Negnevitsky & Pavlovsky, 2005), with numerous algorithms showing strong capability in solving real-world problems (Khan & Yairi, 2018). Particularly, recurrent neural networks (RNNs) excel at processing time series data by using loops to pass information from one time step to the next (Bengio et al., 1994; Hochreiter & Schmidhuber, 1997). Nevertheless, RNNs are

confronted with issues like vanishing or exploding gradients, which limit their capacity to model long-range dependencies. To mitigate this issue, the long short-term memory (LSTM) network was developed, enhancing the capacity to learn from long sequences of data. Variants of LSTM networks have been created to further improve learning for various tasks (Sutskever, 2013). LSTMs have been successfully applied in fields like speech recognition and text translation (Bellegarda & Monz, 2016). Recently, LSTM networks have also been employed in watershed hydrological modeling, showing great promise in predicting river flow and floods (Shen, 2018). LSTM often works with diverse data sources and delivers efficient results even when data is scarce (J. Li et al., 2024). Several studies have explored the application of Long Short-Term Memory (LSTM) networks in estimating hydrological extreme values (Deng et al., 2024; Song et al., 2022). In areas where snow predominates, LSTMs can help estimate streamflow by implicitly learning melt thresholds and rates (Feng et al., 2022).

2.1.2 Long Short-Term Memory (LSTM)

Recurrent neural networks serve as the foundation for the architecture of LSTMs. A feedback loop in the construction of an RNN allows it to imitate time series data. It is unable to recall longer dependencies, though. LSTM uses gates and cell states instead of RNN to overcome the difficulty of memorizing long-term dependencies and gradient explosion (Schmidhuber, 2015). The algorithm's added robustness makes it possible for LSTM to simulate long-term dependent processes, such as snow moisture groundwater recharges and makes its robust prediction technique more appropriate for time series data (Siami-Namini et al., 2019).

2.1.3 LSTM architecture

An LSTM network is made up of an input layer that receives input sequence data, a fully connected layer that provides LSTM cells with input data, an LSTM cell layer that functions as a cell memorizer, and output layers that produce an output vector. Fully connected layers and LSTM cells are the key components of the LSTM architecture (Alizadeh et al., 2021). The cell state and the concealed state, which are carried over to the following phases, are the two primary states found in each LSTM layer as shown in Figure 2-1(Man et al., 2023). The model learnings are retained because of these memory states. This memory is manipulated using three main gates: input, output, and forget. At every sequence, the output gate updates the hidden state, the forget and input gates update the cell state.

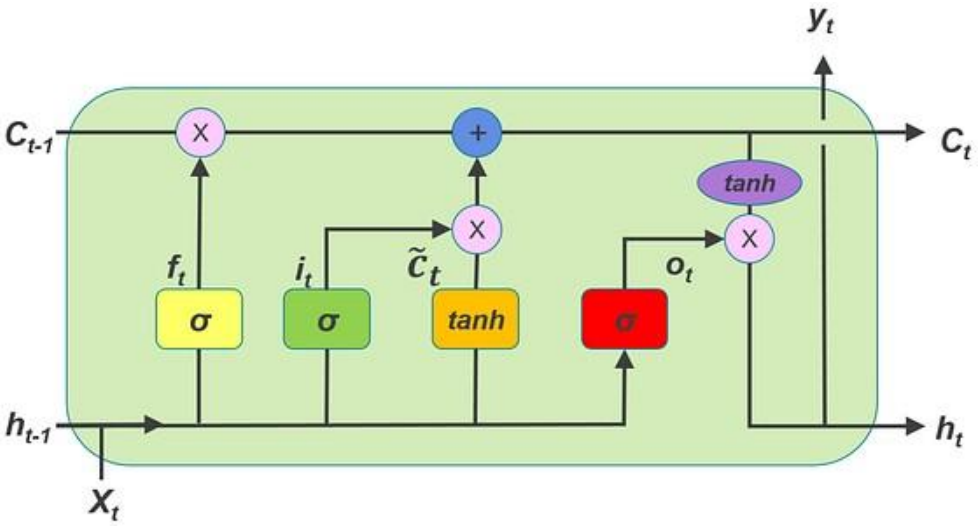

Figure 2-1 Basic LSTM model's architecture

Adopted from Zulqarnain et al. (2021)

Here, the subscript "t" stands for the current time as well as the cell state and concealed state

The LSTM contains three gates when these are rewritten as equations: input, output, forget gate, cell state, and hidden states. The following are the equations for gates:

$$i_t = \sigma\,(w_i[h_{t-1},x_t] + b_i) \quad (1)$$

$$f_t = \sigma\,(w_f[h_{t-1},x_t] + b_f) \quad (2)$$

$$o_t = \sigma\,(w_o[h_{t-1},x_t] + b_o) \quad (3)$$

$$\check{C}_t = \tanh(w_c[h_{t-1},x_t] + b_c) \quad (4)$$

$$C_t = f_t \times C_{t-1} + i_t \times \check{C}_t \quad (5)$$

$$h_t = o_t \times \tanh(C_t) \quad (6)$$

Where x_t represent the input at time t, and b_x denote the bias associated with each gate x. The cell state at time t is C_t, while $\check{C}_t$ refers to the candidate cell state. The sigmoid function is denoted by σ, and the hyperbolic tangent function by tanh. The variables i_t, f_t and o_t map to the input, forget, and output gates respectively, with their corresponding weight matrices w_t.

2.1.4 Applications of LSTM in hydrological modeling

Yuan et al. (2018) presented the LSTM-ALO model, where Ant Lion Optimizer (ALO) optimized the number of neurons within the hidden layers and the learning rate of the LSTM network. Muhammad et al. (2019) developed a hybrid model that combines LSTM and GRU to simulate river flow and provide early flood warnings. Dai et al. (2023) employed a long short-term memory (LSTM) network to transform historical streamflow data into a context vector by an encoder and decoded by another LSTM with the addition of an attention mechanism to enhance the performance of predictions. Kratzert et al. (2019) proposed the Entity-Aware LSTM (EA-LSTM), which outperformed several individually tuned hydrological models in 531 river basins at the regional scale. In some datasets, the correlation information between explanatory and target variables might span a considerable temporal interval, causing gradient vanishing and bursting difficulties in LSTM (X. Zhang et al., 2023). There is also the potential of adopting a multi-timescale architecture, which is computationally more efficient than a naive prediction with different LSTMs on each timescale while maintaining accuracy (Gauch et al., 2021). Yu et al. (2019) explained that standard training of LSTMs by using merely forward propagation may fail to well identify complex relations among predictor and response variables, and thereby use the training information less than optimally. This problem is addressed by Bidirectional LSTM (BiLSTM), where two LSTM layers are used with opposite directions in which sequences pass through so that the model could obtain previous as well as succeeding context at each step. This better awareness of the present sequence position helps to reduce errors in detecting underlying linkages. The architecture of a Bidirectional LSTM (Bi-LSTM) network is illustrated in the Figure 2-2.

.

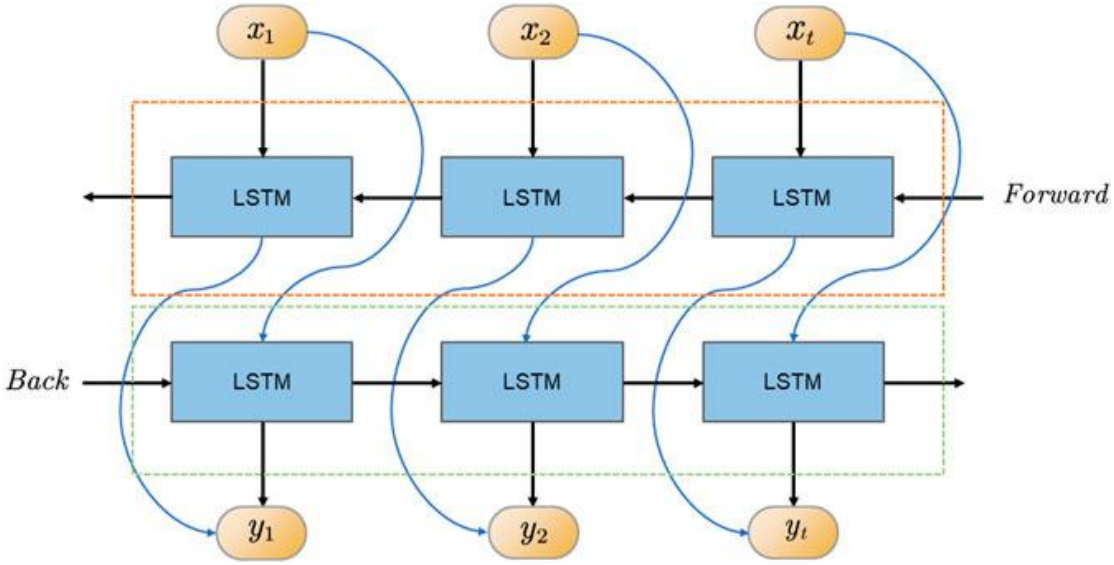

Figure 2-2 Architecture of a Bidirectional LSTM (BiLSTM) network

Adopted from Ni et al. (2023)

2.1.5 Limitation of the LSTM model

LSTM models, like other deep learning methods, have notable drawbacks, including the necessity for large datasets to train the neural networks effectively and challenges in extrapolating conditions beyond the range of existing data. The quality and quantity of training data significantly impact the performance of LSTM models. For example, Kratzert et al. (2018) found that at least 15 years of data is required for daily streamflow simulation, with additional years needed for validation. Gauch et al. (2021) also demonstrated that shorter training periods lead to performance degradation. Similarly, Bai et al. (2021) showed that extending the validation period improves LSTM model performance. Furthermore, regionalization using LSTM requires various catchment physical descriptors. While some descriptors, such as land cover, slope, elevation, and area, are relatively easy to obtain, others, like soil depth and soil porosity, are more challenging to evaluate. As these variables are expected to change gradually or systematically across space, longitude and latitude can be quite helpful to use as proxies for these variables (Arsenault et al., 2023).

2.1.6 Inputs for hydrological modeling using LSTM

The performance of an LSTM model is highly reliant on the selection and preprocessing of input variables. The variables should also adequately represent the physical processes governing the hydrological cycle. For a river basin, the variables selected must represent the basin, spatiotemporally. The input variables can be meteorological (precipitation, temperature, relative humidity, solar

radiation, wind speed, atmospheric pressure), hydrological (discharge, soil moisture, evapotranspiration, snow water equivalent, groundwater levels), topographical and land-use (elevation, slope, aspect, land use/land cover, soil type, drainage area), etc. Several studies with a wide variety of variables have been selected for the creation of LSTM for the prediction of hydrological discharge, and some of the key variables used in some studies are listed in Table 2-1.

Table 2-1 Input variables used in LSTM-based hydrological modeling studies

S.No	Author(s)	Region	Variable Name(s)	Source(s) and Link(s)
1	Deng et al. (2024)	China	Rainfall and air temperature	ERA5-Land dataset (https://cds.climate.copernicus.eu/datasets/reanalysis-era5-single-levels?tab=download)
2	Liang et al. (2023)	China	Air temperature, rainfall, wind velocity, humidity, sunlight duration	China Meteorological Administration (http://data.cma.cn/)
3	Shekar et al. (2023)	India	Wind speed, humidity, solar radiation, elevation, soil data	NASA (https://power.larc.nasa.gov/data-access-viewer/), Food and Agriculture Organization (FAO) Digital Soil Map of the World (DSMW, 1974) (https://earthexplorer.usgs.gov)
4	Zhang et al. (2023)	China	Precipitation, temperature	National Oceanic and Atmospheric Administration (NOAA) (https://www.noaa.gov/)
5	Q. Yu et al. (2024)	China	Rainfall, temperature, evapotranspiration, soil moisture	PERSIANN-CDR (https://chrsdata.eng.uci.edu), MOD11C1 (https://search.earthdata.nasa.gov/search), GLEAM (https://www.gleam.eu/#datasets), GLDAS (Global Land Assimilation Data System) (https://ldas.gsfc.nasa.gov/gldas)
6	Mangukiya et al. (2023)	India	Solar radiation, humidity, wind speed, elevation, slope, watershed characteristics, vegetation indices, and soil properties.	NCEP-CFSR Global Weather Data (https://swat.tamu.edu/data/cfsr), SRTM DEM (https://earthexplorer.usgs.gov/), MODIS Dataset (https://modis.gsfc.nasa.gov/data/), FAO (http://www.fao.org/soils-portal/en/)
7	B. Li et al. (2023)	Tibet, China	Near-surface air temperature, evaporation, rainfall	ERA5 reanalysis, GLEAM v3.5a (https://www.gleam.eu/#datasets), Multi-Source Weighted-Ensemble Precipitation (MSWEP) V2.2 (https://www.gloh2o.org/mswep/)

S.No	Author(s)	Region	Variable Name(s)	Source(s) and Link(s)
8	Man et al. (2023)	China	Land use and land cover categories	Landsat 5 (https://www.usgs.gov/landsat-missions/landsat-5)
9	Choi et al. (2022)	Korea	Leaf area index, evapotranspiration, soil moisture	MODIS global LAI product (MOD15A2H), MODIS ET product (MOD16A2) (https://modis.gsfc.nasa.gov/data/),), SMAP L-band brightness temperature observations (https://nsidc.org/data/spl1btb/versions/3)

2.2 Regionalization and Multi-Basin Hydrological Modeling

2.2.1 Prediction in ungauged basins

There are not many hydrological and meteorological stations in Nepal's upstream region and those that are there are not arranged strategically (Uprety, 2018). Effective management of water resources is hampered by the absence of streamflow gauging stations. This issue is addressed by Prediction in Unguaged Basins (PUB), which estimates hydrological variables at sites where streamflow measurements are not available (Sivapalan et al., 2003). Information is typically transferred to ungauged (target) catchments by utilizing gauged (donor) catchments.

Regionalization of hydrological signatures, regionalization of model parameters, and data-driven approaches/large-sample hydrology are common techniques for PUB approaches. The process of regionalizing model parameters involves estimating parameters for the ungauged basins by relating the calibrated parameters of hydrological models in gauged basins to catchment characteristics (for example, through regression, spatial proximity, or physical similarity). Strong parameter-characteristic relationships, donor similarity, and model selection are critical to this approach's success (Duan et al., 2006). To regionalize hydrological signatures, the signature of ungauged basins is estimated using observable hydrological signatures (such as mean flow and flow duration curve indices) from gauged basins. Data-driven methods frequently use machine learning models. These models are used to forecast flow in ungauged catchments and were trained on sizable datasets of various catchments. They implicitly capture intricate relationships (Kratzert et al., 2019).

2.2.2 Streamflow prediction in ungauged catchments using LSTM regionalization

Unlike conceptual models that employ parameter transfer based on hydrologically proximal or similar gauged catchments, LSTM networks utilize strong regional datasets for the improvement of prediction ability and model performance (Arsenault et al., 2023). Previous efforts to predict streamflow in Nepal have also utilized parameter transfer. Research in the Budhigandaki basin found that spatially transferring calibrated SWAT model parameters to the downstream station resulted in an accurate forecast of daily streamflow (Marahatta et al. 2021). Similarly, Nepal et al. (2017) transferred parameters from a calibrated J2000 model in the Dudhkoshi basin to the adjacent Tamor basin.

LSTM models have been discovered to possess the ability to outperform regular hydrological models in regionalization experiments on leave-one-out cross-

validation (LOOCV). In a comparison of 200 Northwest Russian catchments, Ayzel et al. (2020) discovered that predictive skill for LSTM-based models was better compared to the GR4J regional model with median Nash-Sutcliffe Efficiency (NSE) values of 0.73 compared to 0.61. Nearing et al. (2021) also found that LSTM models trained on regional datasets outperformed those trained on individual basins, with a median NSE improvement of 0.10 using Kratzert et al. (2019) data. Choi et al. (2022) also demonstrated successful regional streamflow modeling with LSTM for 13 catchments in Korea and observed that additional model performance would be possible with increased data coverage. Y. Zhang et al. (2022) also reported improved results from a regional encoder-decoder LSTM network compared to 35 China basins over conceptual hydrological models even in case scenarios with limited available catchment data.

2.2.3 Multi-basin hydrological modeling

The quantity and diversity of training data can have a substantial impact on how well LSTM models perform. Since single-basin models only learn from one catchment, they are less reliable for comprehending data (Kratzert et al., 2024). According to Tayal et al. (2024), adding more basins improves accuracy and boosts the model's predictive performance. A single, shared architecture that has been jointly trained on data from all basins is used by a multi-basin LSTM. Static catchment attributes are combined with time-varying inputs for multi-basin approaches. For each basin, time-varying inputs include meteorological drivers such as temperature, humidity, precipitation, and solar radiation. To distinguish between basins, static catchment attributes are given. Another name for these variables is "basin descriptors."

2.3 Climate Change Impacts on Himalayan Hydrology

Climate change significantly impacts the hydrology of the Himalayan region, a region which holds vast stores of snow and ice feeding major river systems. Rising global temperatures are particularly pronounced at high altitudes, leading to several critical changes. One of the notable effects is the increased rate of glaciers and seasonal snow cover melting. This first increases meltwater runoff, potentially leading to short-term increases in river discharge. The trend in the long run, though, is glacier loss and reduced snow storage, threatening water supply in dry seasons for highly meltwater-dependent river basins downstream, and impacting agriculture and ecosystems. Besides, there are changes to warming that bring changes to precipitation. The height where snowfall rather than rain occurs is growing, reducing the accumulation of snow at low and middle elevations. Furthermore, increases in monsoon intensity and shifts in timing, resulting in

potentially more variable rain, with increasing opportunities for a heavier downpour, are forecast (Moon & Ha, 2020).

A thorough simulation of the Earth's climate system is offered by global climate models. Higher-resolution models have been developed as a result of scientific and computational advancements (Balaji et al., 2022). The atmosphere, ocean, land surface, and sea ice are some of the interdependent elements that make up their structure.

2.3.1 Climate models & SSP scenarios

Global Climate Models (GCMs) are coarse approximations for the extrapolation of future climate conditions and are used extensively for estimation of the potential impacts on regional hydrology. They provide valuable insights into parameters such as temperature, precipitation, and radiation that are the centre of driving Himalayan hydrology. However, GCM outputs cannot be used directly for the simulation of Himalayan hydrology because of some model constraints. Shared Socioeconomic Pathways (SSPs) are conditions developed by the science community to imagine and explore how global society, population, and economy may develop throughout the 21st century.

The SSPs offer different future directions. SSP1, a sustainable future, includes high international cooperation and clean energy transition, leading to the lowest emissions (2.6 W/m^2) and the least extent of warming. SSP2, "Middle of the Road", assumes continuing global trends, leading to moderate emissions (around 4.5 W/m^2) and moderate warming. SSP3, "Regional Rivalry", is a world with low international cooperation and a fragmented world, leading to increased emissions (7.0 W/m^2) and greater warming. Lastly, SSP5, or "Fossil-Fueled Development", prioritizes economic development through the use of fossil fuels, leading to very high emissions (8.5 W/m^2) and maximum warming across the world (Siabi et al., 2023).

2.3.2 Hydrological extremes and their analysis

Hydrological extremes are significant deviations from the natural equilibrium of water flow in a system that create conditions such as excess water in flooding or shortage of water during droughts. Such occurrences violate the normal balance of the water cycle and may lead to an array of problems, such as environmental harm, reduced agricultural productivity, and inconvenience to societies and economies (IPCC, 2014). Hydrological extremes of floods and droughts are studied based on a series of statistical techniques to estimate their frequency, magnitude,

and duration (Lang et al., 1999; Madsen et al., 2014; Van Loon, 2015). The common methods include:

Frequency Analysis: This method estimates how often extreme hydrological events occur by calculating return periods and return levels using probability distributions such as Gumbel, GEV, and Log-Pearson Type III.

Peaks-Over-Threshold (POT): POT is a method that focuses on analysis of all flow events above a given threshold, using the Generalized Pareto Distribution (GPD) to determine specific characteristics of frequent and clustered extreme events.

Threshold Analysis: This technique examines when streamflow exceeds flood levels or drops below drought thresholds (e.g., Q_{90}, Q_{95}) and measures how often, how long, and how intensely these thresholds are crossed. Dahri et al. (2021) investigated some discharge quantiles (Q_5, Q_{10}, Q_{90}, Q_{95}) and concluded that simultaneous changes in high and low flow patterns can indicate complex shifts in overall hydrological risk.

Duration Metrics: It calculates the length of time that high or low flows persist to estimate the severity of flood or drought conditions.

Standardized Indices: Indices such as the Standardized Streamflow Index (SSI) and Standardized Runoff Index (SRI) normalize streamflow data to allow comparison of hydrological extremes across different times and locations.

2.3.3 Challenges in predicting hydrological extremes using LSTM

The hydrological model needs to have strong predicting capabilities for extreme outliers, as they can impact water resource management (Mohammadi et al., 2024). Deep learning models like LSTM demonstrate strong performance in streamflow simulation but face challenges in predicting extreme events (Zarei et al., 2024). While the LSTM architecture addresses long-term dependencies, it tends to smoothen outputs, favouring low variations rather than high variations (Ishii et al., 2023). This underrepresents high-flow conditions during training data, reducing the model's capacity to predict peak discharge events and lowering its reliability when simulating extreme hydrologic conditions. This limitation can be overcome by employing large catchment datasets with sufficient records of extreme flows (Baste et al., 2025; Martel et al., 2024). However, LSTM shows promising results compared to other process-based models to predict low flow conditions (Islam et al., 2025).

3 STUDY AREA

The Koshi River basin spans across China, Nepal, and India. Despite the river's substantial water flow (averaging 1564 cubic meters per second at the main outlet, Chatara Station in Nepal), like other regional basins, it faces significant seasonal variability issues in water availability. The Koshi is the largest of the Himalayan Rivers flowing into the Ganges, with a total catchment area of 87,311 square kilometres. This area is distributed as 33% (28,300 square kilometres) in China, 45% (39,407 square kilometres) in Nepal, and 22% (19,604 square kilometres) in India (Dixit, 2009).

Within Nepal, the Koshi Basin experiences a significant elevation drop, from 8,848 meters at Mt. Everest to 60 meters in the alluvial plains. The basin is divided into four main physiographical regions based on elevation and topography: the Terai region (60-200 meters), the hill regions (200-4000 meters), the mountain regions (above 4000 meters), and the trans-mountain region north of the Himalayas extending into Tibet (Bharati et al., 2014). Rainfall within the Koshi Basin is highly spatially variable due to its changing topography and climate. The average annual rainfall ranges from about 1,755 mm in the mountainous central parts to only 210 mm in the trans-Himalayan region. The average in the eastern mountainous regions is about 1,418 mm, while that in the southern areas of the basin is higher than in the dry northern regions (Chinnasamy et al., 2015).

The climate of the Koshi Basin is diverse from cold in the northern highlands to tropical in the southern plains. There are four distinct seasons in the region: pre-monsoon (March to May), monsoon (June to September), post-monsoon (October to November), and winter (December to February) (Chinnasamy et al., 2015). Precipitation in the Koshi River basin varies greatly, with around 80% occurring during the monsoon season.

The upper basin faces challenges such as snowmelt, water runoff, soil erosion, and land degradation, while the lower basin deals with waterlogging, population growth, agricultural expansion, and urbanisation. The impacts of climate change will compound these difficulties, disrupting seasonal water supply reliability, food, and energy supply reliability, and therefore underscoring the necessity for good water resource management and robust disaster risk reduction policy (Wahid et al., 2017). Communities living in the mid-hills and Terai floodplain are already witnessing climate-related challenges such as irregular monsoon rains, and recurrent floods and droughts. Rainfall pattern change will also alter river flow regimes, potentially destabilizing ecosystems and the services they offer

(Dixit, 2009). Adapting to climate change is challenging due to the dynamic nature of the Earth system and the lack of comprehensive understanding of future climate conditions and their associated uncertainties. Effective climate adaptation relies on high-quality and sufficient hydro-meteorological and environmental data. However, planning for climate adaptation is hindered by the absence of reliable climate information, including uncertainties about the timing and spatial distribution of impacts(Banda et al., 2022). Predicting and quantifying the hydrological impacts and extent of future climate change is essential for developing adaptive measures. These predictions, particularly regarding the effects on hydrological systems and streamflow, are typically made using various modeling approaches, such as the deep learning methods employed in this study.

The project focuses on nine hydrological stations strategically positioned across various watersheds within the Koshi River Basin in Nepal. These include stations on the Bhotekosi River at Barbise, Tamakosi River at Busti, Melamchi River at Helambhu, Balephi River at Jalbire, Tamur River at Majhitar, Dudhakosi River at Rabuwabazar, Khimtikhola at Rasnalu, Likhu River at Sangutar, and Arun River at Simle. The watersheds with their outlets are shown in Figure 3-1. This network of monitoring stations covers key tributaries and watersheds of the Koshi River system, providing essential data for water resource management and flood prediction within this crucial river basin in eastern Nepal.

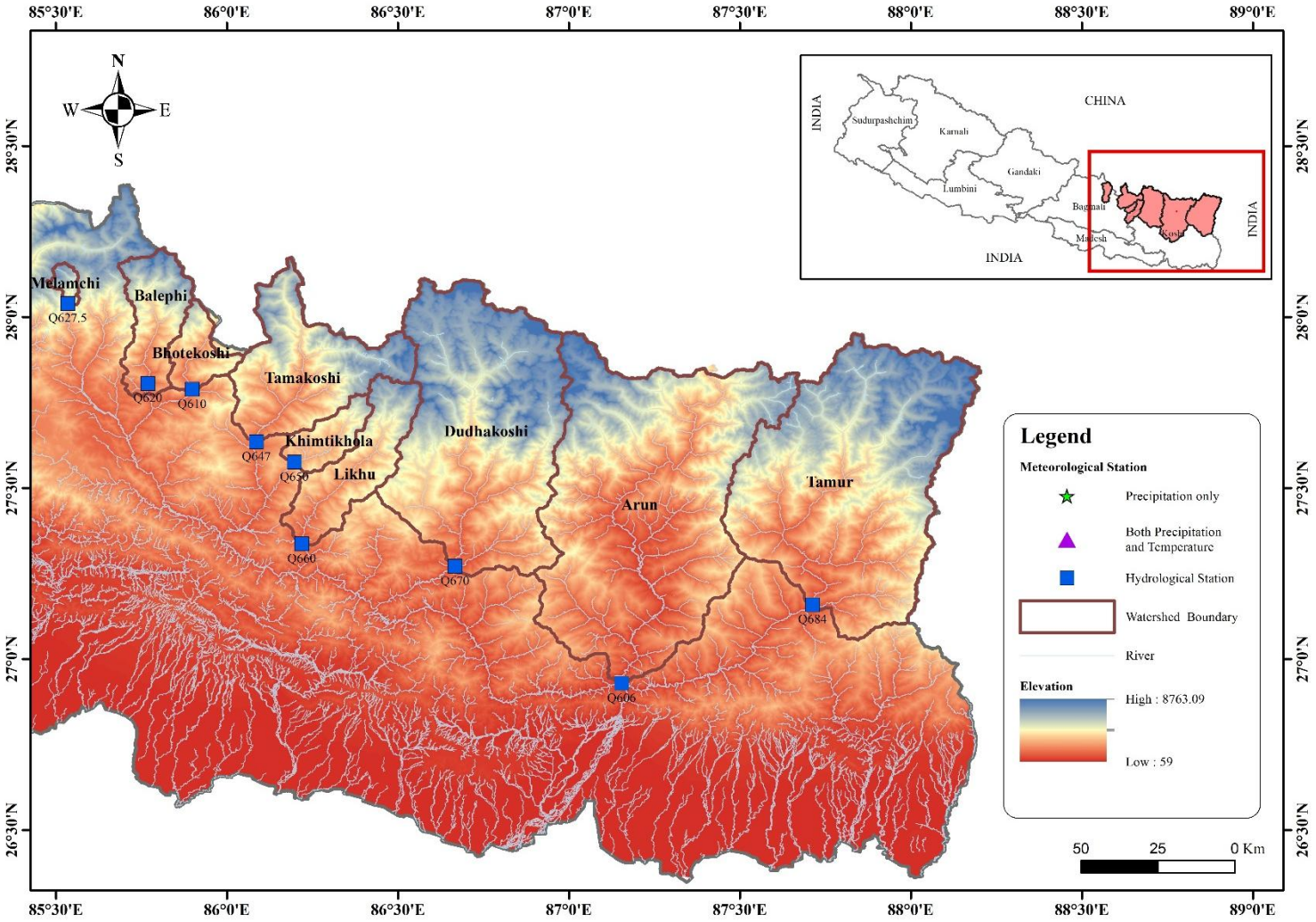

Figure 3-1 Location and topographic variation of study area

4 METHODOLOGY

This study deploys Bidirectional Long Short-Term Memory (BiLSTM) deep learning methodology in hydrological modeling in nine distinct river watersheds. The overall aim is to evaluate the capacity of the model in daily streamflow prediction based on Nash-Sutcliffe Efficiency (NSE), Kling-Gupta Efficiency (KGE), and Root Mean Square Error (RMSE) as key performance metrics of assessment. After validation, the LSTM model trained is deployed to predict impending climate change-induced hydrological extremes. This involves analyzing simulated streamflow generated with bias-corrected outputs from selected CMIP6 Global Climate Model (GCM) datasets under past and two future Shared Socioeconomic Pathways (SSP245 and SSP585). The effect evaluation focuses on streamflow variability and extremes, quantified by comparing specific flow quantiles (Q_5 and Q_{10} for low flows; Q_{90} and Q_{95} for high flows) between the past reference and future projections, primarily as percentage changes. A representation of this overall process is found in Figure 4-1.

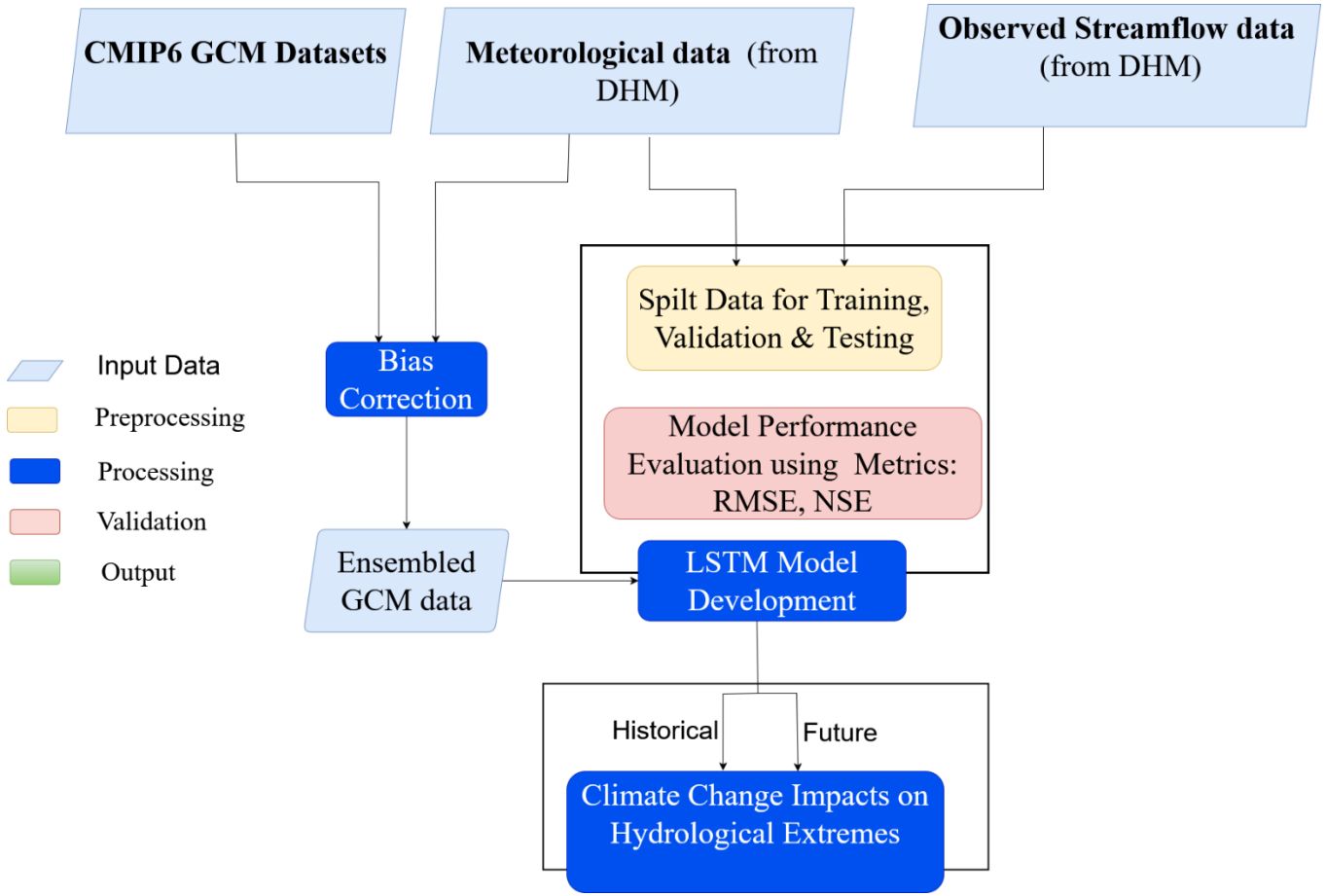

Figure 4-1 Flow diagram of research process

4.1 LSTM Model Development and Evaluation

Robust hydrological modeling relies on large, consistent input data. The selection, procurement, and processing of hydrometeorological observations, static catchment properties, and climate model outputs are critical in making inputs for machine learning-based modeling. The modeling variables are typically categorized into two sets: dynamic and static. Dynamic variables are meteorological and hydrological inputs, i.e., precipitation and temperature that vary over time and directly influence daily streamflow. Static variables, by contrast, are physical and geographical attributes of river watersheds, such as elevation, soil texture, and land cover, that can be assumed to remain constant over time and used to represent basin heterogeneity. Table 4-1 presents an overview of the dynamic and static variables used in the model, their units, and data sources.

Table 4-1 Overview of model input variables

Variable Name	Unit	Source
Dynamic Variables		
Precipitation	mm	DHM/Aphrodite/ERA5
Daily maximum temperature	°C	DHM/ERA5
Daily minimum temperature	°C	
Wind speed at 10 meters	m/s	HAR asia
Shortwave radiation downward	W/m^2	
Longwave radiation downward	W/m^2	
Potential Evapotranspiration	mm/day	Derived from other variables
River discharge (streamflow)	m^3/s	DHM
Static Variables		
The mean elevation of the basin	meters (m)	SRTM DEM (30m resolution)
Elevation range = max - min elevation	meters (m)	
Mean terrain slope of the basin	degrees (°)	
Soil porosity estimated from bulk density (1 - BD/2.65)	dimensionless	HWSD2 / FAO SoilGrids
Fraction of sand content in topsoil	0–1	
Fraction of silt content in topsoil	0–1	
Fraction of clay content in topsoil	0–1	

Variable Name	Unit	Source
Average Leaf Area Index	m^2/m^2	MODIS LAI (MCD15A3H)
Difference between max and min LAI over time	m^2/m^2	
Forest land cover fraction	0–1	MODIS Land Cover (MCD12Q1)
Grassland area fraction	0–1	
Cropland area fraction	0–1	
Permanent snow/ice cover fraction	0–1	
Barren land cover fraction	0–1	
Total basin area	km^2	Derived from basin delineation
Latitude and longitude of basin centroid	decimal degrees	Derived using geometry of basin

4.1.1 Study watersheds and hydrological data

To provide correct basin-scale hydrological modeling, the spatial and geographical properties of the river basins to be examined need to be defined. The study focuses on the watersheds of the Koshi River system of eastern and mid-Nepal, all of which have a hydrological station operated by the Department of Hydrology and Meteorology (DHM). They provide daily discharge data, which form the core observation database for model calibration, validation, and testing. The river's name, coordinates, and catchment area for each hydrological station are presented in Table 4-2.

Table 4-2 Details on hydrological stations

Basin's Name	Location	St no	Coordinate (Lat, Lon)	Area (km^2)
Tamur River	Majhitar	684	87.711887,27.159276	4373.62
Arun River	Simle	606	87.155104,26.923711	5130.67
Dudhakosi River	Rabuwabazar	670	86.65942,27.268532	3706.97
Likhu River	Sangutar	660	86.21832,27.349466	852.20
Khimtikhola	Rasnalu	650	86.202953,27.580536	325.17
Tamakosi River	Busti	647	86.084955,27.63624	1486.41
Balephi River	Jalbire	620	85.766255,27.804756	663.12
Melamchi River	Helambhu	627.5	28.010493, 85.535541	120.91
Bhotekosi River	Barbise	610	27.787359, 85.899338	2370.22

Figure 4-2 shows the discharge data coverage for a daily time series from 1980 to 2019 at nine river watersheds in Nepal: Arun, Balephi, Bhotekoshi, Dudhakoshi, Khimtikhola, Likhu, Melamchi, Tamakoshi, and Tamur. Blue bars represent the

number of days with discharge records, while red bars indicate the number of missing days in a year. Arun and Tamur watersheds, for instance, possess relatively unbroken records after the mid-1980s, whereas Melamchi and Likhu exhibit typical gaps, particularly in the beginning and ending years. Dudhakoshi, Khimtikhola, and Tamakoshi possess more evenly spread data coverage, though intermittent at times. The extent of daily input data was determined based on the availability of daily data from hydrological stations, as shown in Table 4-3**.** The availability of continuous daily records at the watersheds' outlet hydrological stations was used to determine appropriate periods. When choosing appropriate periods, years with very little missing data (less than five daily records) were also taken into consideration. When the model input was being prepared, interpolation was used to fill in the missing data.

Table 4-3 Details on the availability of observed hydrological data

Basin's Name	Station no	Period	Data Availability	Selected Period
Tamur River	684	1986-2019	97.54%	2009-2019
Arun River	606	1986-2019	99.14%	1996-2019
Dudhakosi River	670	1980-2019	97.27%	1985-2008
Likhu River	660	1980-2016	82.00%	2007-2016
Khimtikhola	650	1980-2018	94.05%	1989-2008
Tamakosi River	647	1980-2019	91.97%	1993-2001
Balephi River	620	1980-2019	98.75%	1988-2019
Melamchi River	627.5	1990-2012	91.61%	2001-2012
Bhotekosi River	610	1980-2012	75.15%	1987-1998

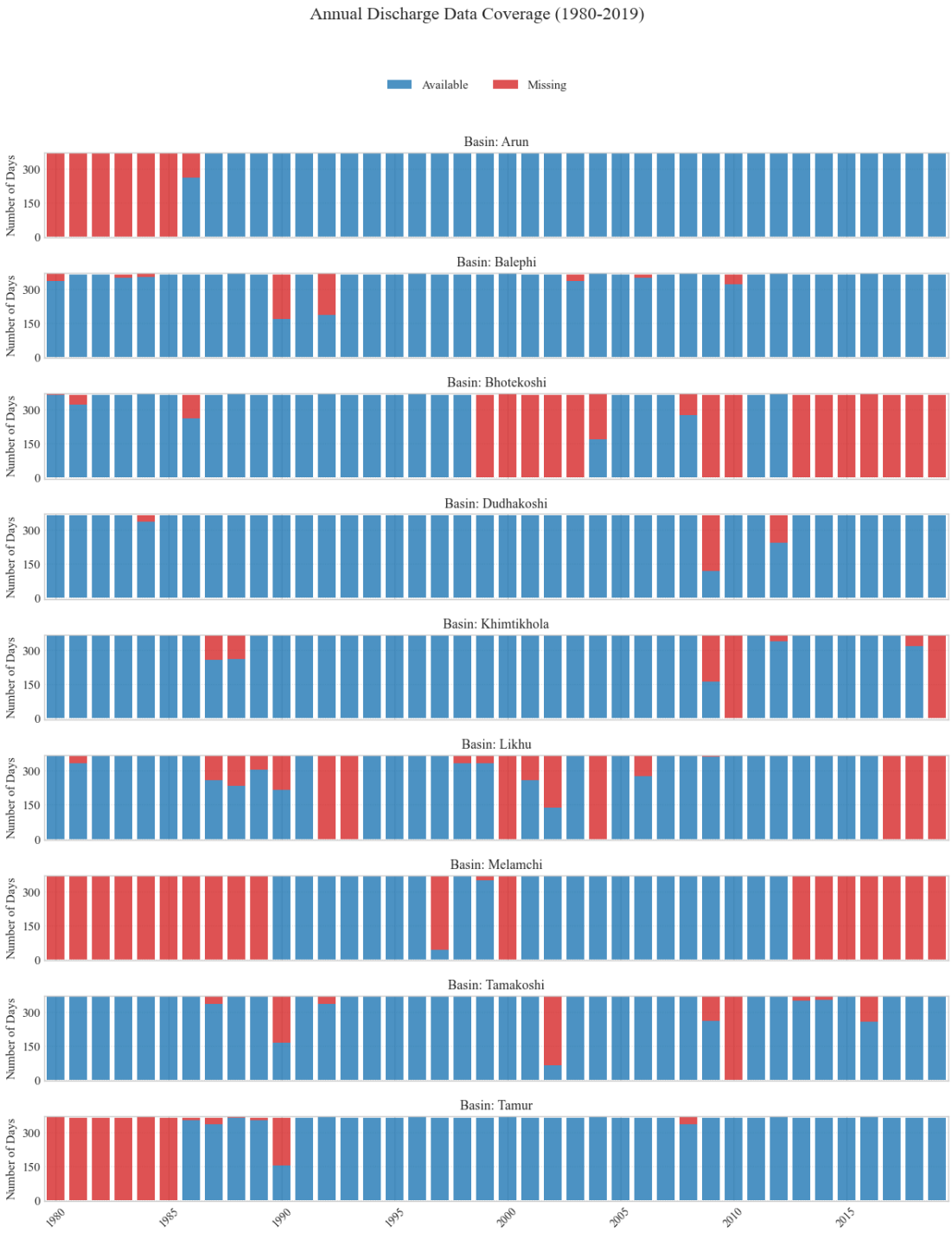

Figure 4-2 Discharge data coverage across nine watersheds (1980–2019)

4.1.2 Meteorological forcing data

To set up the model, daily records from precipitation and temperature stations from the Department of Hydrology and Meteorology (DHM) were used. Daily records from precipitation, temperature and hydrological stations from the Department of Hydrology and Meteorology (DHM) were used as part of in-situ observation for the setting up of the model for nine watersheds - Tamur, Arun,

Dudhakosi, Likhu, Khimtikhola, Tamakoshi, Bhotekoshi, Melamchi and Balephi. Missing temperature data was filled using regression with data from nearby weather stations. For precipitation, Asia-Pacific High-Resolution Observation Data Integration Towards Evaluation of Water Resources (APHRODITE) http://aphrodite.st.hirosaki-u.ac.jp and European Reanalysis Atmosphere 5 (ERA5) https://cds.climate.copernicus.eu/datasets/reanalysis-era5-single-levels gridded datasets were used to estimate the missing values. Monthly regression was used to match the observed precipitation data with the gridded datasets. The list of meteorological stations used for the hydrological modelling at the hydrological stations is shown in Table 4-4.

Table 4-4 Meteorological stations used for hydrological modeling

Basin	**Hydrological**	**Precipitation**	**Temperature**
Arun	606	1301, 1303, 1304, 1305, 1306, 1317, 1321, 1322, 1325	1303, 1304
Balephi	602	-	-
Dudhkoshi	670	1202, 1203, 1204, 1219	-
Khimtikhola	650	-	-
Likhu	660	1224	-
Tamakoshi	647	1101, 1102	-
Tamur	684	1403, 1405, 1406, 1420	1405
Bhotekoshi	610	-	-
Melamchi	627.5	-	-

Potential Evapotranspiration (PET) was estimated by the Hargreaves method (McMahon et al., 2013), an empirical temperature technique applicable in regions with limited meteorological data. The method was utilized by employing the Pyet Python package (https://pypi.org/project/pyet), an efficient computationally package of evapotranspiration calculation from a variety of climatic formulations. For each basin, minimum and maximum daily temperatures and the mean daily temperature, computed as the two's average, were used. These temperatures are derived as basin-averaged values, representing the spatially averaged climate state over the basin. In addition to temperature, the geometric centroid latitude of the basin was utilized to compute the solar radiation component needed for estimating PET. To include future climate change situations, the same approach was utilized for bias-corrected GCM outputs for different Shared Socioeconomic

Pathways (SSP245 and SSP585). For each scenario and GCM, PET was estimated using the corresponding downscaled and corrected temperature data specific to the basin. This technique is widely used in climate and hydrological impact studies due to its simplicity, low data requirements, and ability to perform well in the most diverse geographic regions (Hargreaves & Samani, 1985).

4.1.3 Gridded/reanalysis data integration

Following gridded/reanalysis data products were used in this study: APHRODITE, ERA5, and High-Resolution Atmospheric Reanalysis, version 2 (HAR2)

i) APHRODITE & ERA5: Gridded datasets were used to compensate for the lack of meteorological stations and spatial variability within a watershed. The boundaries of river basins at the location were determined by creating watersheds in ArcGIS using a Digital Elevation Model (DEM) from the Advanced Spaceborne Thermal Emission and Reflection Radiometer (ASTER) (https://www.earthdata.nasa.gov/), which has a spatial resolution of approximately 30 meters at the equator. The grid of the NetCDF file of precipitation from Aphrodite was interpolated to ERA5's grid using the Climate Data Operator (CDO) from the Cygwin terminal available for Windows. After gridding the two datasets into similar grids, linear scaling was performed on a monthly level for both, and a correction factor was calculated. The correction factor was then applied to ERA5's precipitation dataset. The final dataset is a combination of Aphrodite (1980-2015) and the corrected ERA5 dataset (2016-2022). Similarly, ERA5's maximum temperature and minimum temperature datasets were used in this study for temperature. The ERA5 datasets are spatially coarse and may not accurately represent the observation at a grid point, despite having good temporal resolution (Zhao et al., 2022). Therefore, the gridded datasets were downscaled with nearby observation stations using the quantile mapping method, as stated in Section 4.2.2. The location of grids used in this study is given in Table 4-5.

Table 4-5 Spatial grid details for Aphrodite and ERA5 datasets

Basin	**Aphrodite/ERA5 Precipitation**	**ERA5 Temperature**
Arun	87.25_27.25	87.25_27.25
Balephi	-	-
Dudhkoshi	-	86.5_27.5, 86.75_27.5, 86.75_27.75, 86.75_28.0

Basin	Aphrodite/ERA5 Precipitation	ERA5 Temperature
Khimtikhola	-	-
Likhu	86.25_27.5, 86.5_27.75	-
Tamakoshi	86.25_27.75	-
Tamur	87.75_27.75, 88.0_27.75	87.75_27.75, 88.0_27.75
Melamchi	-	-
Bhotekoshi	-	-

Note: The grid in the table is represented in the format Longitude_Latitude. For example, a grid point might be written as 87.25_27.75, where 87.25 is the longitude and 27.75 is the latitude.

The widely used Thiessen polygon method (Zhou et al., 2009) is used to calculate the basin average of forcings such as temperature and precipitation. To do this, the watershed is divided into polygons, each of which is connected to an observed station. It is predicated on the idea that the value recorded at the corresponding station is equal to the value at any point within a polygon. This formula was used to determine the average temperature and precipitation values.

$$P_{avg} = \frac{\sum_{i=1}^{n} A_i * P_i}{A} \qquad (7)$$

The basin average precipitation P_{avg} is calculated as a weighted average of rainfall recorded at each station (P_i), with weights based on the area of the Thiessen polygon (A_i) associated with each station. The total area of basin A is the sum of all A_i and n is the number of stations. This method ensures that each station's contribution is proportional to the area it occupies in the basin. For a Thiessen polygon, a polygon (or Voronoi diagram) must have a minimum of three stations. The criteria for the creation of polygons were not met by small catchments or catchments with fewer meteorological stations, as shown in Table 4-5. This issue was resolved by employing spatial weighting of gridded climate data to calculate basin-averaged daily time series of temperature and precipitation for the chosen basins. The percentage of each overlapping grid cell's area that is inside the basin acts as a weight. Each day's weighted average across all contributing grid cells was determined using these weights. The average values for all forcing in the watersheds of Balephi, Khimtikhola, Melamchi, and Bhotekoshi were determined using this method. Similarly, Melamchi and Bhotekoshi used this method to calculate averages for only temperature datasets.

ii) HAR2: It was selected to include other dynamic hydrometeorological variables because it operates on a finer spatial grid and was created for a specific geographic

region. The High Asia Refined Analysis (HAR) dataset was developed by the Chair of Climatology, Technische Universität Berlin (https://www.tu.berlin/en/klima/research/regional-climatology/high-asia/har). The dataset applies dynamical downscaling of global reanalysis data via the Weather Research and Forecasting (WRF) model to improve resolution and accuracy (X. Wang et al., 2021). It is a high-resolution atmospheric dataset that aims to deliver precise information regarding the climatic conditions in High Mountain Asia (HMA), including the Tibetan Plateau and surrounding mountain systems. It has been demonstrated that HAR2 datasets perform marginally better than ERA5-land datasets and better capture orographic effects (Khadka et al., 2022; Pritchard et al., 2019). The daily time series' meteorological variables, such as radiation and wind speed, covered the years 1980–2022 and were used as additional dynamic inputs for the model.

4.1.4 Static basin attribute derivation

A comprehensive set of physiographic, soil, vegetation, land cover, and climatic attributes for the selected watersheds was derived. A consistent dataset characterizing key environmental factors influencing hydrological processes within each watershed was generated. The procedures involved processing various geospatial raster and vector datasets, extracting information from databases, and performing calculations using established geospatial analysis techniques.

i) Shuttle Radar Topography Mission (SRTM): The topography of each watershed is analyzed using the Shuttle Radar Topography Mission (SRTM) Digital Elevation Model (DEM) with a spatial resolution of 30 meters. It was retrieved through the Earth Explorer facility of the US Geological Survey (USGS) (https://earthexplorer.usgs.gov/). Mean elevation was determined to indicate the average surface height above the mean sea level for each delineated watershed. An average elevation was computed for each watershed polygon by averaging all elevation pixels contained within it. The average elevation, in meters, thus obtained was then used as a defining characteristic for the corresponding watershed. Additionally, the basin elevation range was computed to achieve the relief difference within each watershed. The difference between the two values (i.e., maximum minus minimum elevation) was utilized to compute the total vertical relief or elevation range, also in meters. The mean watershed terrain slope was extracted from a slope raster computed from the SRTM DEM. This mean slope value is a measure of the general steepness of the land surface across the

entire watershed. Figure 4-3 presents the derived elevation, while Figure 4-4 presents the derived slope, presenting the differences in gradients in the area.

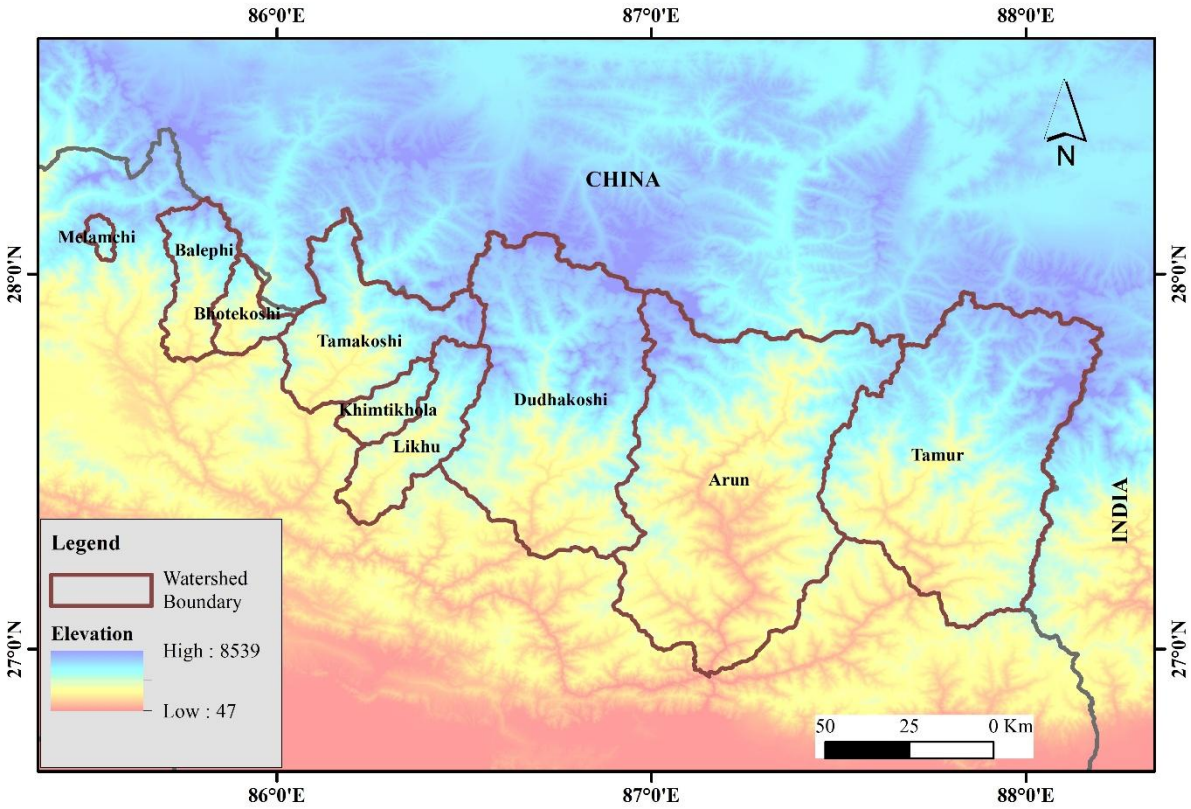

Figure 4-3 Derived elevation across watersheds

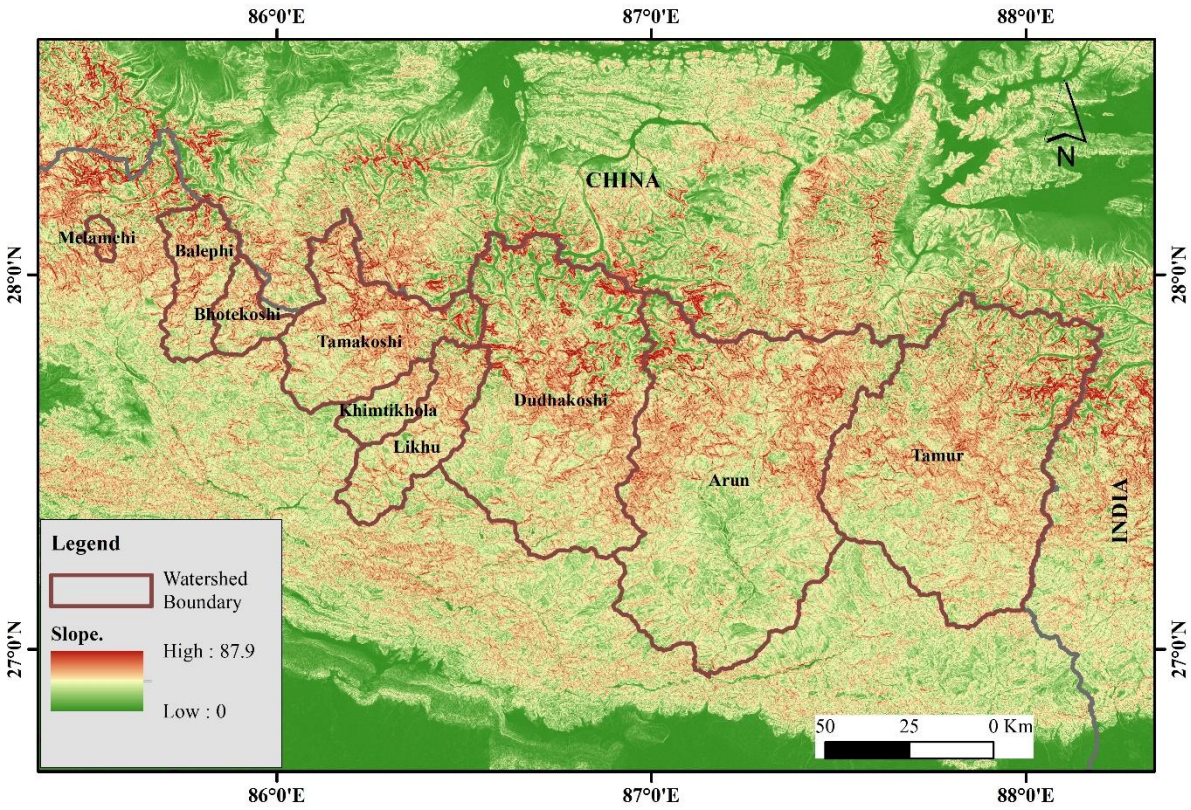

Figure 4-4 Derived slope characteristics of watersheds

ii) HWSD2 / FAO SoilGrids: The Harmonized World Soil Database version 2 (HWSD2) and FAO SoilGrids available on FAO's global soil repository (https://www.fao.org/soils-portal/data-hub/soil-maps-and-databases/harmonized-world-soil-database-v20/en/) are standard global soil datasets providing spatially explicit information on a set of soil properties critical for hydrological modeling. They include soil texture (sand, silt, clay fractions), porosity, bulk density, and organic carbon content, which regulate infiltration, water retention, drainage, and plant water uptake (Hengl et al., 2017). For this study, data were aggregated and disaggregated to the watershed level to represent soil conditions for the watershed. Soil porosity, an important determinant of water holding capacity and infiltration potential, was estimated from bulk density values of HWSD2. Porosity was estimated based on the following equation (Robinson et al., 2022):

$$Porosity = 1 - \frac{BD}{2.65} \qquad (8)$$

Where BD is bulk density (g/cm^3) and 2.65 is the assumed average particle density. A share-weighted average bulk density was calculated for each Soil

Mapping Unit (SMU), and the values were spatially averaged at the basin level using the raster distribution of SMUs to obtain mean basin porosity values. Likewise, sand, silt, and clay contents in topsoil layers were obtained from the HWSD database. For every SMU, the texture values were extracted and normalized such that their sum was equal to unity. Basin-scale averages were then calculated by weighting the SMU values based on their spatial occurrence within each basin polygon. Figure 4-5 presents the soil classification of the study area, as per the FAO Digital Soil Map of the World (DSMW).

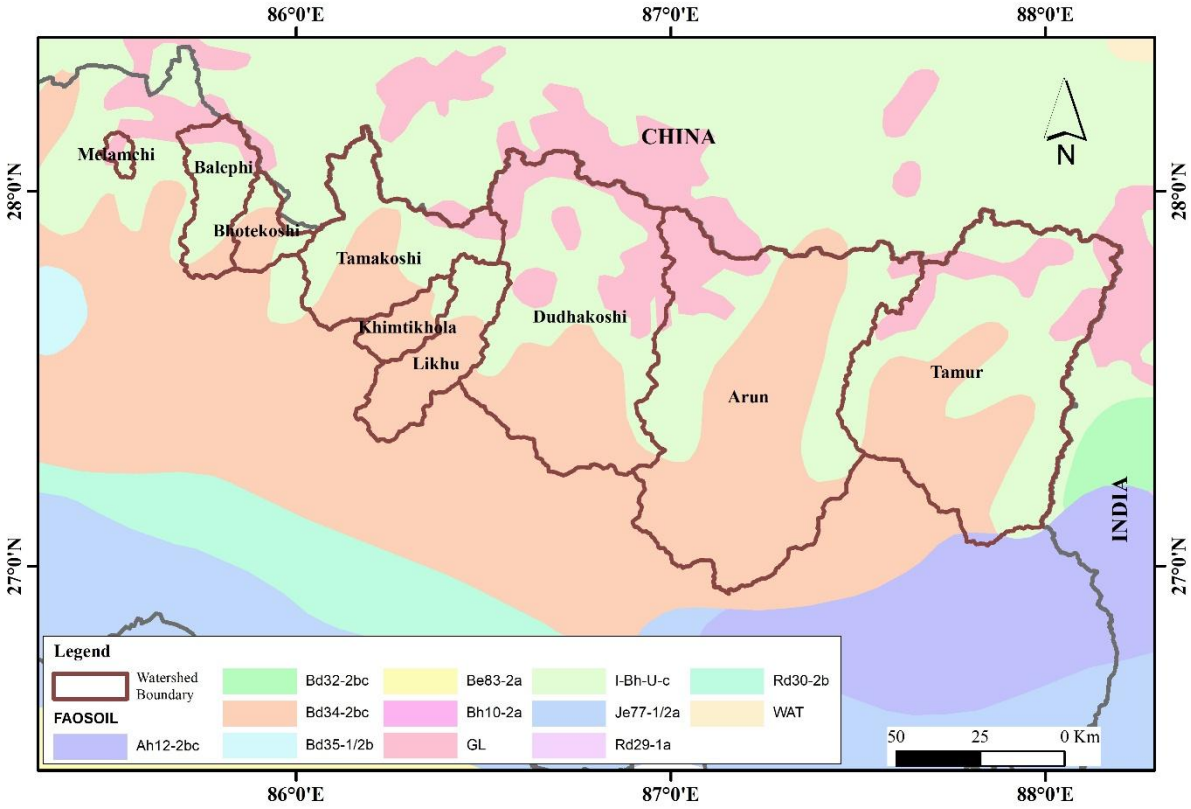

Figure 4-5 Soil classification of the study region

iii) MODIS Leaf Area Index (LAI – MCD15A3H): The MODIS Leaf Area Index (LAI) product, the MCD15A3H Version 6.1, was utilized from the Google Earth Engine (GEE) platform to characterize vegetation dynamics in the study watersheds. The dataset provides 500-meter resolution global LAI estimates at a 4-day temporal frequency, equivalent to the leaf area per unit ground surface (m^2/m^2). To get meaningful indicators from this product, two variables were computed: the mean LAI and LAI range by watershed. The mean LAI illustrated in Figure 4-6 is a measure of the spatial average green leaf area by watershed and was computed by temporally averaging the LAI raster. This produced a representative measure of vegetation density by basin and was used as an input in subsequent eco-

hydrological computation. The LAI range quantifies the degree of spatial heterogeneity in every watershed. It was approximated as the difference between the maximum and minimum LAI values derived from the temporally averaged raster. The topography greatly influences the patterns of vegetation. The Leaf Area Index (LAI) varies by aspect and falls with increasing elevation and slope (W. Zhang et al., 2021). A high LAI range indicates high variability in vegetation cover.

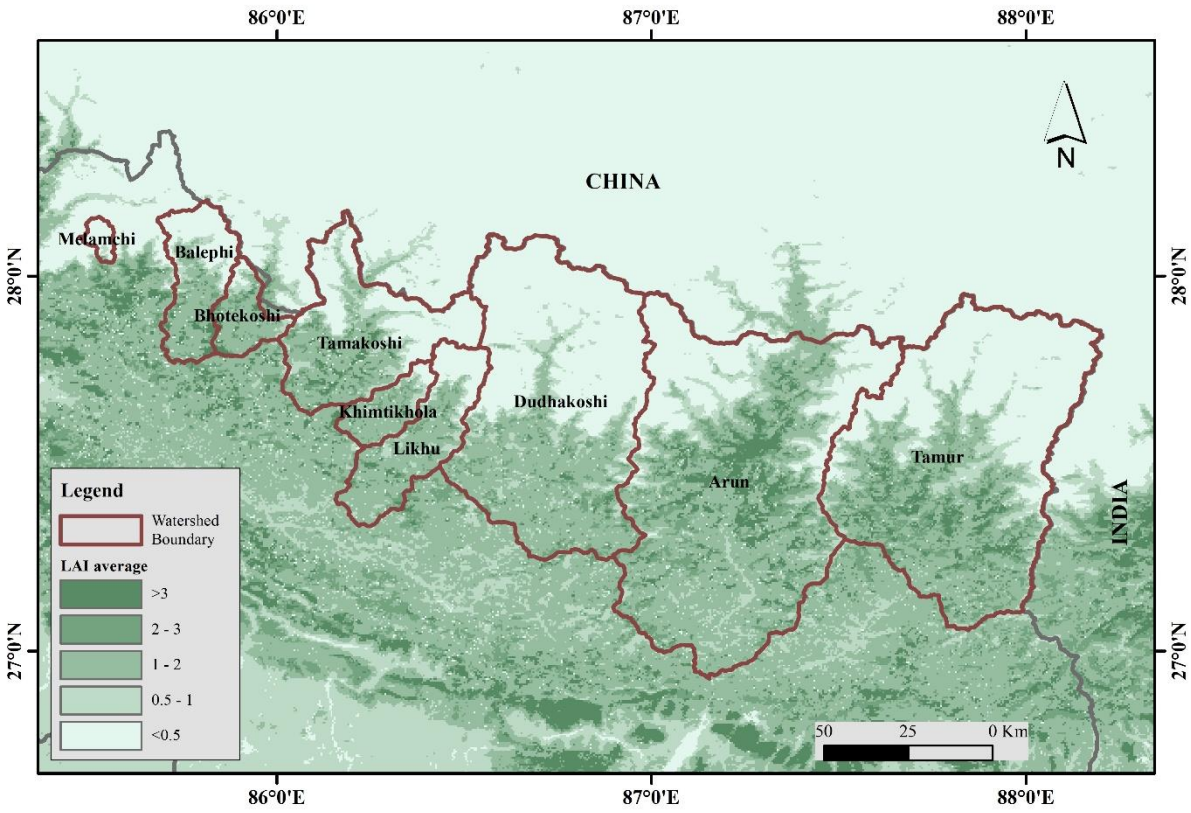

Figure 4-6 Mean LAI across watersheds

iv) MODIS Land Cover (MCD12Q1): MODIS Land Cover product (MCD12Q1 Version 6.1), acquired from Google Earth Engine, is an annual global land cover classification with a spatial resolution of 500 meters. The data classifies the Earth's surface into 17 land cover types ranging from forests, grasslands, and croplands to urban, snow/ice, and barren lands using the International Geosphere-Biosphere Programme (IGBP) classification scheme (Loveland & Belward, 1997). To facilitate easier hydrological interpretation, the land cover codes were combined into broader functional classes: Forest (1–9), Grassland (10), Cropland (12, 14), Snow/Ice (15), and Barren (16). Each land cover class percentage in a watershed was computed using pixel frequency analysis. That is, the total number of pixels in each aggregated class was divided by the total valid land cover pixels in the basin to obtain dimensionless fractions (between 0 and 1)

for each class. These fractions provide a spatial integration of vegetation structure and land use intensity that are essential to parameterize land surface models and examine land use impacts on watershed-scale hydrological response. Figure 4-7 illustrates the geographical coverage of the main land cover classes (forest, grassland, cropland, snow/ice, and barren) in the study basins, as extracted from the mode composite of the MODIS Land Cover Type product (MCD12Q1, Version 6.1) for the period 2001–2024. Land cover was classified by the IGBP scheme and grouped into more general categories.

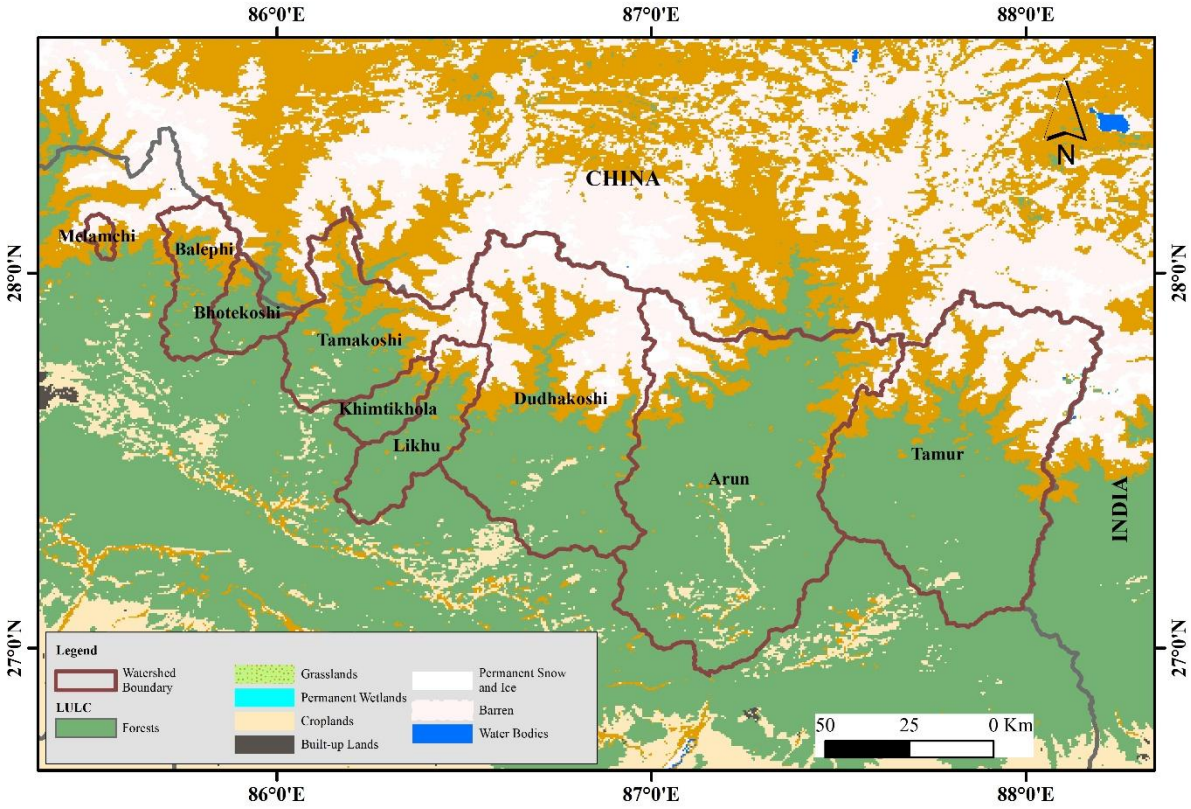

Figure 4-7 Land use land cover classification derived from MODIS (MCD12Q1)

v) Mean Annual Precipitation, Aridity Index and other characteristics: The other characteristics introduced into the final dataset at the watershed level pertain to simple spatial and climatic descriptors that define the geographical identity and hydrometeorological setting of each sub-basin. The total basin area, geographic centroid coordinates (latitude and longitude), Mean Annual Precipitation (MAP), Mean Annual Evapotranspiration (PET), and the Aridity Index (AI) are the additional watershed descriptors. The Aridity Index (AI) was determined by dividing the Mean Annual Precipitation (MAP) by the Mean Annual Potential Evapotranspiration (PET). MAP across different watersheds is presented in Figure 4-8.

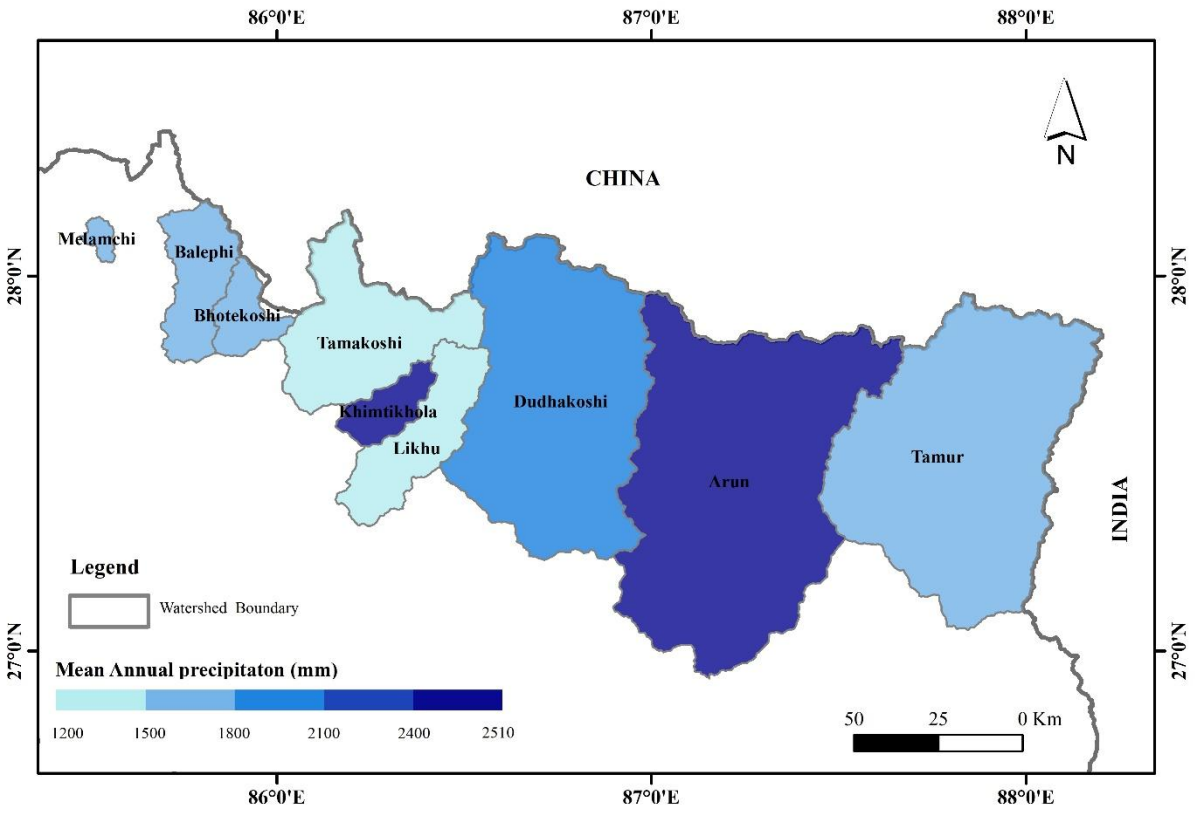

Figure 4-8 MAP across different watersheds

4.1.5 Input data normalization and transformation

Several normalization techniques were employed to harmonize data sets for extreme flow analysis in the study area to provide consistency and reliability of the results. Streamflow data were converted into specific discharge to enable cross-basin comparisons independent of basin size. This was done by dividing streamflow by the product of basin area and mean annual precipitation:

$$Q_{sd} = \frac{Q}{A * P_{avg}} \qquad (9)$$

Here, Q_{sd} is the normalized discharge (dimensionless), Q is the raw streamflow (in m^3/s), A is the watershed area (in km^2), and P_{avg} is the average annual precipitation (in mm/year). This normalization ensures that discharge values reflect hydrological behaviour relative to basin characteristics. To address the positive skew in precipitation and flow data, a logarithmic transformation was applied. This reduces distribution asymmetry and stabilizes variance, using the following equation:

$$x' = \log_{10}(x + 0.1) \qquad (10)$$

x denotes the raw variable (rainfall or specific discharge), and x' is the log-transformed variable. A small constant (0.1) was added to avoid taking the logarithm of zero. The resulting transformed values and all other variables were then standardized using the Z-score method to facilitate statistical analysis across datasets:

$$z = \frac{x_0 - \mu}{\sigma} \qquad (11)$$

Where x_o represents either a transformed or original variable, z is the standardized score, μ is the mean, and σ is the standard deviation of the transformed variable.

4.1.6 Multi-basin BiLSTM model architecture and training

This study employed a two-layer Bidirectional LSTM model to learn temporal patterns in streamflow prediction. The model had 256 and 128 units for the first and second layers, respectively, and a dropout rate of 0.2 after each of the layers to prevent overfitting. Each of the LSTM layers was preceded by batch normalization to regularize and speed up training. A dense layer combined the LSTM output with fixed catchment features such that the model could account for dynamic as well as physical watershed characteristics.

The model was optimized with the Adam optimizer at a learning rate of 0.001, and the Huber loss function for discharge data robustness against outliers. A batch size of 32 was used to strike a balance between computational efficiency and learning performance. Early stopping and learning rate reduction on the plateau were applied based on validation loss to avoid overfitting and improve generalization.60-day dynamic meteorological variable time series were used as input sequences, and discharge was the output variable. The data were divided into 80% for training and 20% for testing purposes, and a portion of the training data (20%) was used for validation. Predictions from each of these splits are evaluated separately to assess the model's performance.

4.1.7 Performance evaluation metrics

The performance of the Long Short-Term Memory (LSTM) model developed for streamflow prediction is critical to ensure the reliability and accuracy of the model in simulating the hydrological process. Model evaluation involves comparing simulated streamflow with observed data using established statistical metrics.

Root Mean Square Error (RMSE), Kling-Gupta Efficiency (KGE) and Nash-Sutcliffe Efficiency (NSE) are the statistical metrics used to assess the model's performance. The fit between simulated and observed data is commonly measured using the NSE by Nash & Sutcliffe (1970). Root Mean Square Error (RMSE) is used to assess the accuracy of simulations by measuring the standard deviation of observed and simulated differences. KGE provides a more diagnostic evaluation by decomposing the model error into three distinct terms: correlation (linear relationship between simulated and observed), bias (ratio of means), and variability (ratio of standard deviations. These metrics are calculated as:

$$NSE = 1 - \frac{\sum_{t=1}^{n}(Q_{obs,t} - Q_{sim,t})^2}{\sum_{t=1}^{n}(Q_{obs,t} - \overline{Q_{obs,t}})^2} \quad (12)$$

$$RMSE = \sqrt{\frac{\sum_{t=1}^{n}(Q_{sim,t} - Q_{obs,t})^2}{n}} \quad (13)$$

$$KGE = 1 - \sqrt{((r-1)^2 + (\beta - 1)^2 + (\gamma - 1)^2)} \quad (14)$$

$$r = \frac{\sum_{t=1}^{n}(Q_{sim,t} - \overline{Q_{sim,t}})*(Q_{obs,t} - \overline{Q_{obs,t}})}{\sqrt{\sum_{t=1}^{n}(Q_{sim,t} - \overline{Q_{sim,t}})^2} * \sqrt{\sum_{t=1}^{n}(Q_{obs,t} - \overline{Q_{obs,t}})^2}} \quad (15)$$

$$\beta = \frac{\overline{Q_{sim,t}}}{\overline{Q_{obs,t}}} \quad (16)$$

$$\gamma = \frac{\sigma_s}{\sigma_o} \quad (17)$$

Where $Q_{sim,t}$ and $Q_{obs,t}$ represent the simulated and observed discharges, respectively; $\overline{Q_{sim,t}}$ and $\overline{Q_{obs,t}}$ are the mean simulated and observed streamflow; and n is the length of the time series. r, β, γ are Pearson correlation coefficients between the simulated and observed time series, the bias ratio component of the KGE score and the variability ratio component of the KGE score. σ_s and σ_o are the standard deviation of predicted and observed values. The NSE and KGE range from −∞ to 1, with values closer to 1 indicating better model performance. For RMSE, values range from 0 to +∞, with lower values indicating better accuracy, and 0 being the ideal outcome.

4.2 Future Streamflow Simulation Under Climate Change

It is indispensable to understand catchment streamflow variations under future climate projections. Due to changes in monsoon rain patterns and several other severe climate change conditions, floods and droughts are very significant. The prediction of streamflow is important for characterizing the potential for extreme events over future periods (Gong et al., 2023).

The developed multi-basin LSTM model, incorporating the maximum number of meteorological stations, is used to evaluate hydrological changes under future climate conditions, utilizing bias-corrected CMIP-6 meteorological data from two Shared Socioeconomic Pathways (SSPs). The projected streamflow was analyzed for variations during 2026-2055 under both SSP245 and SSP585 scenarios.

4.2.1 Future climate data acquisition

For the future climate-induced hydrological impacts on the study watersheds, high-resolution climate projections formulated from the NASA Earth Exchange Global Daily Downscaled Projections for CMIP6 (NEX-GDDP-CMIP6) were utilized. The NEX-GDDP-CMIP6 (https://www.nccs.nasa.gov/services/data-collections/land-based-products/nex-gddp-cmip6) dataset provides daily climate data at a 0.25-degree spatial resolution (~28 km), which is particularly well-suited for watershed-scale analysis. Three GCMs:EC-Earth3, MPI-ESM1-2-LR, and NESM3 were utilized in this research. These GCMs have been identified in earlier research to be the most effective ensemble for analyzing the future effects of climate change on the Indian subcontinent (Kushwaha et al., 2024; Rahman & Pekkat, 2024). Climate data were obtained for two emission pathways: SSP245, a moderate climate policy scenario, and SSP585, a high-emission, fossil-fueled development pathway. Historical simulations for 1985–2014 were used as the reference period, and future projections were used for 2026–2055. The research centres for each selected GCM are listed in Table 4-6.

Table 4-6 Selected CMIP6 Global Climate Models and Characteristics

GCM	Research Center
EC-Earth3	European Community Earth
MPI-ESM1-2-LR	Max Planck Institute for Meteorology
NESM3	Nanjing University of Information Science and Technology

4.2.2 Bias correction of climate model outputs

For hydrological applications, the outputs of the Global Climate Model (GCM) are imprecise due to their coarse resolution. GCM outputs can be adjusted using a statistical downscaling technique called quantile mapping (Dhital et al., 2023; Gautam & Pradhananga, 2024). To increase the accuracy of meteorological forcings, a more popular quantile mapping technique called Empirical Quantile Mapping (EQM) was used as the bias correction method. No theoretical distribution is assumed by this non-parametric approach (Enayati et al., 2021). It

modifies the model variables' distribution to correspond with historical data. Linear interpolation between corresponding quantiles is used to create a mapping function. The SSP245, SSP585, and historical projections are bias-corrected using the same mapping that was obtained from the calibration period (1980–2014). To adjust for frequency correction, EQM for precipitation was only used on days with precipitation of ≥ 1 mm/day. The EQM method can be mathematical expressd as:

$$X_{cor} = F_O^{-1}(F_G(X_G)) \quad (18)$$

$$P_{cor} = \begin{cases} 0 \\ F_O^{-1}(F_{G,wet}(P_G)) \end{cases} if\ P_G < threshold \quad (19)$$

X_{cor} and P_{cor} are bias-corrected values of the other variables (X) and rainfall (P), respectively, derived from the model results, X_G and P_G. FG stands for the Cumulative Distribution Function (CDF) of the gridded data of the calibration period and F_O that of the observed corresponding data. F_O^{-1} is the inverse CDF, or quantile function, of the observed data, taking a probability and returning a variable value. For precipitation, the threshold is used to demarcate wet and dry; values below the threshold are given a value of zero. The wet condition mapping uses F_G, wet, the CDF derived solely from gridded precipitation above the threshold, and calls upon the inverse CDF (F_O^{-1}) derived similarly from observed wet-day precipitation values.

To assess the robustness of the EQM, performance metrics including R^2, NSE, PBIAS, and RSR were calculated between precipitation and temperature datasets for each watershed. The evaluation of the quantile mapping method is based on Moriasi et al. (2007). Systematic quantification of the Evaluation of the EQM method for each watershed is presented in Table 4-7.

Table 4-7 Performance ratings for the evaluation of bias correction

Model Performance	**R^2**	**NSE**	**RSR**	**PBIAS**	**Rating**
Very Good	0.85<D ≤1.00	0.85<N≤1.00	0.00<R≤0.25	P≤ ±5	8
	0.75<D ≤0.85	0.75<N≤0.85	0.25<R≤0.50	±5<P≤ ±10	7
Good	0.70<D ≤0.75	0.70<N≤0.75	0.50<R≤0.55	±10<P≤±12.5	6
	0.65<D ≤0.70	0.65<N≤0.70	0.55<R≤0.60	±12.5<P≤±15	5

Model Performance	R^2	NSE	RSR	PBIAS	Rating
Satisfactory	0.57<D ≤0.65	0.57<N≤0.65	0.60<R≤0.65	±15<P≤ ±20	4
	0.50<D ≤0.57	0.50<N≤0.57	0.65<R≤0.70	±20<P≤ ±255	3
Unsatisfactory	0.40<D ≤0.50	0.40<N≤0.50	0.70<R≤0.80	±25<P≤ ±35	2
Poor	D ≤0.40	N≤0.40	R>0.80	P≥ ±35	1

Source: Ewen, (2011); Gupta et al., (2009); Moriasi et al., (2007)

4.2.3 Projected future climate changes

The bias-corrected ensemble data were used to compute changes in the long-term average of precipitation, maximum temperature, and minimum temperature between the baseline period (1985–2014) and future scenarios (2026–2055). Mean values for each variable were calculated for the historical, and future periods. The differences were expressed as percentage changes for precipitation, to reflect relative changes, and as absolute changes (in °C) for temperatures, to indicate the magnitude of warming.

4.2.4 Climate change impacts on mean annual and seasonal streamflow

Daily streamflow data obtained from model runs of three climate models (EC-Earth3, MPI-ESM1-2-LR, and NESM3) under historical conditions and two emission scenarios (SSP245 and SSP585) were accessed to analyze how climate change impacts streamflow and its temporal patterns. The average annual streamflow was calculated for both the past and future periods, with percentage change used to indicate the extent of streamflow increase or decrease in the future. Monthly mean streamflows were computed for historical and future scenarios to quantify seasonal changes. The variations in streamflow across seasons (pre-monsoon, monsoon, post-monsoon, and winter) were also analyzed.

4.3 Characterization of Hydrological Extremes

4.3.1 Computation of hydrological extremes

Changes in flow extremes were assessed by comparing high and low flow percentiles between historical and future scenarios. High flows were represented by Q_{90} (90^{th} percentile flow) and Q_{95} (95^{th} percentile flow), which correspond to extreme and moderately high flow conditions. Low flows were analyzed using Q_5

(5^{th} percentile flow) and Q_{10} (10^{th} percentile flow), representing conditions of low water availability

4.3.2 Climate change impacts on hydrological extremes.

The percentage changes in these flow metrics from the historical scenario to SSP245 and SSP585 were evaluated to assess future hydrological shifts. For this analysis, 30 years from 1985 to 2014 was selected as the historical baseline, while the future projections were assessed for the period 2026 to 2055, ensuring consistency in the period for comparison.

5 RESULTS AND DISCUSSION

This chapter presents the findings that were achieved by creating and applying the multi-basin Bidirectional Long Short-Term Memory (BiLSTM) hydrological model framework. It begins with an examination of the predictive ability and generalizability of the model across the nine study watersheds. It continues to examine the performance of the climate data bias correction methods utilized. This is followed by the characterization of the expected changes in the most significant climate variables (temperature and precipitation) under future scenarios. Then the concluding section presents, analyzes, and discusses the principal results on the simulated impacts of these climate change scenarios on hydrological extremes (low flows and high flows).

5.1 Multi-Basin BiLSTM Model Performance

The performance of the multi-basin BiLSTM hydrological model was thoroughly examined for nine watersheds employing statistical measures: Nash–Sutcliffe Efficiency (NSE), Kling–Gupta Efficiency (KGE), and Root Mean Square Error (RMSE), for varied training and testing periods. Figure 5-1 presents a boxplot of the general performance of the BiLSTM model across all baselines concerning three metrics: NSE, KGE, and RMSE. The median of the values of NSE during training and testing is between 0.6 and 0.7, and for the testing period, there is a broader range. Similarly, for KGE, the model shows a median of 0.6 to 0.7, with the test phase showing a slightly reduced spread. The RMSE distribution is the same in both training and testing, with the peak values being just below 300 m^3/s in either case.

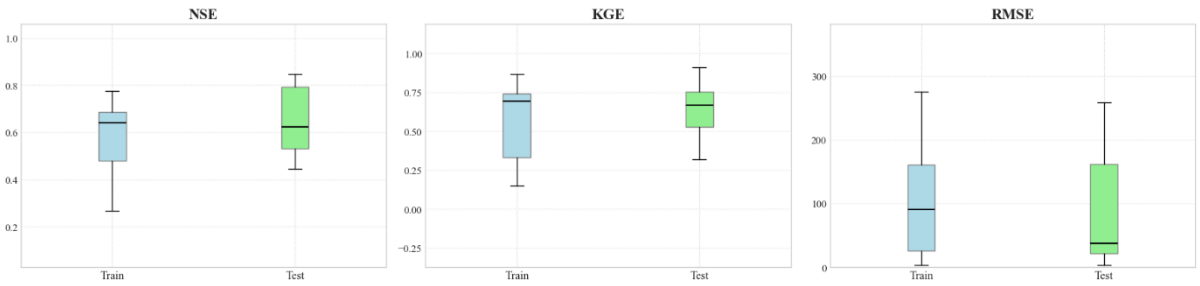

Figure 5-1 Boxplot of performance values for the BiLSTM model across watersheds

Table 5-1 summarizes the training and testing performance of the hydrological model across nine watersheds. The model performed well for the smaller watersheds (Melamchi and Likhu), except for Khimtikhola during training, maintaining strong accuracy levels with NSE values of 0.78 and 0.69, and KGE

values of 0.87 and 0.69, respectively. Among all the watersheds, Melamchi recorded the lowest RMSE (3.28 m^3/s), followed by Likhu (25.35 m^3/s), underscoring the model's capacity to capture streamflow dynamics in smaller catchments. Arun and Balephi also showed relatively good agreement between observed and simulated flows, with NSE values of 0.76 and 0.64 and KGE values of 0.73 and 0.74, respectively. RMSE values for these watersheds were 275.19 m^3/s and 16.31 m^3/s. The best performance during testing was seen in Khimtikhola and Bhotekoshi, with NSE values of 0.85 and 0.82 and KGE values of 0.91 and 0.89, respectively. The Arun also demonstrated strong performance, with NSE of 0.79 and KGE of 0.75, highlighting its reliable predictive ability.

On the other hand, Tamur and Tamakoshi watersheds displayed relatively weaker model performance. Tamur had a test NSE of 0.44 and KGE of 0.32, while Tamakoshi reported similar metrics (NSE- 0.53, KGE- 0.35). These watersheds also showed higher RMSE values of 166.34 m^3/s and 136.99 m^3/s, respectively. Despite these challenges, the model's test performance across most of the cases remained within reasonable bounds, demonstrating its robustness and applicability across a range of watersheds sizes and hydrological conditions. Overall, the multi-watersheds model was very good in various catchments under training and testing scenarios. The reproduction of values such as NSE and KGE across hydrologically and spatially varying basins confirms the strength of the BiLSTM modeling framework.

Table 5-1 Training and testing metrics for the BiLSTM model

	Training			**Testing**		
Watershed	**NSE**	**KGE**	**RMSE**	**NSE**	**KGE**	**RMSE**
Arun	0.76	0.73	275.19	0.79	0.75	258.61
Balephi	0.64	0.74	16.31	0.62	0.57	21.68
Bhotekoshi	0.48	0.48	90.60	0.82	0.89	31.30
Dudhakoshi	0.65	0.74	160.90	0.67	0.71	161.96
Khimtikhola	0.27	0.23	48.56	0.85	0.91	9.40
Likhu	0.69	0.69	25.35	0.50	0.53	37.52
Melamchi	0.78	0.87	3.28	0.58	0.67	3.74
Tamakoshi	0.51	0.33	134.73	0.53	0.35	136.99
Tamur	0.27	0.15	261.46	0.44	0.32	166.34

Details on the performance of a hydrological model simulating river discharge, compared against observed flow data during training and testing across nine watersheds, are graphically represented in Figure 5-2, Figure 5-3, Figure 5-4, Figure 5-5, Figure 5-6, Figure 5-7, Figure 5-8, Figure 5-9 and Figure 5-10 respectively. A visual assessment of time series plots and Flow Duration Curves

comparing observed and simulated discharge indicates that the model consistently underestimates peak flows, particularly high flood events. This underestimation can be attributed in part to the inherent characteristics of the LSTM model, as discussed in Section 2.3.3, which makes it particularly effective for predicting low-flow conditions but less reliable in capturing higher extremes present in training datasets. Another contributing factor is the limited availability of high-quality training sets and the number of catchments included in the dataset for hydrological modeling. Despite the limitation regarding peak flows, the results demonstrate the model's utility as a predictive tool, especially in data-scarce Himalayan areas where it is not always feasible to develop basin-scale models However, applying this model for future projections using CMIP6 GCM datasets restricts the incorporation of other input variables, as those would also require future projections.

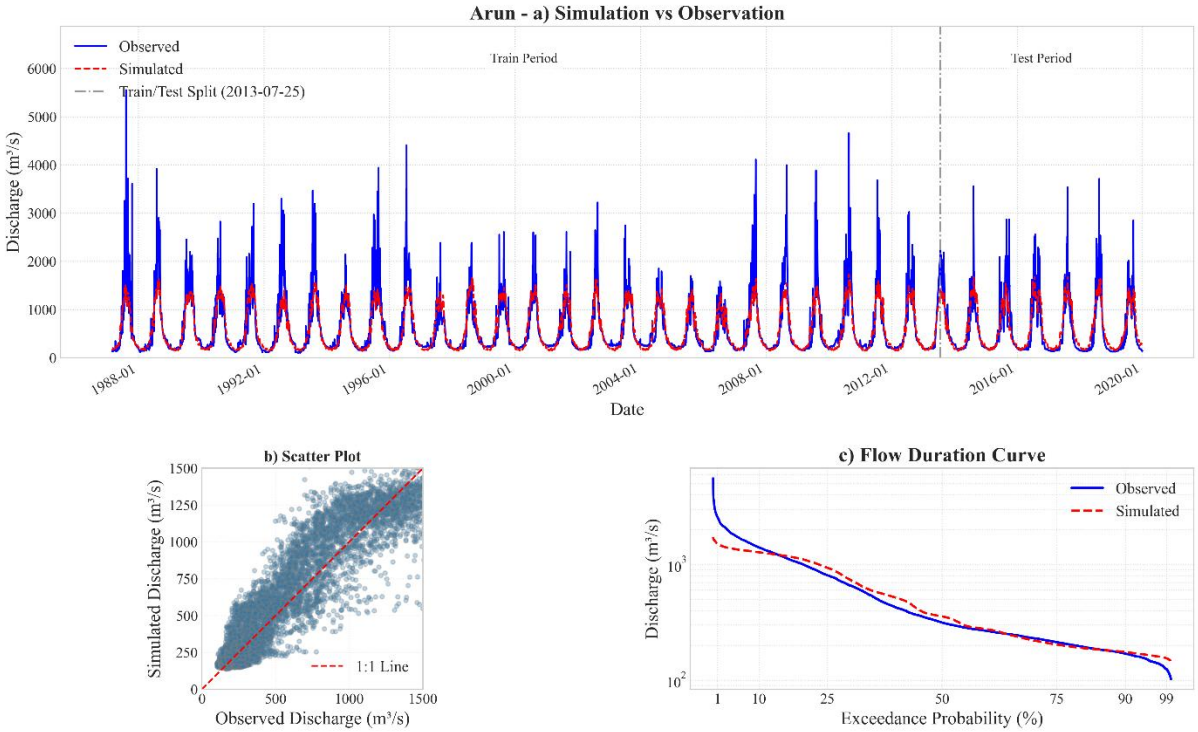

Figure 5-2 Model performance at Simle (Arun River)

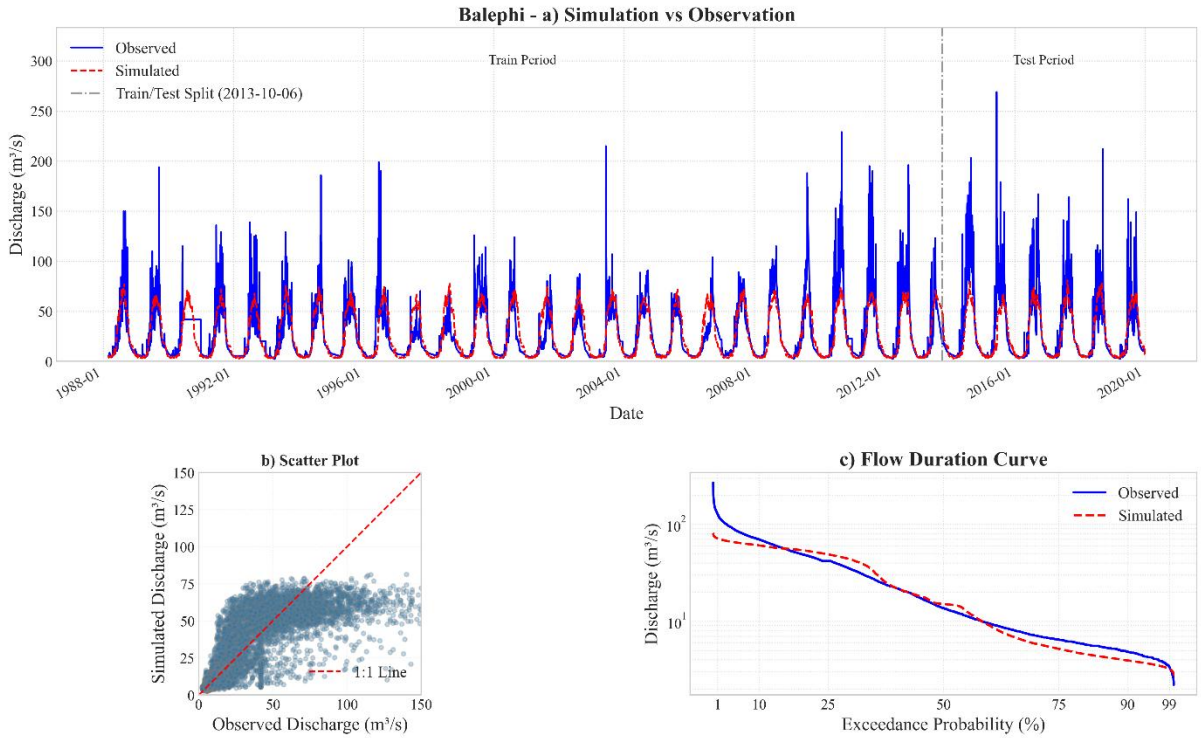

Figure 5-3 Model performance at Jalbire (Balephi River)

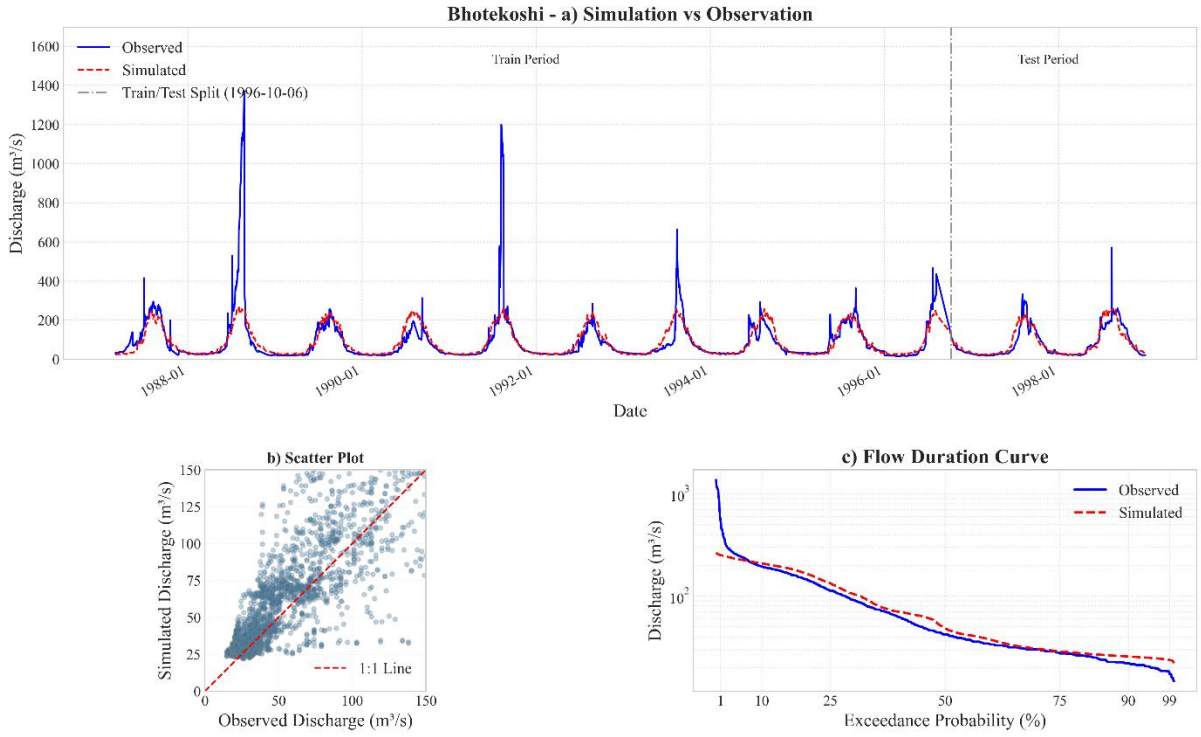

Figure 5-4 Model performance at Barbise (Bhotekoshi River)

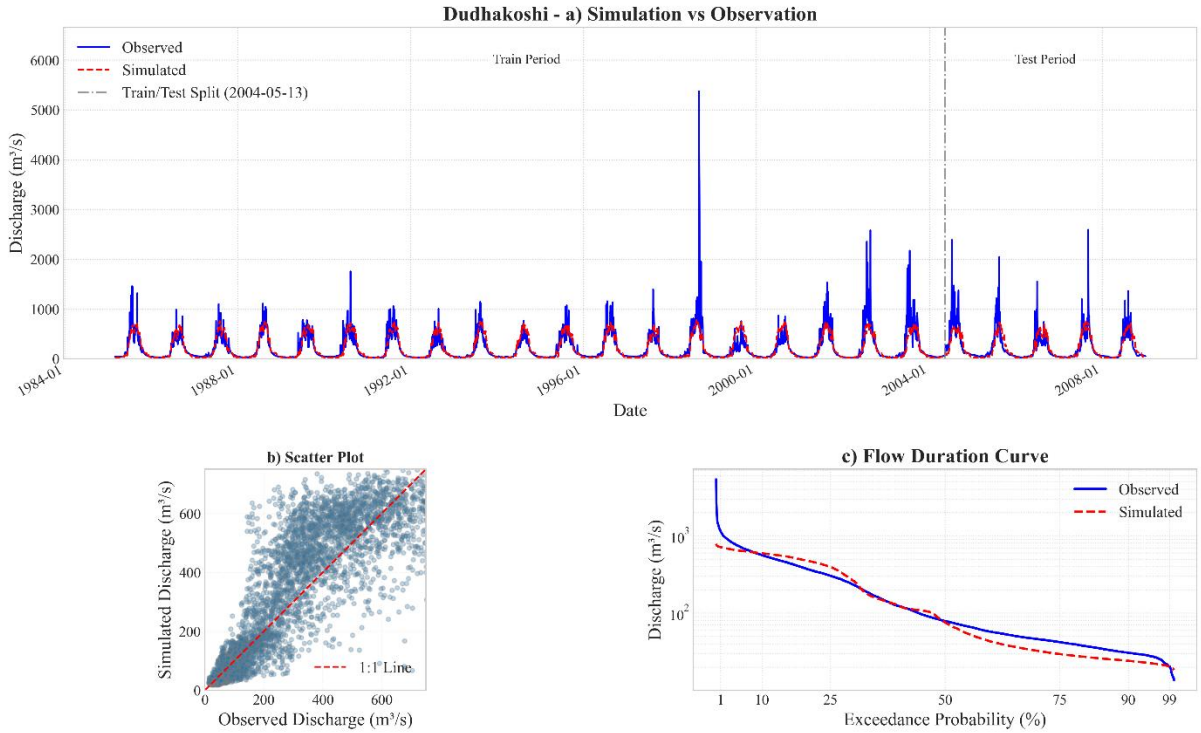

Figure 5-5 Model performance at Rabuwabazar (Dudhakosi River)

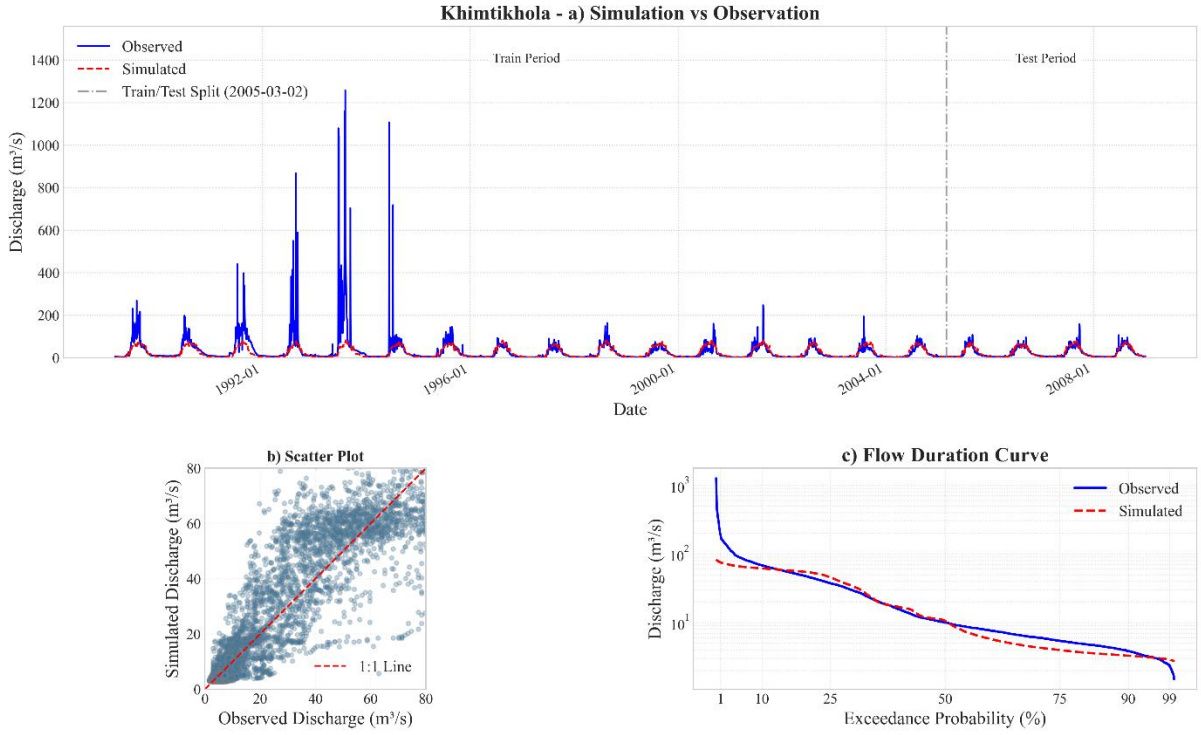

Figure 5-6 Model performance at Rasnalu (Khimtikhola)

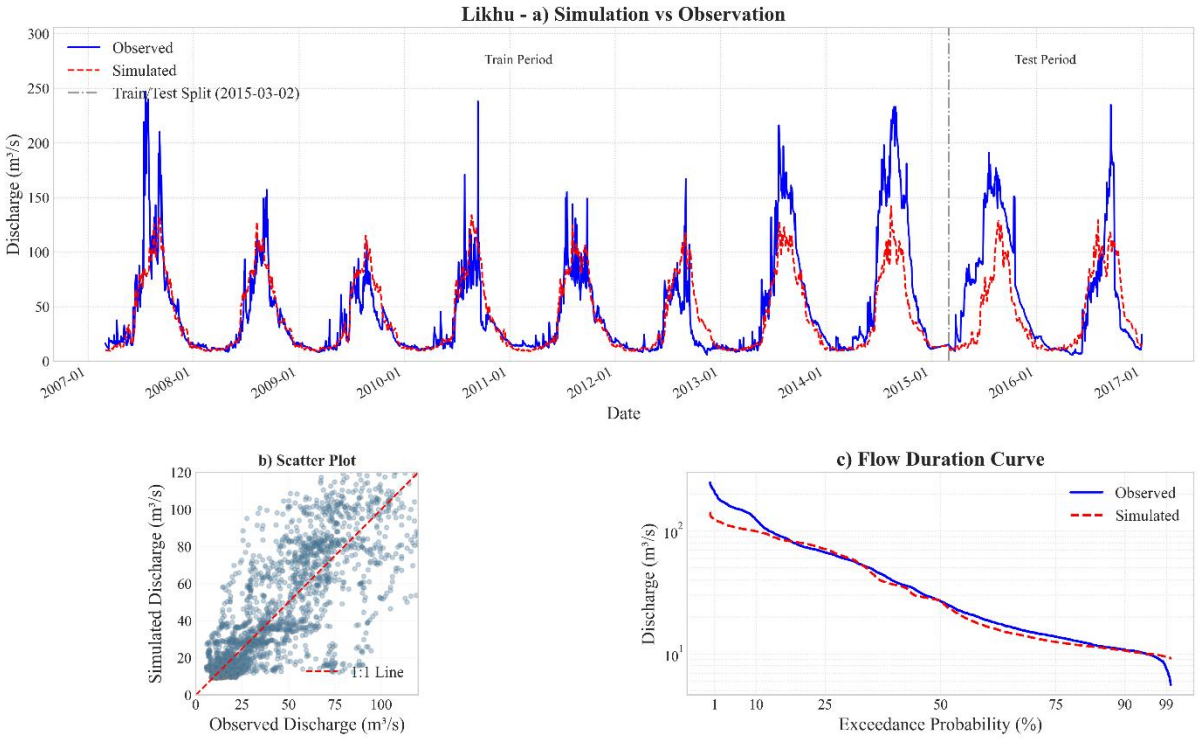

Figure 5-7 Model performance at Sangutar (Likhu River)

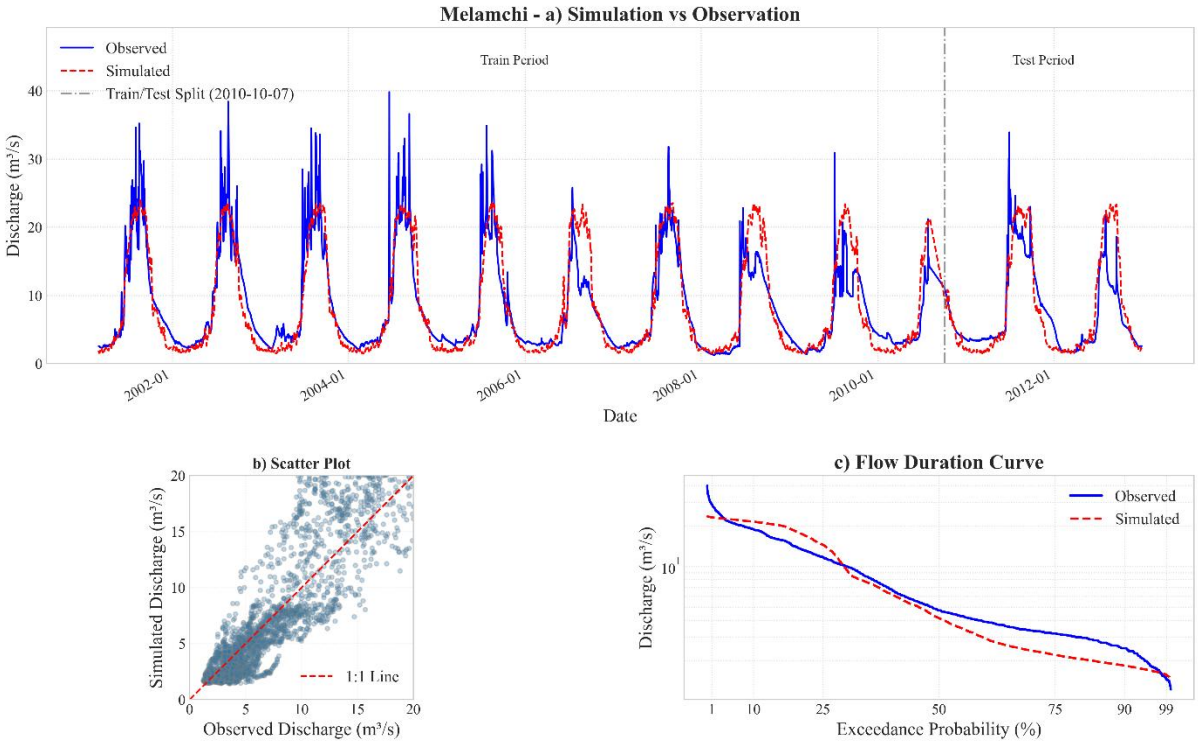

Figure 5-8 Model performance at Helambhu (Melamchi River)

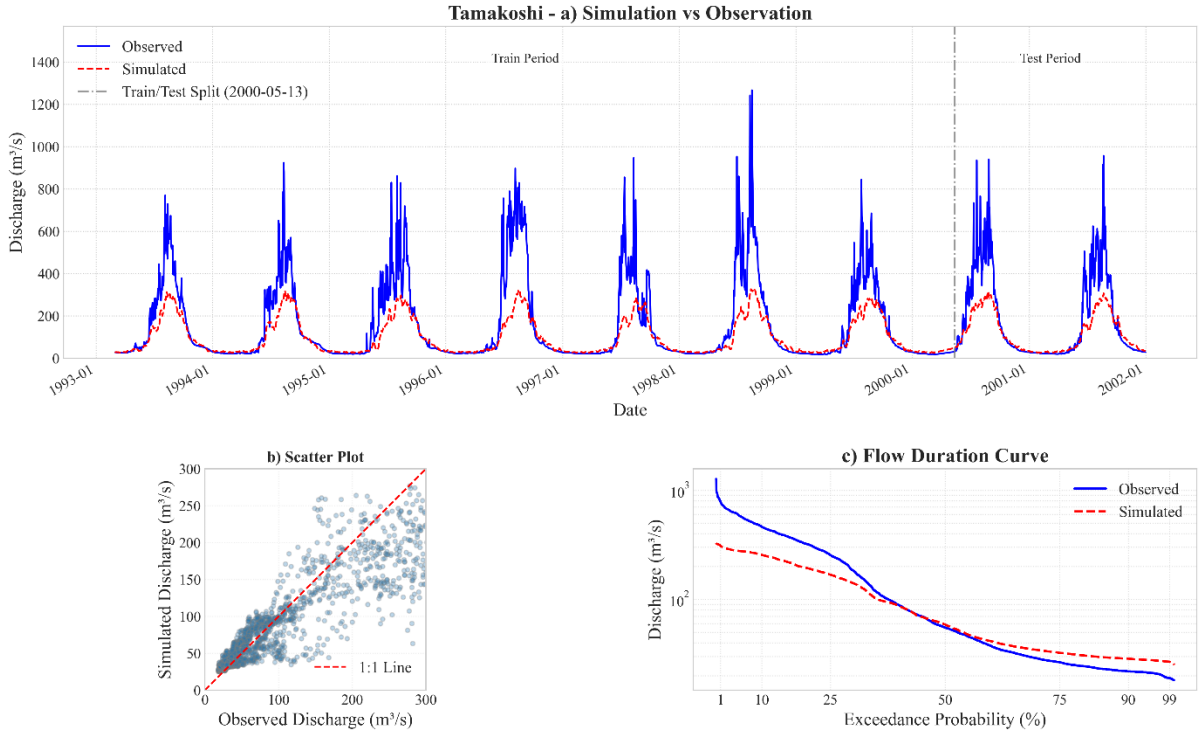

Figure 5-9 Model performance at Busti (Tamakoshi River)

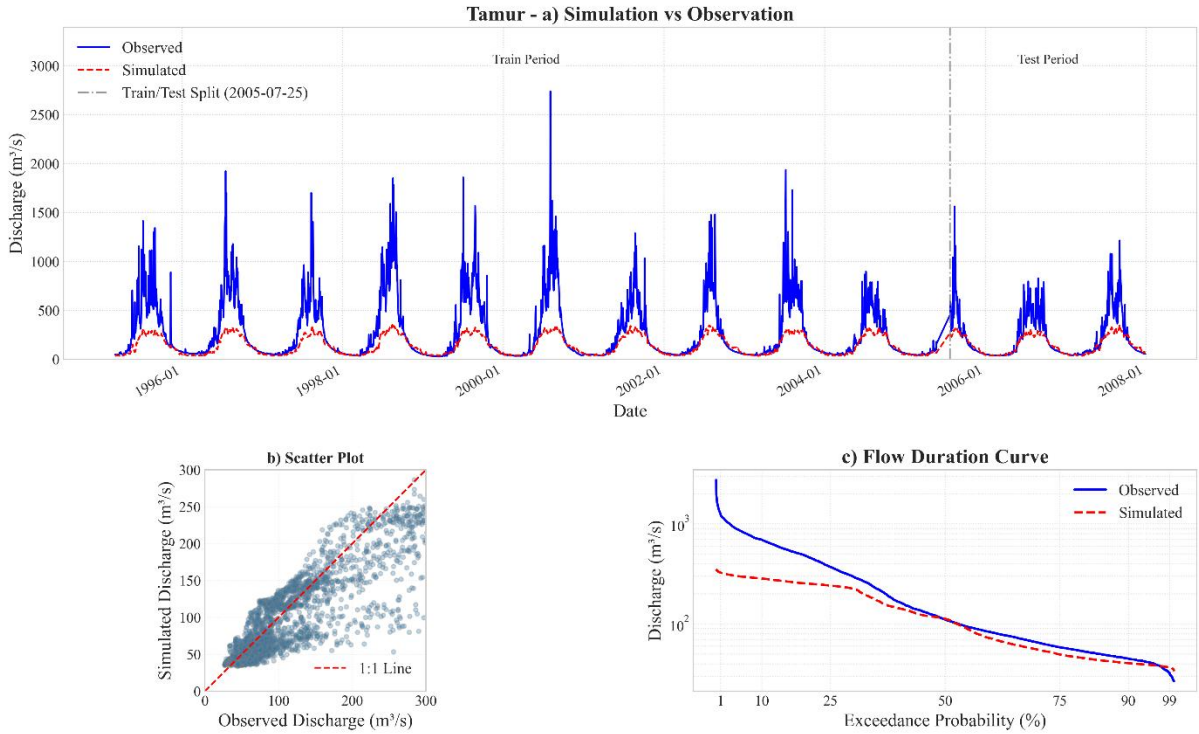

Figure 5-10 Model performance at Majhitar (Tamur River)

5.2 Future Climate Projection

5.2.1 Evaluation of climate data bias correction

The Equidistant Quantile Mapping (EQM) bias correction performance significantly varied across variables and watersheds. The evaluation of the EQM method was quantified using various performance metrics, including R^2, NSE, PBIAS, and RSR, as shown in Table 4-7. The performances of the bias correction method for watersheds for precipitation, maximum temperature and minimum temperature are shown in Figure 5-11, Figure 5-12 and Figure 5-13 respectively. Minimum temperature correction consistently produced a good performance with an average rating of 6.75 to 7.25, signifying excellent agreement with actual values. Correction of maximum temperature was moderate with a rating of between 3.75 and 4.92, showing acceptable agreement. However, there was some difference, particularly in watersheds like Arun and Khimtikhola. In contrast, precipitation correction was done less effectively, averaging typically between 1.83 and 2.75 in all watersheds. This low-performance score for bias-correcting precipitation can be attributed to spatial variability and topographic complexity, which quantile mapping fails to address, as it only adjusts the distribution statistically (Yoshikane & Yoshimura, 2022).

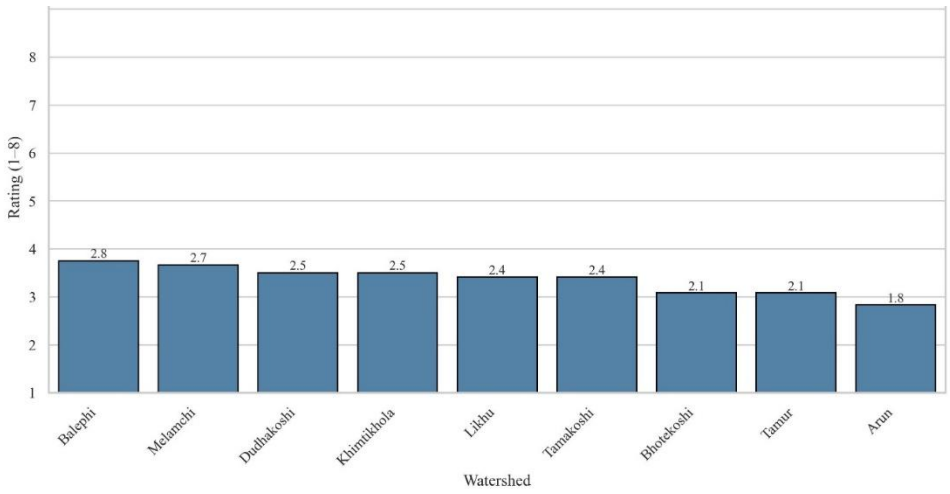

Figure 5-11 Bias correction performance for precipitation

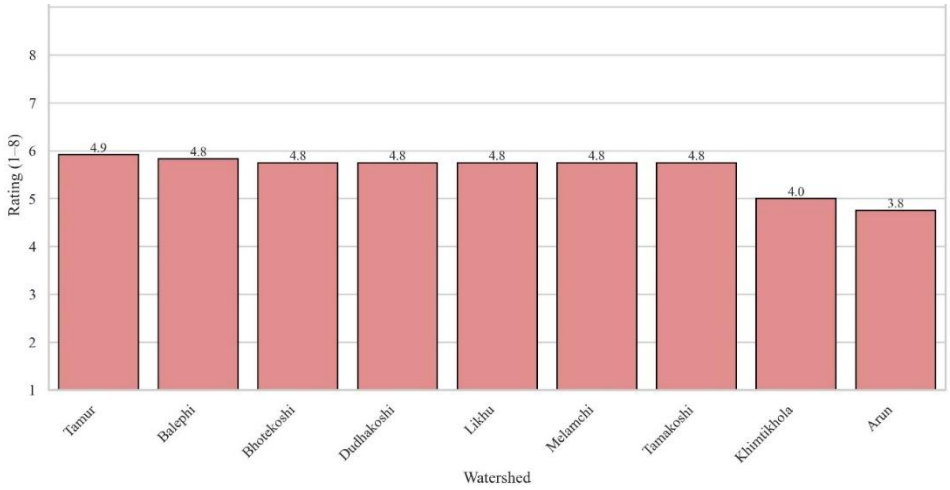

Figure 5-12 Bias correction performance for maximum temperature

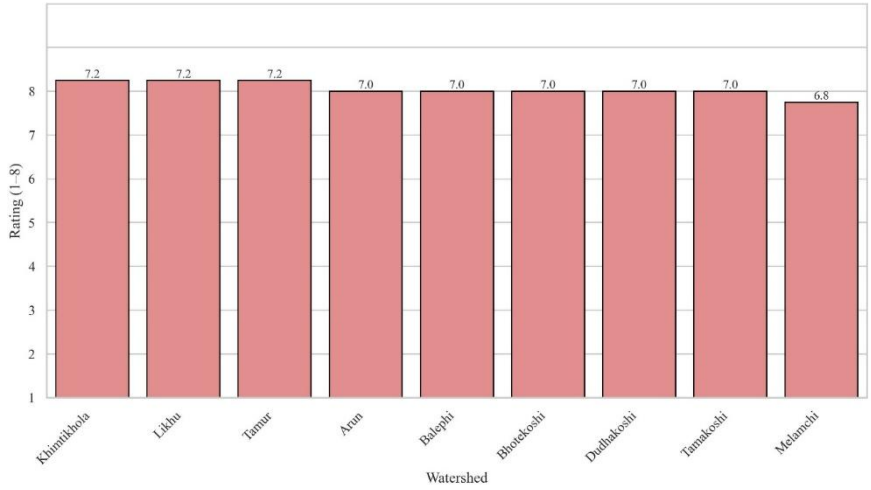

Figure 5-13 Bias correction performance for minimum temperature

5.2.2 Projected future climate changes

Future projections of precipitation, maximum temperature, and minimum temperature over various Himalayan River basins from three CMIP6 models (MPI-ESM1-2-LR, EC-Earth3, and NESM3) under two emission scenarios: SSP245 and SSP585 were compared in this analysis. Daily outputs from these models were analyzed for historical (1985–2014) and future (2026–2055) periods. Relative change between past and future periods was computed for each variable, model, and scenario. Projected changes for precipitation, maximum temperature and minimum temperature are spatially represented across watersheds in Figure 5-14, Figure 5-15, Figure 5-16, Figure 5-17, Figure 5-18 and Figure 5-19 respectively.

For precipitation, MPI-ESM1-2-LR consistently projects a drying trend, with reductions ranging from -3.2% to -9.7%, while EC-Earth3 projects overall wetting between 1.7% and 11.1%. NESM3 shows a more neutral outlook with minor changes close to zero (ranging from -2.7% to 1.4%). This difference is even more apparent under the SSP585 scenario. MPI-ESM1-2-LR models are more intensive drying, reaching -13.0% and NESM3 also shows a projection of drying (-0.7% to -7.0%), whereas EC-Earth3 intensifies its wetting projection up to 16.1%.

Similarly, maximum temperature indicates a warming trend in three models. Under, SSP245, MPI-ESM1-2-LR projects the lowest warming increments (0.67°C to 0.82°C), while EC-Earth3 and NESM3 simulate larger warming, ranging from 0.97°C to 1.46°C. This warming is more pronounced under SSP585, with projections by MPI-ESM1-2-LR up to 0.91°C, EC-Earth3 between 1.12°C to 1.68°C, and NESM3 between 1.43°C to 1.71°C. Despite differences in magnitude, all models suggest warming in the future. For minimum temperature, all the models also project strong warming. In SSP245, MPI-ESM1-2-LR shows increases of 0.60°C to 1.01°C, EC-Earth3 from 0.85°C to 1.30°C, and NESM3 the highest range at 1.12°C to 2.08°C. The trend is more enhanced in SSP585, where MPI-ESM1-2-LR reaches up to 1.20°C, EC-Earth3 up to 1.72°C, and NESM3 again leads at 2.41°C. The overall projection shows that precipitation rises in most watersheds, while mean temperatures continue to rise at a linear rate. All these findings are consistent with findings from a previous study by Pradhan et al. (2023) for the same region.

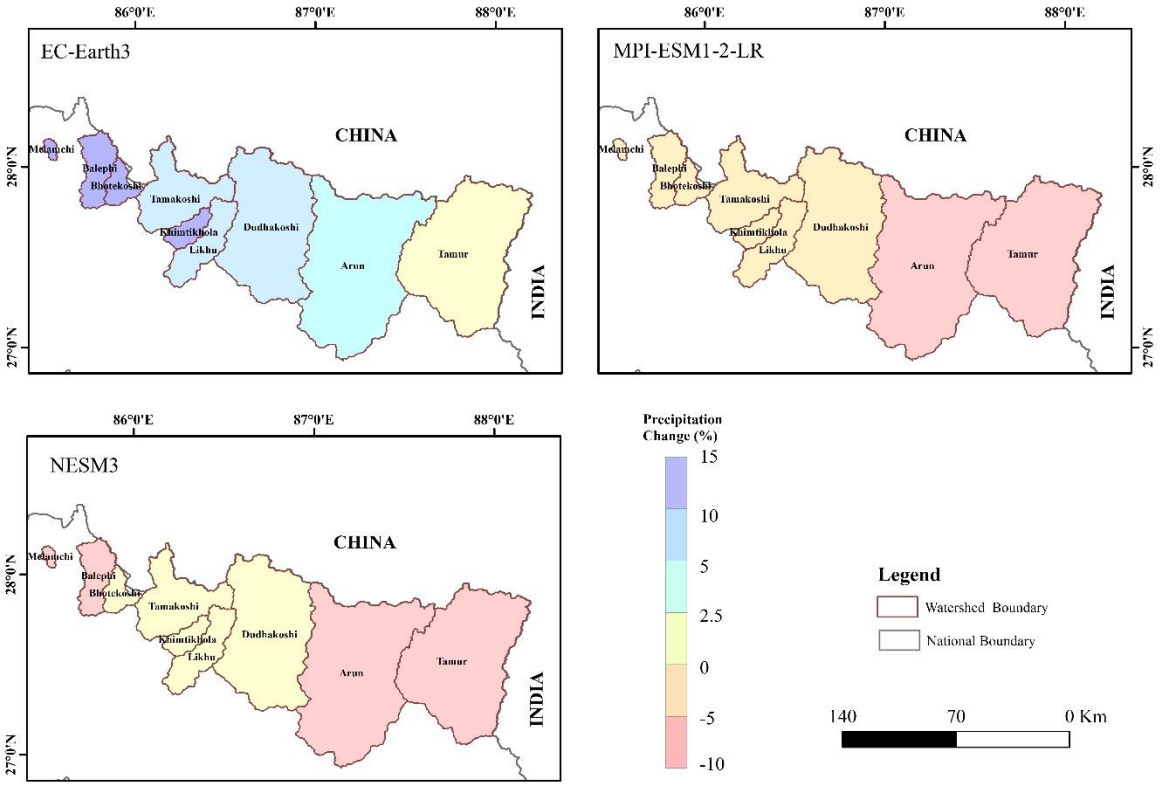

Figure 5-14 Projected change in precipitation under SSP245

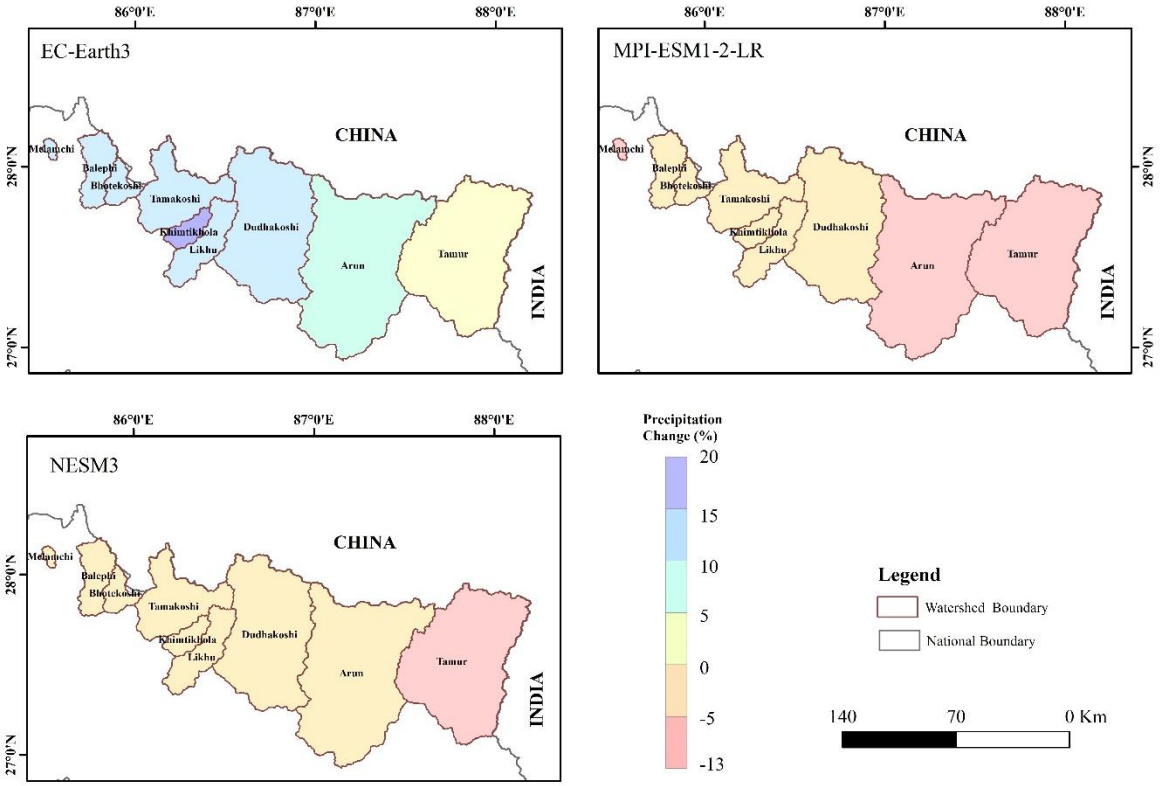

Figure 5-15 Projected change in precipitation under SSP585

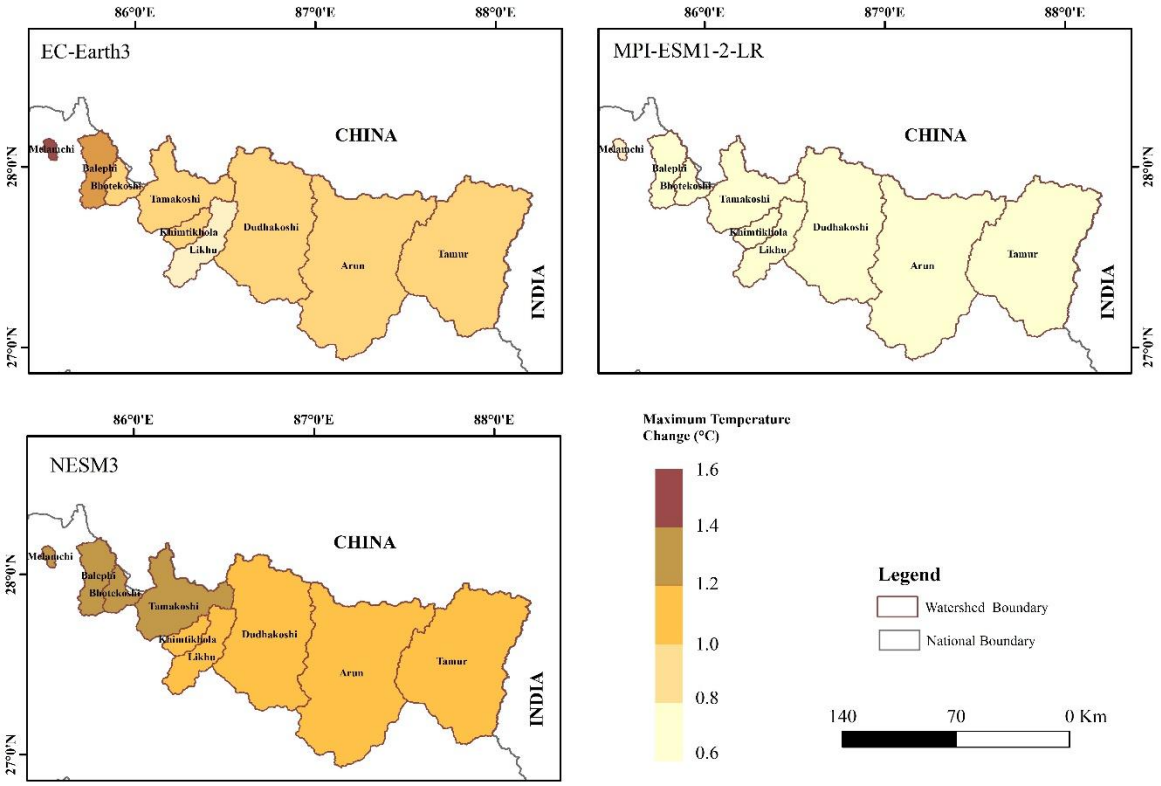

Figure 5-16 Projected change in maximum temperature under SSP245

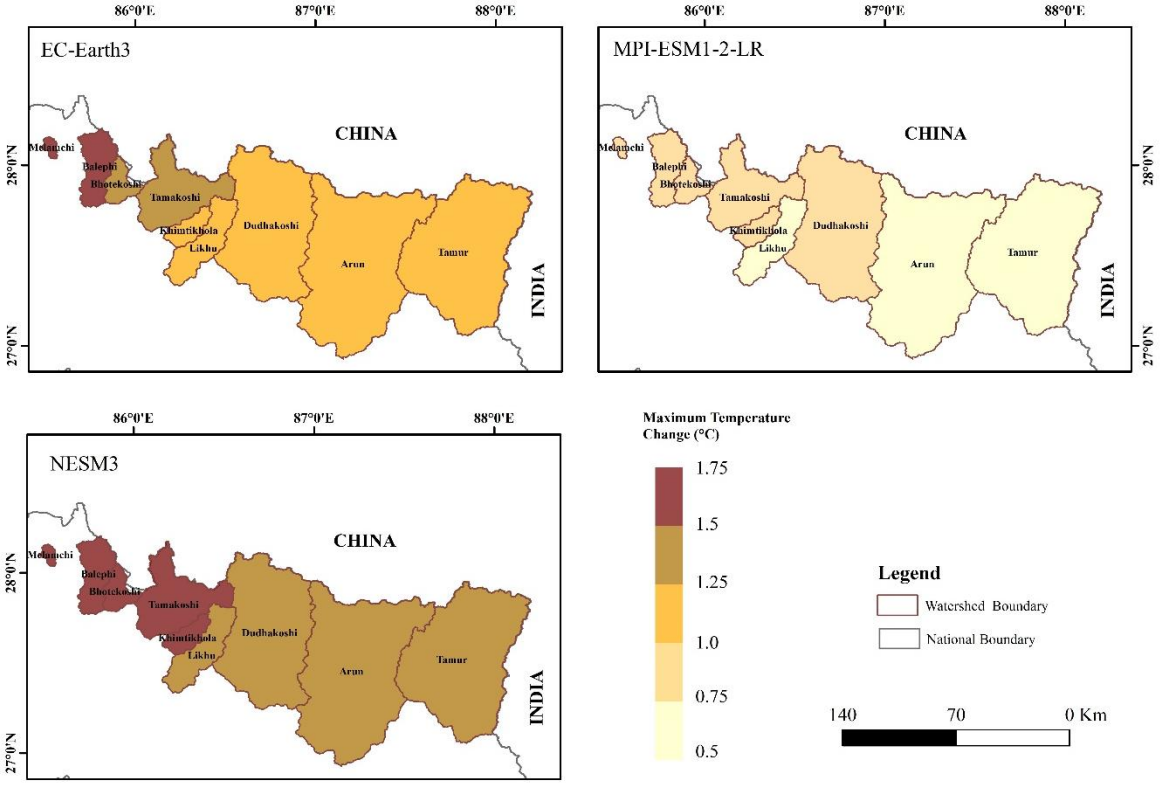

Figure 5-17 Projected change in maximum temperature under SSP585

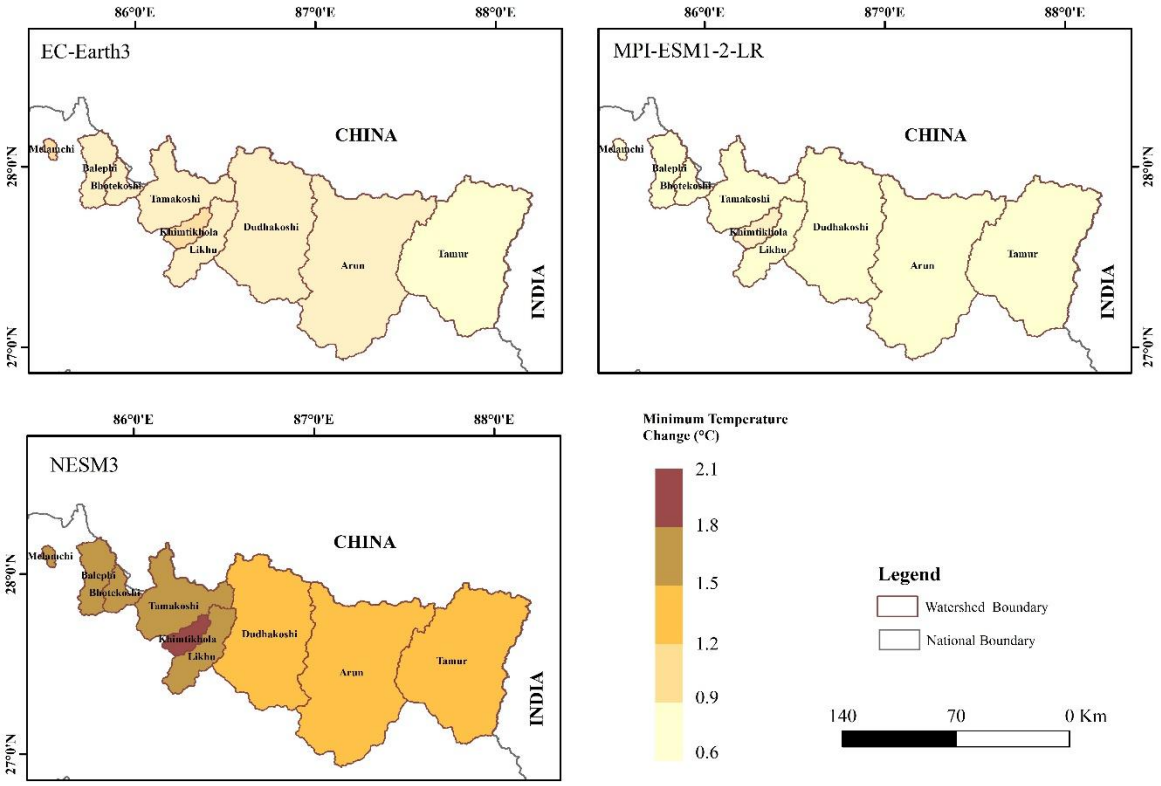

Figure 5-18 Projected change in minimum temperature under SSP245

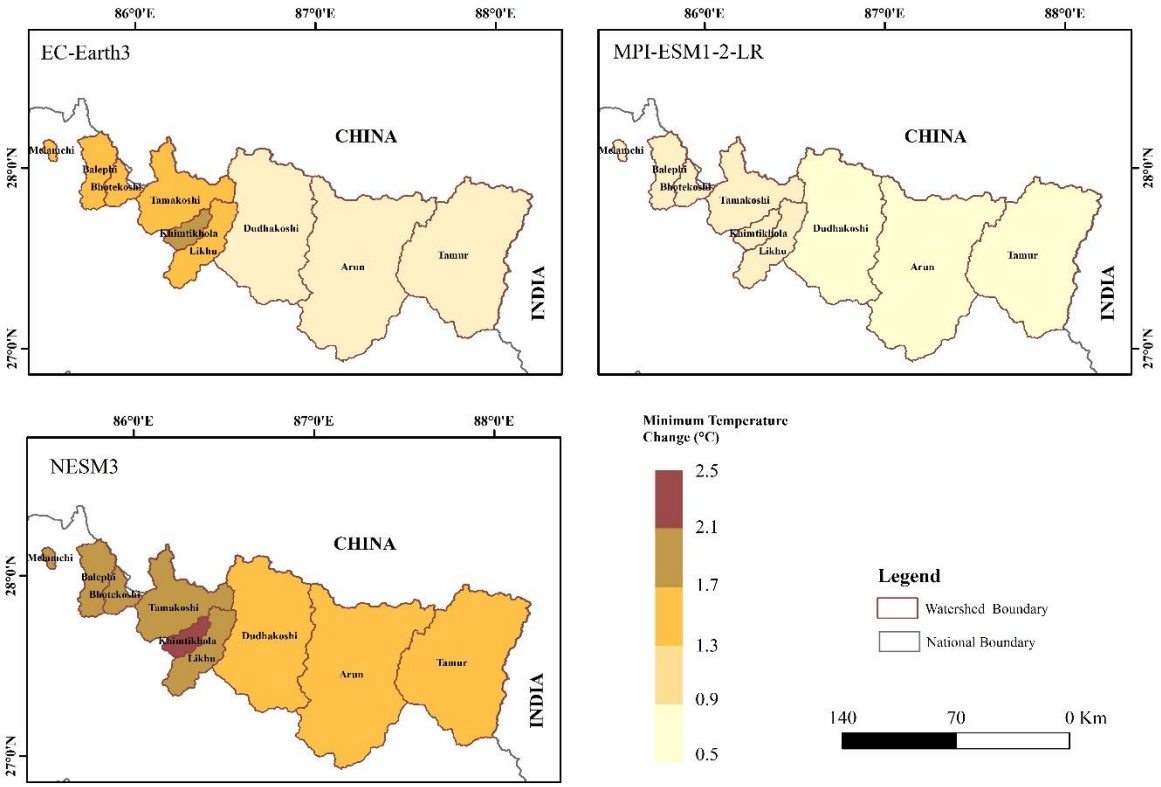

Figure 5-19 Projected change in minimum temperature under SSP585

5.2.3 Changes in long-term mean annual streamflow

The analysis of future changes in streamflow reveals an increase in annual hydrological regime variation across nearly all watersheds under both emission scenarios, with a substantial increase particularly in SSP585 (27.6% under SSP245 and 31.4% under SSP585). When considering mean streamflow changes for three CMIP6 global climate models (EC-Earth3, MPI-ESM1-2-LR, and NESM3), Dudhkoshi shows the highest increase. Conversely, Tamur consistently exhibits the least changes, with a 4.9% increase under SSP245 and a 6% increase under SSP585. High-performing watersheds, based on the results from Table 5-1, show moderate to high annual increases (up to 31.4%), indicating greater confidence in these projections. However, weaker predictive performance watersheds (e.g., Likhu, Tamakoshi, Tamur) display moderate agreement in the direction of change, but with greater uncertainty in precise magnitudes due to poorer model fit.

5.2.4 Changes in seasonal streamflow patterns

Like the Long-Term Mean Annual Streamflow, interseasonal variation is also more pronounced, collectively indicating variations in water supply over a year. The results reflect a potential increase in rainfall in the future across nearly all watersheds. During the monsoon season (June-September), simulations indicate that most watersheds are expected to see the highest increases, with mean values ranging from 6.4% in Tamur to more than 33% in Dudhkoshi under SSP245, and slightly higher increases under SSP585 (7.3% in Tamur, 28% in Likhu, and 36.6% in Dudhkoshi). Pre-monsoon (March-May) shows significant increases in certain watersheds, such as Balephi and Likhu. Post-monsoon variations are moderate (4% to 28%), while winter (December-February) exhibits minimal change, generally less than 10%, indicating more stable baseflow conditions. The changes in average annual flow and the increasing trend across different seasons in this study region align with a study by Kaini et al. (2021). Both annual and seasonal variations across watersheds for the two scenarios (SSP245 and SSP585) are illustrated in Figure 5-20 and Figure 5-21, respectively.

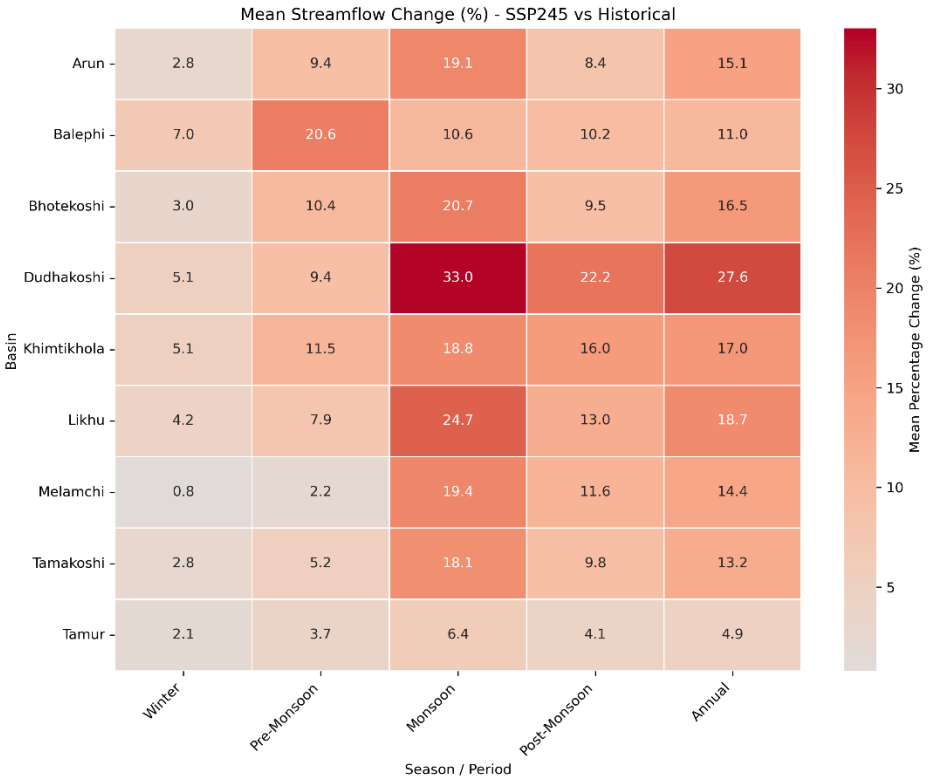

Figure 5-20 Mean projected streamflow change (%) under the SSP245 scenario.

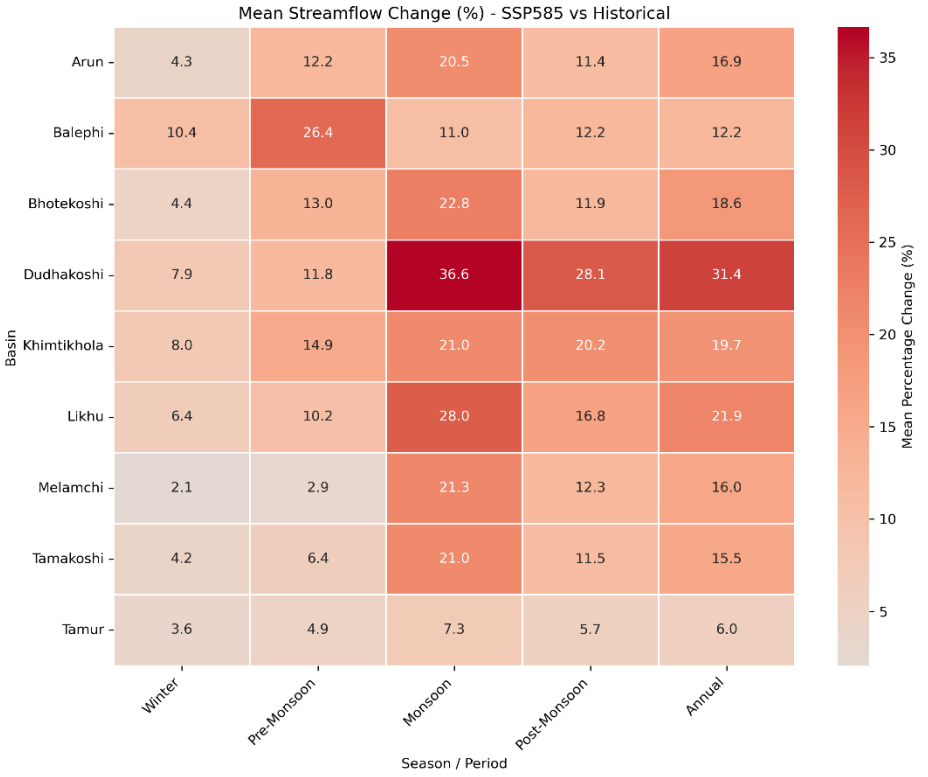

Figure 5-21 Mean projected streamflow change (%) under the SSP585 scenario.

5.3 Projected Climate Change Impacts on Hydrological Extremes

Figure 5-22, Figure 5-23 and Figure 5-24 show simulated hydrological changes in extremes (Q_5, Q_{10}, Q_{90} & Q_{95}) from three global climate models, EC-Earth3, MPI-ESM1-2-LR, and NESM3, evaluated against SSP245 and SSP585 scenarios. All three models capture similar trends but with some distinct differences. The simulations show that the low flow stages, as denoted by Q_5 and Q_{10} percentiles, are simulated to experience modest positive changes between 0% and 8% under the two scenarios for EC-Earth3 (Figure 5-22). The slight increase in low flow conditions reflects an improvement in dryness conditions. However, high flow condition estimates, defined by Q_{90} and Q_{95}, indicate much greater increases, to an approximate 30% under SSP585. Furthermore, the climate models also indicate a large scale of high flow variability, particularly under SSP585 scenarios. The MPI-ESM1-2-LR model shows comparatively lower projections for low and high flows, and the increases in low flows (Q_5 and Q_{10}) tend to be between 0% and 2.5%. Similarly, for high flows (Q_{90} and Q_{95}), MPI-ESM1-2-LR also shows significant increases, albeit relatively lower than those indicated by EC-Earth3 (6% to 23%) as shown in Figure 5-23. The third, NESM3, mirrors closely that of EC-Earth3 in forecasting changes over a wide range. Low flow increases typically vary between 1% and 8%, while the range for high flows is slightly broader for Q_{95} (2% to 30%) than for Q_{90} (5% to 25%) as illustrated in Figure 5-24.

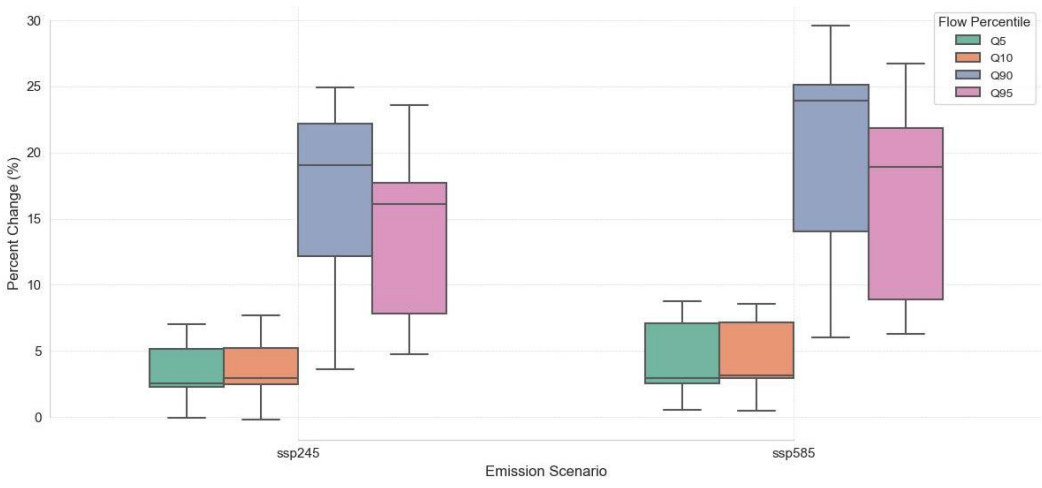

Figure 5-22 Projected changes in hydrological extremes under EC-Earth3

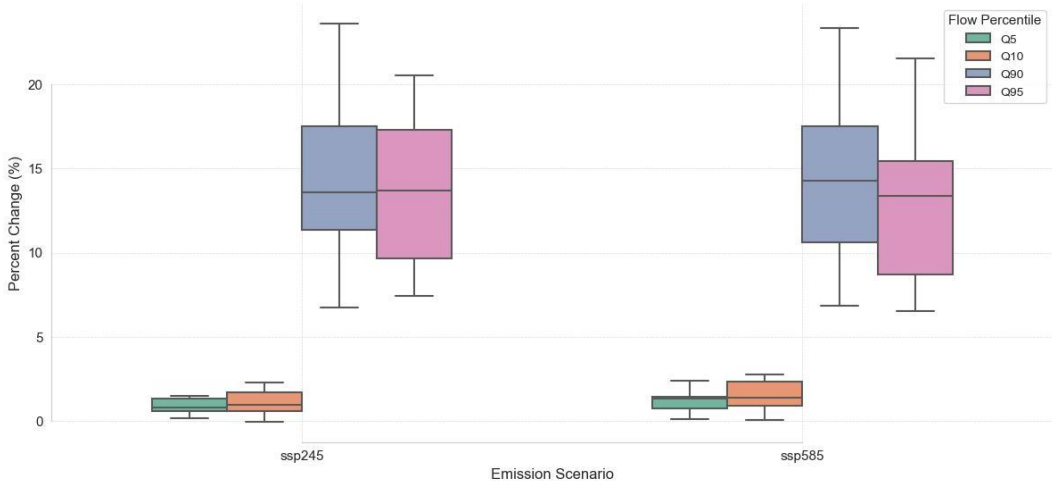

Figure 5-23 Projected changes in hydrological extremes under MPI-ESM1-2-LR

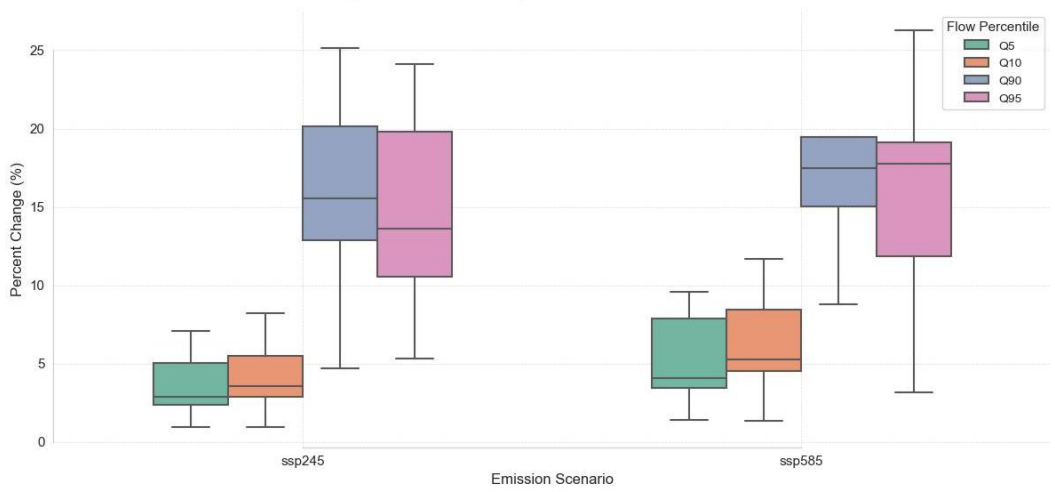

Figure 5-24 Projected changes in hydrological extremes under NESM3

The modest increase in low flows across the three models in both emission scenarios suggests that the severity of drought might not diminish much and even improve slightly. The higher Q_{90} and Q_{95} values in the high-emission scenario suggest the likelihood of more frequent and severe floods in the future. Additionally, the larger range in high flow projections, particularly under SSP585, highlights the large uncertainty involved in predicting extreme flood magnitudes. To synthesize these impacts across watersheds, Figure 5-25 and Figure 5-26 depict boxplots of percentage increases in low flows (Q_5, Q_{10}) and high flows (Q_{90}, Q_{95}) aggregated across all watersheds and GCM models for SSP245 and SSP585 scenarios relative to the historical reference (1985–2014). Dudhkoshi appears especially susceptible, with the largest percentage increase of around 23.32% in

SSP245 and 24.69% in SSP585. Bhotekoshi follows closely behind it, with an enormous increase in high flow values of 19.85% in SSP245 and 22.30% in SSP585, which show a large magnification of flood sizes. Similarly, Likhu shows dramatic increases in high flow percentiles, with an estimate of 19.13% for SSP245 and 21.63% for SSP585. Melamchi, Arun, and Tamakoshi have relatively moderate high-flow changes. Low flow changes are less than 10% in most cases, except in small watersheds such as Khimtikhola and Balephi, where values exceed 10% in certain circumstances.

Briefly, the outcomes indicate a twofold water management challenge of enhanced baseflow conditions that potentially support dry-season water supply, along with extremely enhanced flood magnitudes, especially under SSP585. The outcomes emphasize the urgent development of basin-level integrated water resource and disaster management plans capable of addressing improved water availability as well as augmented flood exposure in the future climatic scenario.

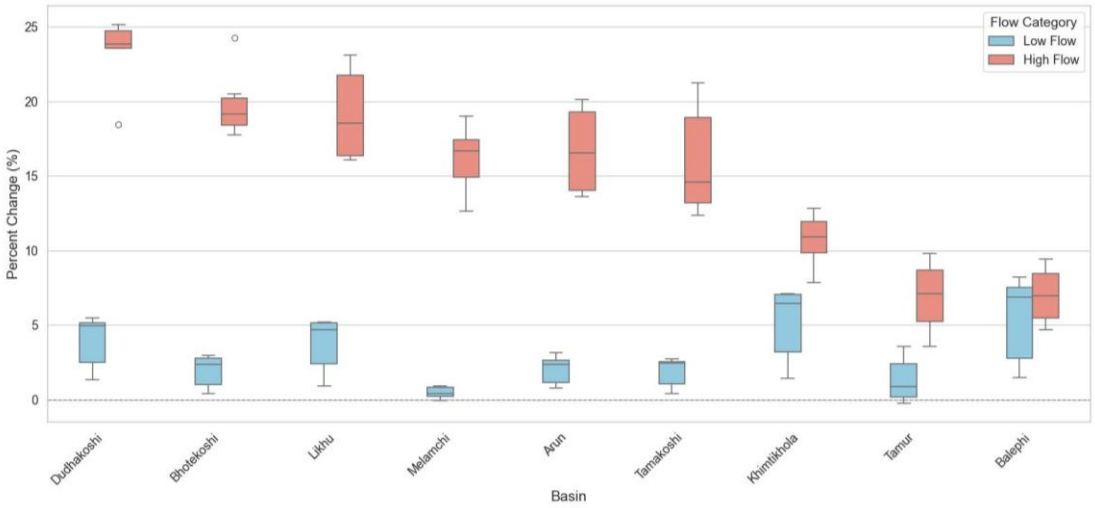

Figure 5-25 Boxplot summary of projected changes under SSP245 across the watersheds

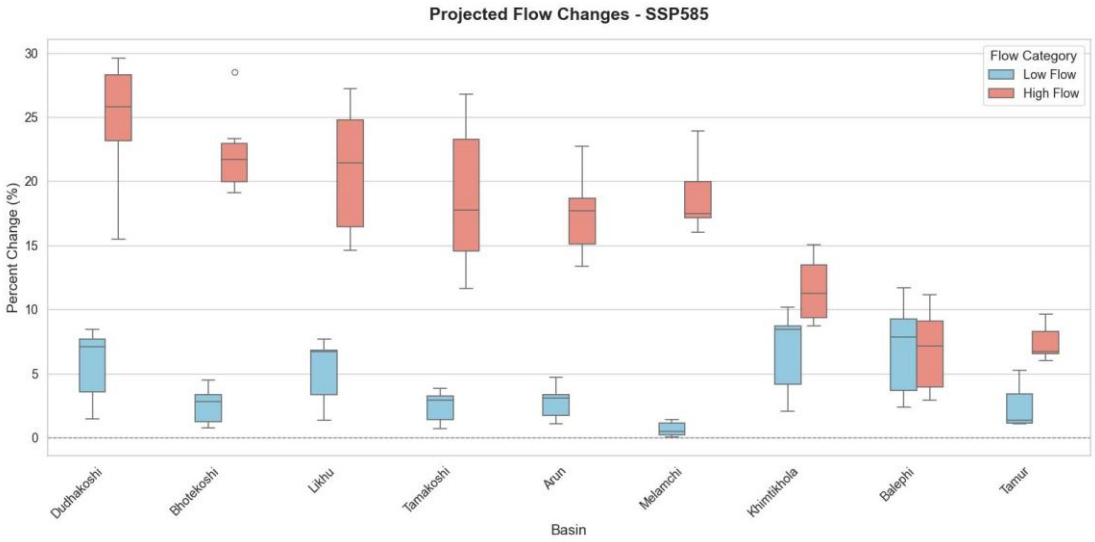

Figure 5-26 Boxplot summary of projected changes under SSP585 across the watersheds

6 CONCLUSIONS AND RECOMMENDATIONS

The key findings of the research on the use of a multi-basin BiLSTM model for hydrological modeling and climate change impact assessment in the Himalayan river basins are synthesized in this chapter. Implications for water management and further research are drawn from these findings.

6.1 Conclusions

The conclusions are summarized in the following points:

- The multi-basin BiLSTM was developed using diverse dynamic meteorological forcing and watershed attributes to address heterogeneity across watersheds. It demonstrated satisfactory performance in simulating daily streamflow for most of the nine heterogeneous Himalayan watersheds, achieving NSE > 0.6 and KGE > 0.6 on test sets, indicating its ability to predict unseen data effectively.
- Daily streamflow simulations for the period 2026–2055 using the validated BiLSTM model driven by CMIP6 climate projections under SSP245 and SSP585 scenarios reveal a clear climate change signal. The analysis reveals a consistent pattern of increased mean annual streamflow across most watersheds and scenarios, with median rises ranging from approximately 5% to 34%. Significant increases are anticipated during the monsoon and pre-monsoon seasons.
- The BiLSTM simulations, driven by future climate scenarios, consistently projected a divergence in hydrological extremes when historical and future periods are compared using flow percentiles. Low flow percentiles (Q_5, Q_{10}) showed modest positive changes (typically <10%), while high flow percentiles (Q_{90}, Q_{95}) indicated substantial intensification (increases up to 30% or more under SSP585), suggesting increased flood risks.

6.2 Recommendations

The conclusions of this thesis, lead to the following specific recommendations:

I. For further research:

- The integration of explicit snow and glacier melt process representations within the LSTM framework can be investigated to possibly improve simulations in Himalayan basins, mitigating constraints in the representation of some physical processes.

- Explainable AI (XAI) techniques can be applied to explain the trained LSTM model for enhanced interpretability over its "black-box" nature.
- The development or application of high-resolution gridded meteorological datasets specifically appropriate for complex Himalayan topography can be conducted to achieve a potential model forcing accuracy improvement.
- The potential benefits of a hybrid modeling approach that integrates the LSTM network with elements of process-based hydrological models may be explored.

II. For policy and practice:

- Integrated water resource management strategies for the Koshi Basin may be developed and implemented to proactively plan for the dual challenge of significantly increased flood risk and simultaneously affected dry-season water availability in projected future climate conditions.
- Strengthening and developing the hydrometeorological network in the Koshi Basin, especially in mid- and high-elevation ranges, is recommended for improving data for modeling and forecasting.

REFERENCES

Adamowski, J., & Sun, K. (2010). Development of a coupled wavelet transform and neural network method for flow forecasting of non-perennial rivers in semi-arid watersheds. *Journal of Hydrology*, *390*(1), 85–91. https://doi.org/10.1016/j.jhydrol.2010.06.033

Alizadeh, B., Bafti, A. G., Kamangir, H., Zhang, Y., Wright, D. B., & Franz, K. J. (2021). A novel attention-based LSTM cell post-processor coupled with bayesian optimization for streamflow prediction. *Journal of Hydrology*, *601*, 126526.

Arsenault, R., Martel, J.-L., Brunet, F., Brissette, F., & Mai, J. (2023). Continuous streamflow prediction in ungauged basins: Long short-term memory neural networks clearly outperform traditional hydrological models. *Hydrology and Earth System Sciences*, *27*(1), 139–157. https://doi.org/10.5194/hess-27-139-2023

ASCE. (2000). Artificial Neural Networks in Hydrology. I: Preliminary Concepts. *Journal of* Hydrologic *Engineering*, *5*(2), 115–123. https://doi.org/10.1061/(ASCE)1084-0699(2000)5:2(115)

Ayzel, G., Kurochkina, L., Kazakov, E., & Zhuravlev, S. (2020). Streamflow prediction in ungauged basins: Benchmarking the efficiency of deep learning. *E3S Web of Conferences*, *163*, 01001. https://doi.org/10.1051/e3sconf/202016301001

Bai, P., Liu, X., & Xie, J. (2021). Simulating runoff under changing climatic conditions: A comparison of the long short-term memory network with two conceptual hydrologic models. *Journal of Hydrology*, *592*, 125779.

Bajracharya, S., Mool, P., & Shrestha, B. (2006). *The impact of global warming on the glaciers of the Himalaya*.

Balaji, V., Couvreux, F., Deshayes, J., Gautrais, J., Hourdin, F., & Rio, C. (2022). Are general circulation models obsolete? *Proceedings of the National Academy of Sciences*, *119*(47), e2202075119.

Banda, V. D., Dzwairo, R. B., Singh, S. K., & Kanyerere, T. (2022). Hydrological Modelling and Climate Adaptation under Changing Climate: A Review with a Focus in Sub-Saharan Africa. *Water*, *14*(24), Article 24. https://doi.org/10.3390/w14244031

Baste, S., Klotz, D., Espinoza, E. A., Bardossy, A., & Loritz, R. (2025). Unveiling the Limits of Deep Learning Models in Hydrological Extrapolation Tasks. *EGUsphere*, 1–24. https://doi.org/10.5194/egusphere-2025-425

Bateni, S. M., Jeng, D.-S., & Melville, B. W. (2007). Bayesian neural networks for prediction of equilibrium and time-dependent scour depth around bridge piers. *Advances in Engineering Software*, *38*(2), 102–111.

Bellegarda, J. R., & Monz, C. (2016). State of the art in statistical methods for language and speech processing. *Computer Speech & Language*, *35*, 163–184.

Bengio, Y., Simard, P., & Frasconi, P. (1994). Learning long-term dependencies with gradient descent is difficult. *IEEE* Transactions *on Neural Networks*, *5*(2), 157–166.

Bharati, L., Gurung, P., Jayakody, P., Smakhtin, V., & Bhattarai, U. (2014). The projected impact of climate change on water availability and development in the Koshi Basin, Nepal. *Mountain Research and Development*, *34*(2), 118–130.

Chinnasamy, P., Bharati, L., Bhattarai, U., Khadka, A., Dahal, V., & Wahid, S. (2015). Impact of planned water resource development on current and future water demand in the Koshi River basin, Nepal. *Water International*, *40*(7), 1004–1020.

Choi, J., Lee, J., & Kim, S. (2022). Utilization of the Long Short-Term Memory network for predicting streamflow in ungauged basins in Korea. *Ecological Engineering*, *182*, 106699. https://doi.org/10.1016/j.ecoleng.2022.106699

Dahri, Z. H., Ludwig, F., Moors, E., Ahmad, S., Ahmad, B., Ahmad, S., Riaz, M., & Kabat, P. (2021). Climate change and hydrological regime of the high-altitude Indus basin under extreme climate scenarios. *Science of The Total Environment*, *768*, 144467. https://doi.org/10.1016/j.scitotenv.2020.144467

Dai, Z., Zhang, M., Nedjah, N., Xu, D., & Ye, F. (2023). A Hydrological Data Prediction Model Based on LSTM with Attention Mechanism. *Water (Switzerland)*, *15*(4). https://doi.org/10.3390/w15040670

Daniell, T. (1991). Neural networks. Applications in hydrology and water resources engineering. *National Conference Publication- Institute of Engineers. Australia*.

Deng, C., Yin, X., Zou, J., Wang, M., & Hou, Y. (2024). Assessment of the impact of climate change on streamflow of Ganjiang River catchment via LSTM-based models. *Journal of Hydrology: Regional Studies*, *52*, 101716. https://doi.org/10.1016/j.ejrh.2024.101716

Dhital, H. P., Joshi, M., & Budhathoki, N. (2023). Impacts of climate change on temperature and precipitation in nepal: Projections and bias correction. *Journal of Sustainability and Environmental Management*, *2*(4), 203–212.

Dixit, A. (2009). Kosi embankment breach in Nepal: Need for a paradigm shift in responding to floods. *Economic* and *Political Weekly*, 70–78.

Duan, Q., Schaake, J., Andréassian, V., Franks, S., Goteti, G., Gupta, H., Gusev, Y. M., Habets, F., Hall, A., Hay, L., & others. (2006). Model Parameter Estimation Experiment (MOPEX): An overview of science strategy and major results from the second and third workshops. *Journal of Hydrology*, *320*(1–2), 3–17.

Enayati, M., Bozorg-Haddad, O., Bazrafshan, J., Hejabi, S., & Chu, X. (2021). Bias correction capabilities of quantile mapping methods for rainfall and temperature variables. *Journal of Water and Climate Change*, *12*(2), 401–419.

Evin, G., Le Lay, M., Fouchier, C., Penot, D., Colleoni, F., Mas, A., Garambois, P.-A., & Laurantin, O. (2024). Evaluation of hydrological models on small mountainous catchments: Impact of the meteorological forcings. *Hydrology and Earth System Sciences*, *28*(1), 261–281.

Ewen, J. (2011). Hydrograph matching method for measuring model performance. *Journal of Hydrology*, *408*(1–2), 178–187.

Feng, D., Liu, J., Lawson, K., & Shen, C. (2022). Differentiable, Learnable, Regionalized Process-Based Models With Multiphysical Outputs can Approach State-Of-The-Art Hydrologic Prediction Accuracy. *Water Resources Research*, *58*(10), e2022WR032404. https://doi.org/10.1029/2022WR032404

Gauch, M., Kratzert, F., Klotz, D., Nearing, G., Lin, J., & Hochreiter, S. (2021). Rainfall-runoff prediction at multiple timescales with a single Long Short-Term Memory network. *Hydrology and Earth System Sciences*, *25*(4), 2045–2062. https://doi.org/10.5194/hess-25-2045-2021

Gautam, D. K., & Pradhananga, R. D. (2024). Verification and bias correction of rainfall and temperature forecasts over the babai river basin of nepal. *Journal of Hydrology and* Meteorology, *12*(1), 1–10.

Ghimire, G. R., Sharma, S., Panthi, J., Talchabhadel, R., Parajuli, B., Dahal, P., & Baniya, R. (2020). Benchmarking Real-Time Streamflow Forecast Skill in the Himalayan Region. *Forecasting*, *2*(3), Article 3. https://doi.org/10.3390/forecast2030013

Gong, L., Zhang, X., Pan, G., Zhao, J., & Zhao, Y. (2023). Hydrological responses to co-impacts of climate change and land use/cover change based on CMIP6

in the Ganjiang River, Poyang Lake basin. *Anthropocene*, *41*, 100368. https://doi.org/10.1016/j.ancene.2023.100368

Gupta, H. V., Kling, H., Yilmaz, K. K., & Martinez, G. F. (2009). Decomposition of the mean squared error and NSE performance criteria: Implications for improving hydrological modelling. *Journal of Hydrology*, *377*(1–2), 80–91.

Hargreaves, G. H., & Samani, Z. A. (1985). Reference crop evapotranspiration from temperature. Applied *Engineering in Agriculture*, *1*(2), 96–99.

Hengl, T., Jesus, J. M. de, Heuvelink, G. B. M., Gonzalez, M. R., Kilibarda, M., Blagotić, A., Shangguan, W., Wright, M. N., Geng, X., Bauer-Marschallinger, B., Guevara, M. A., Vargas, R., MacMillan, R. A., Batjes, N. H., Leenaars, J. G. B., Ribeiro, E., Wheeler, I., Mantel, S., & Kempen, B. (2017). SoilGrids250m: Global gridded soil information based on machine learning. *PLOS ONE*, *12*(2), e0169748. https://doi.org/10.1371/journal.pone.0169748

Hochreiter, S., & Schmidhuber, J. (1997). Long short-term memory. *Neural Computation*, *9*(8), 1735–1780.

IPCC. (2014). *Climate change 2014: Impacts, adaptation, and vulnerability. Summary for policymakers*. https://www.ipcc.ch/site/assets/uploads/2018/02/ar5_wgII_spm_en.pdf

Ishii, T., Ueda, R., & Miyao, Y. (2023). *Empirical Analysis of the Inductive Bias of Recurrent Neural Networks by Discrete Fourier Transform of Output Sequences* (No. arXiv:2305.09178). arXiv. https://doi.org/10.48550/arXiv.2305.09178

Islam, K., Daraio, J. A., Cheema, M., Sabau, G., & Galagedara, L. (2025). Improved streamflow prediction accuracy in Boreal climate watershed using a LSTM model: A comparative study. *PLOS Water*, *4*(4), e0000359. https://doi.org/10.1371/journal.pwat.0000359

Kaini, S., Nepal ,Santosh, Pradhananga ,Saurav, Gardner ,Ted, & and Sharma, A. K. (2021). Impacts of climate change on the flow of the transboundary Koshi River, with implications for local irrigation. *International Journal of Water Resources Development*, *37*(6), 929–954. https://doi.org/10.1080/07900627.2020.1826292

Kay, A., Dunstone, N., Kay, G., Bell, V., & Hannaford, J. (2024). Demonstrating the use of UNSEEN climate data for hydrological applications: Case studies for extreme floods and droughts in England. *Natural Hazards and Earth System Sciences Discussions*, *2024*, 1–23.

Khadka, A., Wagnon, P., Brun, F., Shrestha, D., Lejeune, Y., & Arnaud, Y. (2022). Evaluation of ERA5-Land and HARv2 Reanalysis Data at High Elevation in

the Upper Dudh Koshi Basin (Everest Region, Nepal). *Journal of Applied Meteorology and Climatology*, *61*(8), 931–954. https://doi.org/10.1175/JAMC-D-21-0091.1

Khan, S., & Yairi, T. (2018). A review on the application of deep learning in system health management. Mechanical *Systems and Signal Processing*, *107*, 241–265.

Kim, J.-B., & Bae, D.-H. (2021). The Impacts of Global Warming on Climate Zone Changes Over Asia Based on CMIP6 Projections. *Earth and Space Science*, *8*(8), e2021EA001701. https://doi.org/10.1029/2021EA001701

Kratzert, F., Gauch, M., Klotz, D., & Nearing, G. (2024). HESS opinions: Never train a long short-term memory (LSTM) network on a single basin. *Hydrology and Earth System Sciences*, *28*(17), 4187–4201.

Kratzert, F., Klotz, D., Brenner, C., Schulz, K., & Herrnegger, M. (2018). Rainfall-runoff modelling using Long Short-Term Memory (LSTM) networks. *Hydrology and Earth System Sciences*, *22*(11), 6005–6022. https://doi.org/10.5194/hess-22-6005-2018

Kratzert, F., Klotz, D., Shalev, G., Klambauer, G., Hochreiter, S., & Nearing, G. (2019). Towards learning universal, regional, and local hydrological behaviors via machine learning applied to large-sample datasets. *Hydrology and Earth System Sciences*, *23*(12), 5089–5110. https://doi.org/10.5194/hess-23-5089-2019

Kushwaha, P., Pandey, V. K., Kumar, P., & Sardana, D. (2024). CMIP6 model evaluation for mean and extreme precipitation over India. *Pure and Applied Geophysics*, *181*(2), 655–678.

Lang, M., Ouarda, T. B. M. J., & Bobée, B. (1999). Towards operational guidelines for over-threshold modeling. *Journal of Hydrology*, *225*(3), 103–117. https://doi.org/10.1016/S0022-1694(99)00167-5

Li, B., Li, R., Sun, T., Gong, A., Tian, F., Khan, M. Y. A., & Ni, G. (2023). Improving LSTM hydrological modeling with spatiotemporal deep learning and multi-task learning: A case study of three mountainous areas on the Tibetan Plateau. *Journal of Hydrology*, *620*, 129401. https://doi.org/10.1016/j.jhydrol.2023.129401

Li, J., Wu, G., Zhang, Y., & Shi, W. (2024). Optimizing flood predictions by integrating LSTM and physical-based models with mixed historical and simulated data. *Heliyon*, *10*(13).

Liang, W., Chen, Y., Fang, G., & Kaldybayev, A. (2023). *Machine learning method is an alternative for the hydrological model in an alpine catchment in the Tianshan region, Central Asia*. https://doi.org/10.1016/j.ejrh.2023.101492

Loveland, T. R., & Belward, A. S. (1997). The International Geosphere Biosphere Programme Data and Information System global land cover data set (DISCover). *Acta Astronautica*, *41*(4–10), 681–689. USGS Publications Warehouse. https://doi.org/10.1016/S0094-5765(98)00050-2

Lundquist, J. D., & Cayan, D. R. (2007). Surface temperature patterns in complex terrain: Daily variations and long-term change in the central Sierra Nevada, California. *Journal of Geophysical Research: Atmospheres*, *112*(D11).

Madsen, H., Lawrence, D., Lang, M., Martinkova, M., & Kjeldsen, T. R. (2014). Review of trend analysis and climate change projections of extreme precipitation and floods in Europe. *Journal of Hydrology*, *519*, 3634–3650. https://doi.org/10.1016/j.jhydrol.2014.11.003

Man, Y., Yang, Q., Shao, J., Wang, G., Bai, L., & Xue, Y. (2023). Enhanced LSTM Model for Daily Runoff Prediction in the Upper Huai River Basin, China. *Engineering*, *24*, 229–238. https://doi.org/10.1016/j.eng.2021.12.022

Mangukiya, N. K., Sharma, A., & Shen, C. (2023). How to enhance hydrological predictions in hydrologically distinct watersheds of the Indian subcontinent? *Hydrological Processes*, *37*(7), e14936. https://doi.org/10.1002/hyp.14936

Marahatta, S., Devkota, L. P., & Aryal, D. (2021). Application of swat in hydrological simulation of complex mountainous river basin (Part i: Model development). *Water (Switzerland)*, *13*(11). https://doi.org/10.3390/w13111546

Martel, J.-L., Arsenault, R., Turcotte, R., Castañeda-Gonzalez, M., Brissette, F., Armstrong, W., Mailhot, E., Pelletier-Dumont, J., Lachance-Cloutier, S., Rondeau-Genesse, G., & Caron, L.-P. (2024). Exploring the ability of LSTM-based hydrological models to simulate streamflow time series for flood frequency analysis. *EGUsphere*, 1–32. https://doi.org/10.5194/egusphere-2024-2134

McMahon, T. A., Peel, M. C., Lowe, L., Srikanthan, R., & McVicar, T. R. (2013). Estimating actual, potential, reference crop and pan evaporation using standard meteorological data: A pragmatic synthesis. *Hydrology and Earth System Sciences*, *17*(4), 1331–1363. https://doi.org/10.5194/hess-17-1331-2013

Mohammadi, M., Gato-Trinidad, S., & King Kuok, K. (2024). The limitation of machine learning methods for water supply and demand forecasting: A case study for Greater Melbourne, Australia. *Water Supply*, *24*(11), 3848–3861. https://doi.org/10.2166/ws.2024.225

Moon, S., & Ha, K.-J. (2020). Future changes in monsoon duration and precipitation using CMIP6. *Npj Climate and Atmospheric Science*, *3*(1), 1–7. https://doi.org/10.1038/s41612-020-00151-w

Moriasi, D. N., Arnold, J. G., Van Liew, M. W., Bingner, R. L., Harmel, R. D., & Veith, T. L. (2007). Model evaluation guidelines for systematic quantification of accuracy in watershed simulations. *Transactions of the ASABE*, *50*(3), 885–900.

Muhammad, A. U., Li, X., & Feng, J. (2019). Using LSTM GRU and hybrid models for streamflow forecasting. Machine *Learning and Intelligent Communications: 4th International Conference, MLICOM 2019, Nanjing, China, August 24–25, 2019, Proceedings 4*, 510–524.

Nayak, P. C., Sudheer, K., Rangan, D., & Ramasastri, K. (2004). A neuro-fuzzy computing technique for modeling hydrological time series. *Journal of Hydrology*, *291*(1–2), 52–66.

Nearing, G. S., Kratzert, F., Sampson, A. K., Pelissier, C. S., Klotz, D., Frame, J. M., Prieto, C., & Gupta, H. V. (2021). What Role Does Hydrological Science Play in the Age of Machine Learning? *Water Resources Research*, *57*(3). https://doi.org/10.1029/2020WR028091

Negnevitsky, M., & Pavlovsky, V. (2005). Neural networks approach to online identification of multiple failures of protection systems. *IEEE Transactions on Power Delivery*, *20*(2), 588–594.

Nepal, S., Flügel, W.-A., Krause, P., Fink, M., & Fischer, C. (2017). Assessment of spatial transferability of process-based hydrological model parameters in two neighbouring catchments in the Himalayan Region. *Hydrological Processes*, *31*(16), 2812–2826. https://doi.org/10.1002/hyp.11199

Neupane, P., Shrestha, S., & Ghimire, S. (2022). Climate change impact on the hydrological extremes of a river basin in the hindu kush himalayan region: A case study of the marsyangdi river basin, nepal. In *Handbook of himalayan ecosystems and sustainability, volume 2* (pp. 111–136). CRC Press.

Ni, G., Zhang, X., Ni, X., Cheng, X., & Meng, X. (2023). A WOA-CNN-BiLSTM-based multi-feature classification prediction model for smart grid financial markets. *Frontiers in Energy Research*, *11*. https://doi.org/10.3389/fenrg.2023.1198855

Nourani, V. (2017). An emotional ANN (EANN) approach to modeling rainfall-runoff process. *Journal of Hydrology*, *544*, 267–277.

Perkins-Kirkpatrick, S. E., & Lewis, S. C. (2020). Increasing trends in regional heatwaves. *Nature Communications*, *11*(1), 3357. https://doi.org/10.1038/s41467-020-16970-7

Pradhan, P., Shrestha, S., & Shanmugam, M. S. (2023). Potential impacts of climate change on ecologically relevant flows: A case study in the Himalayan River basin. *AQUA - Water* Infrastructure*, Ecosystems and Society*, *72*(11), 2109–2125. https://doi.org/10.2166/aqua.2023.284

Pritchard, D. M. W., Forsythe, N., Fowler, H. J., O'Donnell, G. M., & Li, X.-F. (2019). Evaluation of Upper Indus Near-Surface Climate Representation by WRF in the High Asia Refined Analysis. Journal *of Hydrometeorology*, *20*(3), 467–487. https://doi.org/10.1175/JHM-D-18-0030.1

Rahman, A., & Pekkat, S. (2024). Identifying and ranking of CMIP6-global climate models for projected changes in temperature over Indian subcontinent. *Scientific Reports*, *14*(1), 3076.

Robinson, D. A., Thomas, A., Reinsch, S., Lebron, I., Feeney, C. J., Maskell, L. C., Wood, C. M., Seaton, F. M., Emmett, B. A., & Cosby, B. J. (2022). Analytical modelling of soil porosity and bulk density across the soil organic matter and land-use continuum. *Scientific Reports*, *12*(1), 7085. https://doi.org/10.1038/s41598-022-11099-7

Schmidhuber, J. (2015). Deep learning in neural networks: An overview. *Neural Networks*, *61*, 85–117.

Shekar, P. R., Mathew, A., Pandey, A., & Bhosale, A. (2023). A comparison of the performance of SWAT and artificial intelligence models for monthly rainfall–runoff analysis in the Peddavagu River Basin, India. *Aqua Water Infrastructure, Ecosystems and Society*, *72*(9), 1707–1730. https://doi.org/10.2166/aqua.2023.048

Shen, C. (2018). A transdisciplinary review of deep learning research and its relevance for water resources scientists. *Water Resources Research*, *54*(11), 8558–8593.

Siabi, E. K., Awafo, E. A., Kabo-bah, A. T., Derkyi, N. S. A., Akpoti, K., Mortey, E. M., & Yazdanie, M. (2023). Assessment of Shared Socioeconomic Pathway (SSP) climate scenarios and its impacts on the Greater Accra region. *Urban Climate*, *49*, 101432. https://doi.org/10.1016/j.uclim.2023.101432

Siami-Namini, S., Tavakoli, N., & Namin, A. S. (2019). The performance of LSTM and BiLSTM in forecasting time series. *2019 IEEE International Conference on Big Data (Big Data)*, 3285–3292.

Singh, R., Pandey, V. P., & Kayastha, S. P. (2021). Hydro-climatic extremes in the himalayan watersheds: A case of the marshyangdi watershed, nepal. *Theoretical and Applied Climatology*, *143*(1), 131–158.

Sivapalan, M., Takeuchi, K., Franks, S., Gupta, V., Karambiri, H., Lakshmi, V., Liang, X., McDonnell, J., Mendiondo, E. M., O'connell, P., & others. (2003). IAHS decade on predictions in ungauged basins (PUB), 2003–2012: Shaping an exciting future for the hydrological sciences. *Hydrological Sciences Journal*, *48*(6), 857–880.

Song, Y. H., Chung, E.-S., & Shahid, S. (2022). Differences in extremes and uncertainties in future runoff simulations using SWAT and LSTM for SSP scenarios. *Science of the Total Environment*, *838*, 156162.

Sutskever, I. (2013). Training *recurrent neural networks* [Phd].

Tabari, H. (2020). Climate change impact on flood and extreme precipitation increases with water availability. *Scientific Reports*, *10*(1), 13768. https://doi.org/10.1038/s41598-020-70816-2

Tanty, R., & Desmukh, T. S. (2015). Application of Artificial Neural Network in Hydrology- A Review. *International Journal of Engineering Research & Technology*, *4*(6). https://doi.org/10.17577/IJERTV4IS060247

Tayal, K., Renganathan, A., & Lu, D. (2024). Improving streamflow predictions across CONUS by integrating advanced machine learning models and diverse data. *Environmental Research Letters*, *19*(10), 104009.

Uprety, M. (2018, July). *Nepal flood 2017: Wake up call for effective preparedness and response*.

Van Loon, A. F. (2015). Hydrological drought explained. *WIREs Water*, *2*(4), 359–392. https://doi.org/10.1002/wat2.1085

Wahid, S. M., Kilroy, G., Shrestha, A. B., Bajracharya, S. R., & Hunzai, K. (2017). Opportunities and challenges in the trans-boundary koshi river basin. *River System Analysis and Management*, 341–352.

Wang, W., & Ding, J. (2003). Wavelet network model and its application to the prediction of hydrology. *Nature and Science*, *1*(1), 67–71.

Wang, X., Tolksdorf, V., Otto, M., & Scherer, D. (2021). WRF-based dynamical downscaling of ERA5 reanalysis data for high mountain asia: Towards a new version of the high asia refined analysis. *International Journal of Climatology*, *41*(1), 743–762.

Winstral, A., Elder, K., & Davis, R. E. (2002). Spatial snow modeling of wind-redistributed snow using terrain-based parameters. *Journal of Hydrometeorology*, *3*(5), 524–538.

Xu, W., Jiang, Y., Zhang, X., Li, Y., Zhang, R., & Fu, G. (2020). Using long short-term memory networks for river flow prediction. *Hydrology Research*, *51*(6), 1358–1376. https://doi.org/10.2166/NH.2020.026

Yoshikane, T., & Yoshimura, K. (2022). A bias correction method for precipitation through recognizing mesoscale precipitation systems corresponding to weather conditions. *PLOS Water*, *1*(5), e0000016. https://doi.org/10.1371/journal.pwat.0000016

Yu, Q., Tolson, B. A., Shen, H., Han, M., Mai, J., & Lin, J. (2024). Enhancing long short-term memory (LSTM)-based streamflow prediction with a spatially distributed approach. *Hydrology and Earth System Sciences*, *28*(9), 2107–2122. https://doi.org/10.5194/hess-28-2107-2024

Yuan, X., Chen, C., Lei, X., Yuan, Y., & Muhammad Adnan, R. (2018). Monthly runoff forecasting based on LSTM–ALO model. *Stochastic Environmental Research and Risk Assessment*, *32*, 2199–2212.

Zarei, E., Saleh, F. N., & Dalir, A. N. (2024). Comparing the hybrid-lumped-LSTM model with a semi-distributed model for improved hydrological modeling. *Journal of Water and Climate Change*, *15*(8), 4099–4113. https://doi.org/10.2166/wcc.2024.269

Zhang, W., Jin, H., Shao, H., Li, A., Li, S., & Fan, W. (2021). Temporal and Spatial Variations in the Leaf Area Index and Its Response to Topography in the Three-River Source Region, China from 2000 to 2017. *ISPRS International Journal of Geo-Information*, *10*(1), Article 1. https://doi.org/10.3390/ijgi10010033

Zhang, X., Qi, Y., Liu, F., Li, H., & Sun, S. (2023). Enhancing daily streamflow simulation using the coupled SWAT-BiLSTM approach for climate change impact assessment in Hai-River Basin. *Scientific Reports*, *13*(1). https://doi.org/10.1038/s41598-023-42512-4

Zhang, Y., Ragettli, S., Molnar, P., Fink, O., & Peleg, N. (2022). Generalization of an Encoder-Decoder LSTM model for flood prediction in ungauged catchments. *Journal of Hydrology*, *614*, 128577. https://doi.org/10.1016/j.jhydrol.2022.128577

Zhao, P., Gao, L., Ma, M., & Du, J. (2022). Bias correction of ERA-Interim reanalysis temperature for the Qilian Mountains of China. *Frontiers in Environmental Science*, *10*. https://doi.org/10.3389/fenvs.2022.1033202

Zhou, Q., Liu, G., & Zhang, Z. (2009). Improvement and optimization of Thiessen polygon method boundary treatment program. *2009 17th International Conference on Geoinformatics*, 1–5. https://doi.org/10.1109/GEOINFORMATICS.2009.5293458

Zulqarnain, M., Ghazali, R., Hassim, Y. M. M., & Aamir, M. (2021). An enhanced gated recurrent unit with auto-encoder for solving text classification problems. *Arabian Journal for Science and Engineering*, *46*(9), 8953–8967.

APPENDIX

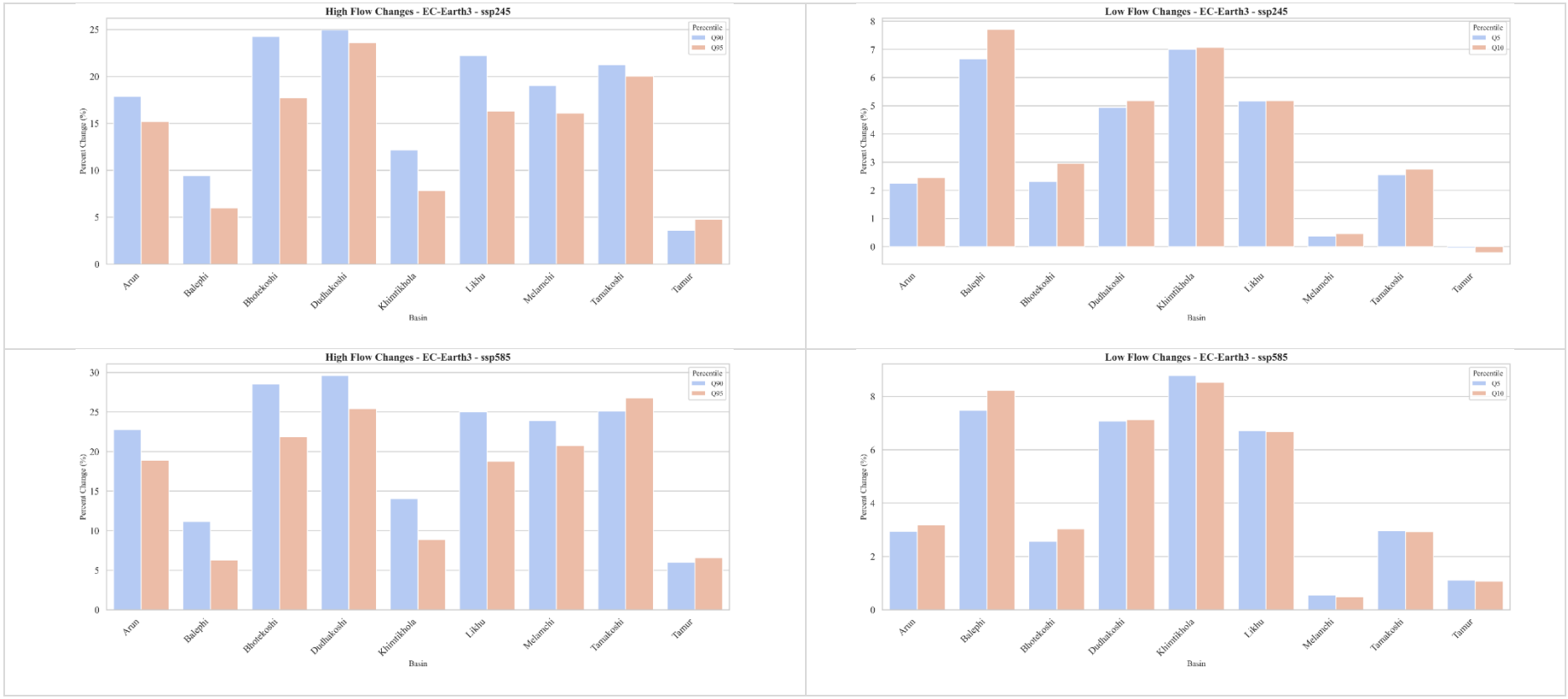

Fig A: Percentile-based streamflow changes under EC-Earth3

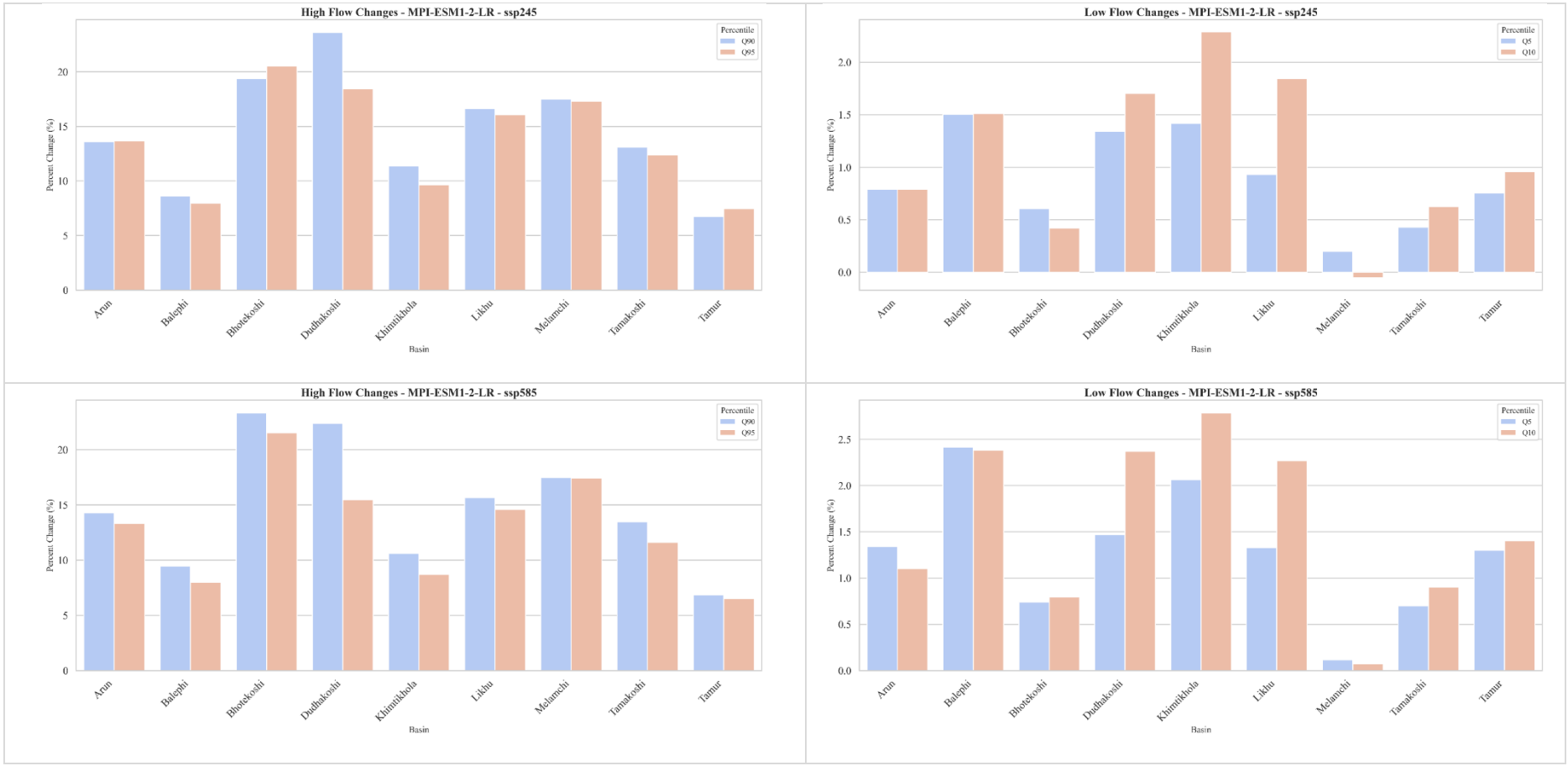

Fig B: Percentile-based streamflow changes under MPI-ESM1-2-LR

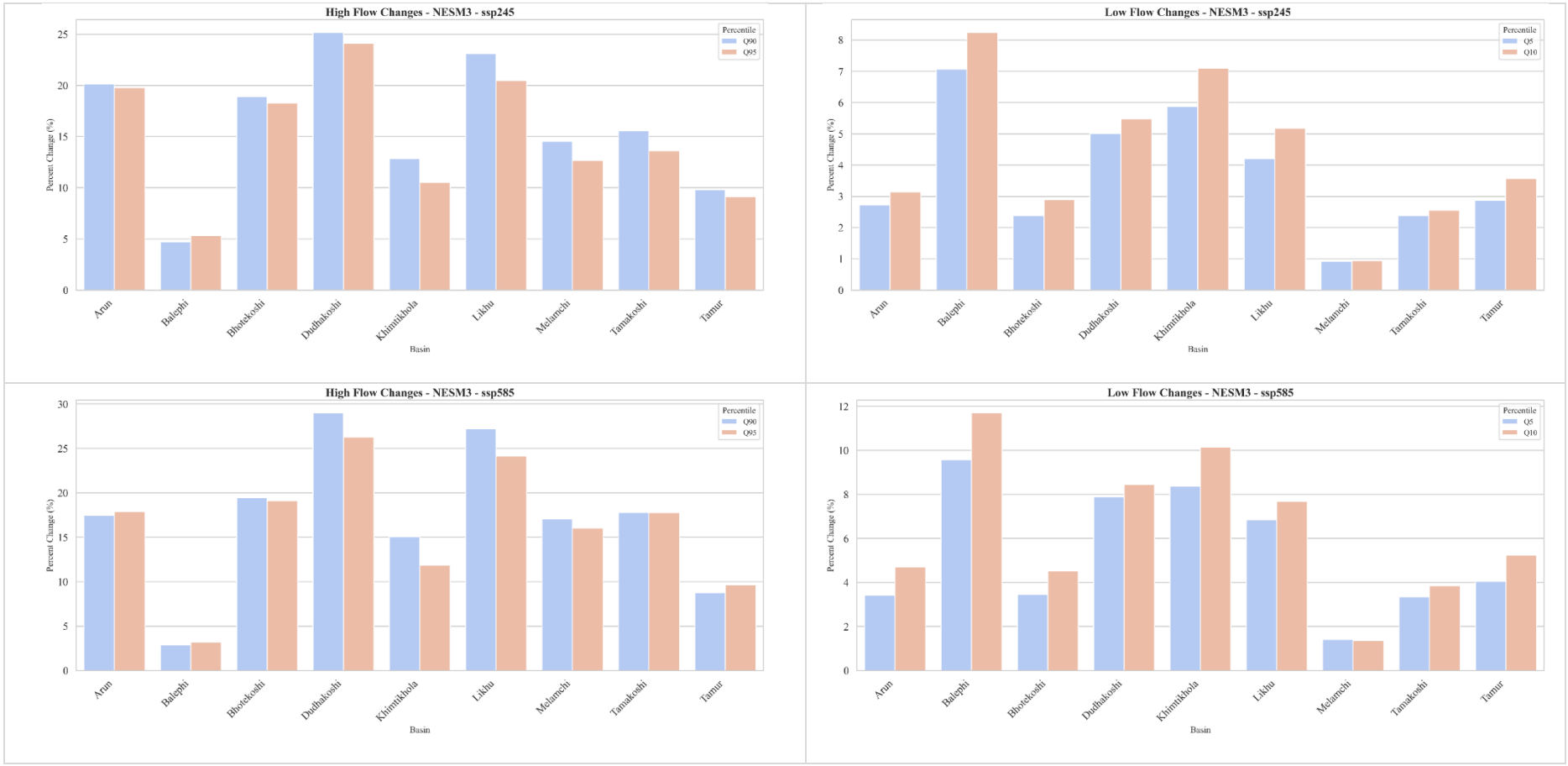

Fig C: Percentile-based streamflow changes under NESM3

Table A: Watershed characteristics

Watershed	Melamchi	Khimtikhola	Bhotekoshi	Balephi	Likhu	Tamakoshi	Dudhakoshi	Tamur	Arun
Elevation Mean (m)	4307.81	2771.6	2516.54	3217.23	2833.02	3410.46	3746.13	3396.08	2361.24
Elevation Range (m)	3460	3872	4585	6153	6251	5936	8212	7952	7892
Slope Mean (°)	32.06	24.85	28.7	29.54	27.62	30.62	28.04	28.26	26.82
Porosity	1.967	1.227	1.490	1.925	1.362	1.704	1.664	1.704	1.463
Sand Fraction	0.448	0.468	0.493	0.498	0.480	0.503	0.462	0.485	0.472
Silt Fraction	0.314	0.312	0.306	0.305	0.310	0.304	0.312	0.307	0.311
Clay Fraction	0.238	0.221	0.201	0.198	0.211	0.193	0.226	0.207	0.218
Mean LAI	0.268	1.328	1.571	1.096	1.187	0.963	0.764	1.064	1.383
Range LAI	2.450	3.493	3.932	4.058	3.624	4.207	3.866	4.216	4.480
LC Forest	0.107	0.842	0.835	0.545	0.748	0.482	0.453	0.576	0.758
LC Grass	0.490	0.133	0.144	0.239	0.139	0.283	0.203	0.172	0.118
LC Crop	0.000	0.000	0.006	0.003	0.003	0.019	0.011	0.004	0.029
LC Snow/Ice	0.033	0.000	0.001	0.048	0.015	0.028	0.054	0.056	0.025
LC Barren	0.371	0.025	0.014	0.165	0.096	0.189	0.279	0.192	0.071
Area (km^2)	74.05	325.17	326.11	663.12	852.2	1486.41	3706.97	4373.62	5130.67
Latitude (°)	28.1	27.65	27.9	27.99	27.57	27.86	27.67	27.52	27.45
Longitude (°)	85.53	86.3	85.91	85.79	86.38	86.23	86.74	87.83	87.23
MAP (mm)	1580.63	2421.53	1582.16	1606.92	1493.88	1229.3	2048	1686.08	2509.8
Aridity Index (AI)	1.79	3.07	1.77	1.79	1.76	1.43	2.35	2.11	2.9

Table B: Climate Change Impacts on Precipitation and Temperature: Mean Annual Perspective

Basin	Model	Scenario	Precipitation Change (%)	Tma Change (°C)	Tmin Change (°C)
Arun	EC-Earth3	ssp245	4.47	1.02	0.94
Arun	EC-Earth3	ssp585	7.49	1.23	1.22
Arun	MPI-ESM1-2-LR	ssp245	-7.90	0.67	0.64
Arun	MPI-ESM1-2-LR	ssp585	-10.28	0.71	0.77
Arun	NESM3	ssp245	-0.86	1.13	1.33
Arun	NESM3	ssp585	-4.48	1.47	1.57
Balephi	EC-Earth3	ssp245	10.84	1.33	1.14
Balephi	EC-Earth3	ssp585	13.53	1.54	1.54
Balephi	MPI-ESM1-2-LR	ssp245	-3.35	0.79	0.81
Balephi	MPI-ESM1-2-LR	ssp585	-4.82	0.86	0.93
Balephi	NESM3	ssp245	-0.96	1.33	1.60
Balephi	NESM3	ssp585	-2.76	1.64	1.80
Bhotekoshi	EC-Earth3	ssp245	11.11	1.20	1.10
Bhotekoshi	EC-Earth3	ssp585	13.98	1.37	1.50
Bhotekoshi	MPI-ESM1-2-LR	ssp245	-3.47	0.75	0.82
Bhotekoshi	MPI-ESM1-2-LR	ssp585	-4.20	0.81	0.94
Bhotekoshi	NESM3	ssp245	0.43	1.26	1.64
Bhotekoshi	NESM3	ssp585	-1.46	1.56	1.86
Dudhakoshi	EC-Earth3	ssp245	7.37	1.08	0.96
Dudhakoshi	EC-Earth3	ssp585	11.26	1.24	1.24
Dudhakoshi	MPI-ESM1-2-LR	ssp245	-3.81	0.71	0.69
Dudhakoshi	MPI-ESM1-2-LR	ssp585	-4.34	0.75	0.82
Dudhakoshi	NESM3	ssp245	0.31	1.17	1.43
Dudhakoshi	NESM3	ssp585	-1.79	1.47	1.64
Khimtikhola	EC-Earth3	ssp245	10.67	1.02	1.30

Table B: Climate Change Impacts on Precipitation and Temperature: Mean Annual Perspective

Basin	Model	Scenario	Precipitation Change (%)	Tma Change (°C)	Tmin Change (°C)
Khimtikhola	EC-Earth3	ssp585	16.12	1.18	1.72
Khimtikhola	MPI-ESM1-2-LR	ssp245	-4.73	0.71	1.01
Khimtikhola	MPI-ESM1-2-LR	ssp585	-4.83	0.76	1.20
Khimtikhola	NESM3	ssp245	1.37	1.19	2.08
Khimtikhola	NESM3	ssp585	-1.17	1.51	2.41
Likhu	EC-Earth3	ssp245	8.98	0.97	1.05
Likhu	EC-Earth3	ssp585	13.57	1.12	1.36
Likhu	MPI-ESM1-2-LR	ssp245	-3.66	0.68	0.79
Likhu	MPI-ESM1-2-LR	ssp585	-4.03	0.71	0.93
Likhu	NESM3	ssp245	1.34	1.12	1.64
Likhu	NESM3	ssp585	-0.67	1.43	1.89
Melamchi	EC-Earth3	ssp245	10.27	1.46	1.20
Melamchi	EC-Earth3	ssp585	12.62	1.68	1.59
Melamchi	MPI-ESM1-2-LR	ssp245	-3.32	0.82	0.80
Melamchi	MPI-ESM1-2-LR	ssp585	-5.92	0.91	0.92
Melamchi	NESM3	ssp245	-2.65	1.39	1.55
Melamchi	NESM3	ssp585	-4.37	1.71	1.75
Tamakoshi	EC-Earth3	ssp245	9.07	1.16	1.11
Tamakoshi	EC-Earth3	ssp585	12.93	1.32	1.47
Tamakoshi	MPI-ESM1-2-LR	ssp245	-3.25	0.74	0.82
Tamakoshi	MPI-ESM1-2-LR	ssp585	-3.89	0.81	0.96
Tamakoshi	NESM3	ssp245	0.54	1.24	1.68
Tamakoshi	NESM3	ssp585	-1.16	1.54	1.90
Tamur	EC-Earth3	ssp245	1.65	1.04	0.85
Tamur	EC-Earth3	ssp585	2.92	1.25	1.11

Table B: Climate Change Impacts on Precipitation and Temperature: Mean Annual Perspective

Basin	Model	Scenario	Precipitation Change (%)	Tma Change (°C)	Tmin Change (°C)
Tamur	MPI-ESM1-2-LR	ssp245	-9.66	0.70	0.60
Tamur	MPI-ESM1-2-LR	ssp585	-13.04	0.73	0.72
Tamur	NESM3	ssp245	-2.64	1.14	1.24
Tamur	NESM3	ssp585	-7.03	1.43	1.44

Acceptance Letter for Submitted Paper

त्रिभुवन विश्वविद्यालय
Tribhuvan University
इन्जिनियरिङ्ग अध्ययन संस्थान
Institute of Engineering
थापाथली क्याम्पस
THAPATHALI CAMPUS
Accredited By University Grants Commission (UGC) Nepal, 2024

GPO Box- 280, Thapathali, Kathmandu
Tel: 01-5339766
E-mail: info@tcioe.edu.np
Website: www.tcioe.edu.np
गोस्वारा पो. नं. २८०, थापाथली, काठमाडौं
फोन: ०१-५३३९७६६

Date: April 21, 2025

To Whom It May Concern:

This is to certify that the paper titled **"Evaluating Streamflow Variability in the Arun River Basin with Long Short-Term Memory (LSTM) Model and CMIP6 Climate Projections"** (Submission# **541**) submitted by **Pramesh Karki** as the first author, which had been accepted for presentation after the peer-review process, has successfully been presented at the 16th IOE Graduate Conference held during April 18 - 20, 2025. Kindly note that the final revision of the papers and publication process of the conference proceedings is still underway and hence inclusion of the accepted manuscript in the conference proceedings is contingent upon timely response to further edits during the publication process.

INSTITUTE OF ENGINEERING
16th IOE Graduate Conference
THAPATHALI

Dr. Raj Kumar Chaulagain,
Convener,
16th IOE Graduate Conference

Certificate of Participation

IOE Graduate Conference

Certificate of Participation

THIS CERTIFICATE IS AWARDED TO

Pramesh Karki

in recognition of an invaluable contribution as

PAPER PRESENTER

at the 16th IOE Graduate Conference

Organized by Tribhuvan University, IOE, Thapathali Campus in association with IOE, Office of the Dean held from April 18-20, 2025 at Thapathali Campus, Kathmandu, Nepal.

Dr. Raj Kumar Chaulagain
Convener
16th IOE Graduate Conference

Dr. Khem Gyanwali
Campus Chief
Thapathali Campus

Prof. Dr. Sushil Bahadur Bajracharya
Dean
Institute of Engineering

Paper Submitted to 16th IOE Graduate Conference

IOE Graduate Conference
[Placeholder for Publication Information]

Evaluating the impact of Climate Change on Hydrological Extremes using LSTM.

Pramesh Karki [a], Vishnu Prasad Pandey [b], Laxmi Prasad Devkota [c]

[a] *Department of Climate Change and Development, Pulchowk Campus, Institute of Engineering, Tribhuvan University, Nepal*
[b] *Center for Water Resources Studies, Institute of Engineering, Tribhuvan University, Nepal*
[c] *Water Modeling Solutions Pvt.Ltd, Kathmandu, Nepal*
[a] pramkar112@gmail.com , [b] vishnu.pandey@pcampus.edu.np , [c] lpdevkota1@gmail.com

Abstract
Climate drivers are closely linked to the occurrence of extreme hydrological events, which significantly impact the environment, livelihoods, and the economy, especially in the Himalayan river basins. Traditional process-based models struggle to capture extreme events due to coarse or missing data, whereas deep learning models, particularly Long Short-Term Memory (LSTM) networks, excel in identifying intricate patterns in climate data. This study aims to develop an LSTM model for the Simle outlet in the Arun River Basin to characterize hydrological extremes and improve water resource management. LSTM model trained on observed hydrometeorological data performed satisfactorily, with Nash-Sutcliffe Efficiency (NSE) values above 0.6 across training and testing phases. Future streamflow projections were generated using bias-corrected precipitation and temperature data from three CMIP6 Global Climate Models (GCMs) under historical, SSP2-4.5, and SSP5-8.5 scenarios. The simulation results indicate an increase in high flows, with Q_5 and Q_{10} rising by 8.56% and 8.49% under SSP2-4.5, and by 11.20% and 10.85% under SSP5-8.5. Low flows (Q_{90} and Q_{95}) also showed moderate increases, reaching 2.40% and 2.01% under SSP5-8.5. This study highlights the robustness and versatility of the LSTM model as a data-driven approach for hydrological modeling, particularly for long-term flow forecasting when integrated with climate data from Global Circulation Models (GCMs)

Keywords
LSTM (Long Short-Term Memory), Hydrological Modeling, Climate Change, Streamflow Prediction, CMIP6 GCMs, Arun River Basin, Extreme Flow Events

1. Introduction

Climate drivers are closely linked to the occurrence of extreme hydrological events [1]. The environment, people's lives, and the economy are all impacted by these issues, which are made worse in the Himalayan river basins [2]. These concerns highlight the need for more effective strategies for water management and disaster risk reduction [3]. These extremes can be accessed using a hydrological model and ensemble climate data, which helps with safe and efficient water resource management [4].

Traditional process-based models are not reliable for assessing extreme events, as the data input is either coarse or missing in most cases [5]. These techniques cannot capture the stochastic volatility of medium- and long-term runoff [6]. On the other hand, data-driven models are known for their ability to make accurate predictions [7, 8]. Deep learning models identify intricate patterns and features in climate data more effectively than any traditional statistical model [9] . The long short-term memory (LSTM) network was specifically designed to improve how well models learn from long sequences of data [10]. LSTM uses gates and cell states instead of RNN to overcome the difficulty of memorizing long-term dependencies and gradient explosion [11]. The added robustness of the algorithm makes it possible for LSTM to simulate long-term dependent processes, such as snow moisture groundwater recharges, and makes its robust prediction technique more appropriate for time series data [12]. LSTM often works with diverse data sources and delivers efficient results even when data is scarce [13].

Several studies [14, 15] have explored the application of LSTM in estimating hydrological extreme values. The LSTM model excels at capturing intricate relationships between precipitation and particularly during extreme events like floods or droughts, making it a useful tool for hydrological study [16]. The objective of this study is to develop an LSTM (Long Short-Term Memory) model for the Simle outlet in the Arun River Basin and to characterize hydrological extremes in the region.

2. Study Area

The Arun River, a transboundary river, lies in the eastern part of Nepal. The Arun River is one of the seven main tributaries of the Saptakoshi River. The Koshi River has been suffering from frequent flooding over the last decade, and the Arun River contributes significantly to the flow of the Saptakoshi [17]. The elevation of the basin varies greatly, ranging from approximately 202 meters above mean sea level to the towering peak of Mount Everest at over 8,848 meters [18]. This basin is of great importance due to its potential for hydropower production and rich natural resources [19]. The watershed of the Arun River at the Simle outlet, along with the spatially distributed meteorological stations, is shown in Figure 1.

Pages: 1 – 6

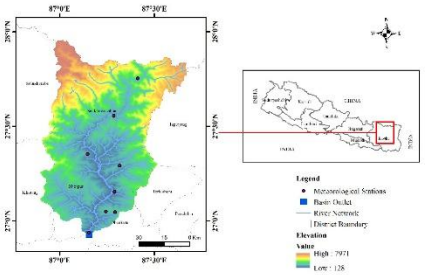

Figure 1: Study Map

3. Methodology

3.1 LSTM Model Development

3.1.1 Model Architecture

An LSTM network is made up of an input layer that receives input sequence data, a fully connected layer that provides LSTM cells with input data, an LSTM cell layer that functions as a cell memorizer, and output layers that produce an output vector. Fully connected layers and LSTM cells are the key components of the LSTM architecture [20] The cell state and the concealed state, which are carried over to the following phases, are the two primary states found in each LSTM layer as shown in the figure below [21] The model learnings are retained because of these memory states. This memory is manipulated using three main gates: input, output, and forget. At every sequence, the output gate updates the hidden state, the forget and input gates update the cell state. The LSTM contains three gates when these are rewritten as equations: input, output, forget gate, cell state, and hidden states. The LSTM gating mechanisms and cell state updates are defined as follows:

$$i_t = \sigma(W_i[h_{t-1}, x_t] + b_i) \tag{1}$$

$$f_t = \sigma(W_f|h_{t-1}, x_t] + b_f) \tag{2}$$

$$o_t = \sigma(W_o[h_{t-1}, x_t] + b_o) \tag{3}$$

$$\tilde{C}_t = \tanh(W_c|h_{t-1}, x_t] + b_c) \tag{4}$$

$$C_t = f_t \cdot C_{t-1} + i_t \cdot \tilde{C}_t \tag{5}$$

$$h_t = o_t \cdot \tanh(C_t) \tag{6}$$

where x_t is the input, b_x represents the biases for each gate x, C_t is the cell state at time step t, and $\tilde{C}_t$ is the candidate cell state. The activation functions σ and tanh represent the sigmoid and hyperbolic tangent functions, respectively. The input, forget, and output gates are denoted by i_t, f_t, and o_t, while W_x represents the weight matrix associated with each gate. Generalized architecture of an LSTM cell is shown in the Figure 2.

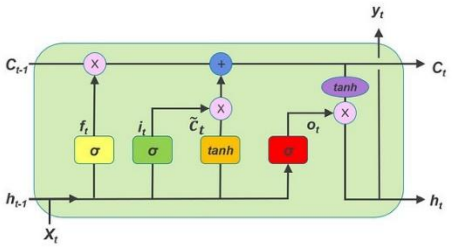

Figure 2: LSTM architecture [22]

The LSTM model is trained only through forward propagation, which fails to effectively capture the potential linear or nonlinear correlations between the explanatory and target variables, resulting in less usage of training data [23]. BiLSTM solves this problem by stacking two or three reversed LSTMs to examine past and future correlation information between explanatory and target variables at each time step. This better awareness of the present sequence position helps to reduce errors in detecting underlying linkages. This study used a three-layer LSTM model to recognize patterns in sequential data. The model had 256, 128, and 64 units in its first, second, and third layers, with a 0.3 dropout rate after each layer to help prevent overfitting.

The training was done using the Adam optimizer with a 0.001 learning rate for efficient and stable learning. Mean Average Error (MAE) was chosen as the loss function. A batch size of 32 was chosen to balance speed and performance. To avoid overfitting and improve accuracy, early stopping was applied based on validation loss. The input and output variables for the LSTM model are divided into 70% for training, 15% for validation, and 15% for testing. Predictions from each of these splits are evaluated separately to assess the model's performance.

3.1.2 Input Data

To set up the model for the Arun River basin, daily records of ten precipitation, one hydrological, and two temperature stations from the Department of Hydrology and Meteorology(DHM) were used. The details of these stations are listed in Table 1. The datasets were considered from 1996 to 2019. Missing temperature data was filled using regression with data from nearby weather stations. For precipitation, Asia-Pacific High-Resolution Observation Data Integration Towards Evaluation of Water Resources (APHRODITE)`http://aphrodite.st.hirosaki-u.ac.jp` and European Reanalysis Atmosphere 5 (ERA5) `https://cds.climate.copernicus.eu/datasets/reanalysis-era5-single-levels?tab=overview` gridded datasets to estimate the missing values. Monthly

regression was used to match the observed precipitation data with the gridded datasets.

Table 1: Station Information

Station ID	Station Name	Longitude	Latitude	Elevation (m)	Type
1301	Num	87.285	27.555	1494	P
1303	Chainpur (East)	87.317	27.292	1277	P,T
1304	Pakhribas	87.292	27.046	1720	P,T
1305	Leguwa Ghat	87.289	27.153	446	P
1306	Muga	87.244	27.050	1457	P
1317	Chepuwa	87.412	27.753	2039	P
1322	Machhuwaghat	87.155	26.938	168	P
1325	Dingla	87.146	27.353	1169	P
606	Simple	87.155	26.923	512	H

Note: P = Precipitation, T = Temperature, and H: Hydrological stations

Different methods of normalization were applied to various data sets for the region under study. The MinMaxScaler method was used to normalize the maximum and minimum temperatures:

$$x_{\text{scaled}} = \frac{x - x_{\min}}{x_{\max} - x_{\min}} \tag{7}$$

where x_{scaled} is the normalized value, and $x_{\min}$ and $x_{\max}$ are the minimum and maximum values of the temperature series, respectively. Streamflow values were normalized by dividing them by the watershed area and mean annual precipitation to make them dimensionless for standardized comparison [24]:

$$Q_{\text{sd}} = \frac{Q}{A \times P_{\text{avg}}} \tag{8}$$

where Q_{sd} represents the specific discharge, Q is the observed streamflow (m^3/s), A denotes the watershed area (km^2), and P_{avg} is the mean annual precipitation (mm/year). This conversion allows for the assessment of hydrological response relative to precipitation input and watershed size. Since a log transformation reduces skewness, it was applied to address the right-skewed nature of precipitation and streamflow data [25].

$$x' = \log_{10}(\sqrt{x} + 0.1) \tag{9}$$

where x' is the transformed value, x is the original variable (precipitation or specific discharge), and a small positive constant (0.1) is added to prevent undefined values for zero or near-zero inputs. The Z-Score method was then used to standardize the transformed data:

$$z = \frac{x' - \mu}{\sigma} \tag{10}$$

where z is the standardized value, μ is the mean, and σ is the standard deviation of the transformed variable.

3.1.3 Evaluation Metrics

Root Mean Square Error (RMSE) and Nash-Sutcliffe Efficiency (NSE) are the statistical metrics used to assess the model's performance. The fit between simulated and observed data is commonly measured using the NSE by Nash & Sutcliffe (1970). As a measure of how well the simulations match the real data, RMSE stands for sample standard deviation of the differences between the mean values of simulated and observed data.

The model performance is evaluated using the Nash-Sutcliffe Efficiency (NSE) and Root Mean Square Error (RMSE) metrics:

$$NSE = 1 - \frac{\sum_{t=1}^{n}(Q_{\text{sim},t} - Q_{\text{obs},t})^2}{\sum_{t=1}^{n}(Q_{\text{obs},t} - \bar{Q}_{\text{obs},t})^2} \tag{11}$$

$$RMSE = \sqrt{\frac{\sum_{t=1}^{n}(Q_{\text{sim},t} - Q_{\text{obs},t})^2}{n}} \tag{12}$$

where $Q_{\text{sim},t}$ and $Q_{\text{obs},t}$ represent the simulated and observed discharges, respectively; $\bar{Q}_{\text{obs},t}$ is the mean observed streamflow; and n is the length of the time series. The NSE ranges from $-\infty$ to 1, with values closer to 1 indicating better model performance. For RMSE and MAE, values range from 0 to $+\infty$, with lower values indicating better accuracy, and 0 being the ideal outcome.

3.2 Assessment of Climate Change Impact on Hydrology

3.2.1 GCM Data Acquisition and Selection

The outputs from climate models in the CMIP6 project, including daily precipitation, maximum temperature, and minimum temperature data, were extracted from the World Climate Research Programme (WCRP) repository (`https://esgf-node.llnl.gov/search/cmip6/`). Three CMIP6 General Circulation Models (GCMs)—EC-Earth3, MPI-ESM1-2-LR, and NESM3—were chosen for analysis under historical, SSP2-4.5, and SSP5-8.5 scenarios. These GCMs have been identified in earlier research to be the most effective ensemble for analyzing the future effects of climate change on the Indian subcontinent [26, 27]. Detailed information on the resolutions and the respective research centers associated with each selected GCM is provided in Table 2.

Table 2: General Circulation Models and their characteristics

GCM	Spatial Resolution (°)	Research Center
EC-Earth3	0.7018 × 0.7031	European Community Earth
MPI-ESM1-2-LR	1.5 × 1.5	Max Planck Institute for Meteorology
NESM3	1.88 × 1.88	Nanjing University of Information Science and Technology

3.2.2 Bias Correction and Ensemble of Data

The extracted daily series were bias-corrected using observational data from DHM through quantile mapping with the qmap package in R [28, 29]. The optimal bias correction method was selected based on the evaluation of each function using Nash-Sutcliffe Efficiency (NSE) and R^2. The Bernoulli-Gamma function was applied to precipitation, smooth spline to maximum temperature, and a linear function to minimum temperature as per the result of the evaluation. Bias-corrected data for each station were then ensembled across the three GCMs. The ensembled outputs for the three scenarios were subsequently used in the LSTM model to generate daily streamflow series.

3.3 Computing Climate Change Impact on Hydrological Extremes

Changes in flow extremes were assessed by comparing high and low flow percentiles between historical and future scenarios. High flows were represented by Q_5 (5th percentile flow) and Q_{10} (10th percentile flow), which correspond to extreme and moderately high flow conditions. Low flows were analyzed using Q_{90} (90th percentile flow) and Q_{95} (95th percentile flow), representing conditions of low water availability. The percentage changes in these flow metrics from the historical scenario to SSP245 and SSP585 were evaluated to assess future hydrological shifts. For this analysis, a 30-year period from 1985 to 2014 was selected as the historical baseline, while the future projections were assessed for the period 2026 to 2055, ensuring consistency in the time span for comparison.

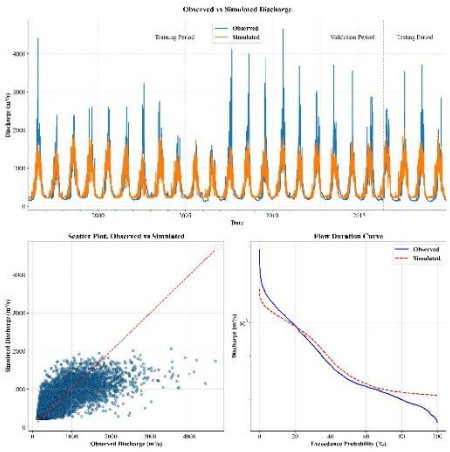

Figure 3: Model Performance at Simle of Arun River

4. Results and Discussion

4.1 Model Performance Evaluation

Early stopping limited the training period to 148 epochs, and the best model weights were found at the end of the 108^{th} epoch. The best weights were restored, and training metrics (NSE and RMSE) were separately calculated for training, validation, and testing. The results are shown in Table 3. The model achieves an NSE (Nash-Sutcliffe Efficiency) above 0.6 across all phases, which is considered satisfactory for hydrological applications. This suggests the need for incorporating additional hydrological variables, such as soil moisture, evapotranspiration, land use, or snowmelt, to improve the model's performance.

Table 3: Training, Validation, and Testing Metrics

Metric	Training	Validation	Testing
RMSE	337.79	323.14	351.40
NSE	0.60	0.59	0.66

However, the hydrograph as shown in Figure 3, reveals a weakness in the model's ability to accurately capture extreme events, such as high and low flows.

The model was developed for a single basin, treating the LSTM as a lumped model rather than a process-based model. This approach leads to relatively poorer performance compared to using LSTM as a regional model, which can leverage spatial variability and shared patterns across multiple basins.

4.2 Climate Change Impact on Hydrological Extremes

4.2.1 Projected Future Climates

Climate change analysis was performed using ensemble bias-corrected data from selected GCMs. When the annual average precipitation was computed for the baseline period (1985–2014) and future scenarios (2026–2055), a decreasing trend was observed for both SSP2-4.5 and SSP5-8.5. On average, precipitation decreased by 2.65% under SSP2-4.5 and by 4.06% under SSP5-8.5. Similarly, the maximum temperature increased by an average of 0.64°C under SSP2-4.5 and by 0.8°C under SSP5-8.5, while the minimum temperature increased by 0.89°C and 1.1°C, respectively. The results indicate a decline in precipitation, whereas both maximum and minimum temperatures show an increasing trend.

4.2.2 Climate Change Impact on Hydrological Extremes

The trained model was used for future predictions based on the ensembled data from three CMIP6 GCMs. For Station 606, the model projected a significant increase in high-flow events. Under SSP2-4.5, Q_5 and Q_{10} flows increased by 8.56% and 8.49%, respectively. A larger increase was observed under SSP5-8.5, where Q_5 rose by 11.20% and Q_{10} by 10.85%. These findings suggest a potential intensification of high-flow extremes under warming scenarios. In contrast, low-flow metrics also showed slight increases. Q_{90} and Q_{95} under SSP2-4.5 increased by 2.19% and 1.69%, respectively. Under SSP5-8.5, the increments were slightly higher, with Q_{90} increasing by 2.40% and Q_{95} by 2.01%. These variations are illustrated in Figure 4.

The projected rise in both high and low flows can be attributed to complex climatic interactions. While reduced precipitation may limit overall runoff, rising temperatures likely enhance snow and glacier melt in higher elevations, contributing to elevated streamflow during specific periods. Additionally, increased evapotranspiration may offset some of the precipitation losses. These trends, consistent with other

Himalayan studies [30], highlight the evolving hydrological behavior in the region and reinforce the importance of forward-looking water resource planning and adaptive flood management strategies.

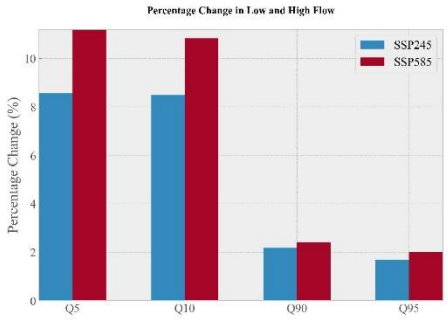

Figure 4: Percentage Change in Low and High Flow

5. Conclusion

The Long Short-Term Memory network, a data-driven deep learning approach, was used to investigate the impact of climate change on hydrological extremes in the Arun River Basin. The model was developed using observed hydrometeorological data to simulate daily streamflow at the Simle outlet. A Bidirectional Long Short-Term Memory (BiLSTM) model performed well with Nash-Sutcliffe Efficiency (NSE) values above 0.6 across training and testing phases. The model exhibited limitations in capturing hydrological extremes due to the absence of other basin descriptors such as soil moisture, evaporation, or snow melt. To assess future streamflow dynamics, climate projections from three CMIP6 GCMs (EC-Earth3, MPI-ESM1-2-LR, and NESM3) under SSP2-4.5 and SSP5-8.5 scenarios were bias-corrected using quantile mapping and used as inputs to the trained model. Results showed a consistent rise in temperature and a decline in precipitation, contributing to noticeable changes in streamflow characteristics. For Station 606, high flows (Q_5 and Q_{10}) increased by 8.56% and 8.49% under SSP2-4.5, and by 11.20% and 10.85% under SSP5-8.5, respectively. Low flows (Q_{90} and Q_{95}) also increased slightly under both scenarios, indicating a shift toward more stable baseflow conditions.

These anticipated changes are likely driven by the combined impact of declining precipitation and rising temperatures, which affect snowmelt dynamics and increase evapotranspiration—especially in mountainous areas. The observed rise in both high and low flow percentiles suggests a shift in the seasonal distribution of water, potentially influencing strategies for water storage, allocation, and disaster risk management.

References

[1] Reeta Singh, Vishnu Prasad Pandey, and Sadhana Pradhanang Kayastha. Hydro-climatic extremes in the himalayan watersheds: a case of the marshyangdi watershed, nepal. *Theoretical and Applied Climatology*, 143(1):131–158, 2021.

[2] Prajwal Neupane, Sangam Shrestha, and Suwas Ghimire. Climate change impact on the hydrological extremes of a river basin in the hindu kush himalayan region: A case study of the marsyangdi river basin, nepal. In *Handbook of Himalayan Ecosystems and Sustainability, Volume 2*, pages 111–136. CRC Press, 2022.

[3] Shahriar M Wahid, Garrett Kilroy, Arun B Shrestha, Sagar Ratna Bajracharya, and Kiran Hunzai. Opportunities and challenges in the trans-boundary koshi river basin. *River system analysis and management*, pages 341–352, 2017.

[4] Alison Kay, Nick Dunstone, Gillian Kay, Victoria Bell, and Jamie Hannaford. Demonstrating the use of unseen climate data for hydrological applications: case studies for extreme floods and droughts in england. *Natural Hazards and Earth System Sciences Discussions*, 2024:1–23, 2024.

[5] Hossein Tabari. Statistical analysis and stochastic modelling of hydrological extremes, 2019.

[6] Xiaohui Yuan, Chen Chen, Xiaohui Lei, Yanbin Yuan, and Rana Muhammad Adnan. Monthly runoff forecasting based on lstm–alo model. *Stochastic environmental research and risk assessment*, 32:2199–2212, 2018.

[7] Vahid Nourani. An emotional ann (eann) approach to modeling rainfall-runoff process. *Journal of Hydrology*, 544:267–277, 2017.

[8] Rakesh Tanty and Tanweer S Desmukh. Application of artificial neural network in hydrology—a review. *Int. J. Eng. Technol. Res*, 4(6):184–188, 2015.

[9] Étienne Plésiat, Robert Dunn, Markus Donat, Colin Morice, Thomas Ludwig, Hannes Thiemann, and Christopher Kadow. Using artificial intelligence to reconstruct missing climate data in extreme events datasets. In *EGU General Assembly Conference Abstracts*, pages EGU–13507, 2023.

[10] S Hochreiter. Long short-term memory. *Neural Computation MIT-Press*, 1997.

[11] Jürgen Schmidhuber. Deep learning in neural networks: An overview. *Neural networks*, 61:85–117, 2015.

[12] Sima Siami-Namini, Neda Tavakoli, and Akbar Siami Namin. The performance of lstm and bilstm in forecasting time series. In *2019 IEEE International conference on big data (Big Data)*, pages 3285–3292. IEEE, 2019.

[13] Jun Li, Guofang Wu, Yongpeng Zhang, and Wenhui Shi. Optimizing flood predictions by integrating lstm and physical-based models with mixed historical and simulated data. *Heliyon*, 10(13), 2024.

[14] Chao Deng, Xin Yin, Jiacheng Zou, Mingming Wang, and Yukun Hou. Assessment of the impact of climate change on streamflow of ganjiang river catchment via lstm-based models. *Journal of Hydrology: Regional Studies*, 52:101716, 2024.

[15] Young Hoon Song, Eun-Sung Chung, and Shamsuddin Shahid. Differences in extremes and uncertainties in future runoff simulations using swat and lstm for ssp scenarios. *Science of the Total Environment*, 838:156162, 2022.

[16] Sujan Ghimire, Zaher Mundher Yaseen, Aitazaz A Farooque, Ravinesh C Deo, Ji Zhang, and Xiaohui Tao. Streamflow prediction using an integrated methodology

based on convolutional neural network and long short-term memory networks. *Scientific Reports*, 11(1):17497, 2021.

[17] Rajiv Sinha, Alok Gupta, Kanchan Mishra, Shivam Tripathi, Santosh Nepal, SM Wahid, and Somil Swarnkar. Basin-scale hydrology and sediment dynamics of the kosi river in the himalayan foreland. *Journal of Hydrology*, 570:156–166, 2019.

[18] Bernd Hoffmann, Sarah J Feakins, Bodo Bookhagen, Stephanie M Olen, Danda P Adhikari, Janardan Mainali, and Dirk Sachse. Climatic and geomorphic drivers of plant organic matter transport in the arun river, e nepal. *Earth and Planetary Science Letters*, 452:104–114, 2016.

[19] Rana Muhammad Ali Washakh, Ningsheng Chen, Tao Wang, Sundas Almas, Sajid Rashid Ahmad, and Mahfuzur Rahman. Glof risk assessment model in the himalayas: A case study of a hydropower project in the upper arun river. *Water*, 11(9):1839, 2019.

[20] Babak Alizadeh, Alireza Ghaderi Bafti, Hamid Kamangir, Yu Zhang, Daniel B Wright, and Kristie J Franz. A novel attention-based lstm cell post-processor coupled with bayesian optimization for streamflow prediction. *Journal of Hydrology*, 601:126526, 2021.

[21] Yuanyuan Man, Qinli Yang, Junming Shao, Guoqing Wang, Linlong Bai, and Yunhong Xue. Enhanced lstm model for daily runoff prediction in the upper huai river basin, china. *Engineering*, 24:229–238, 2023.

[22] Muhammad Zulqarnain, Rozaida Ghazali, Yana Mazwin Mohmad Hassim, and Muhammad Aamir. An enhanced gated recurrent unit with auto-encoder for solving text classification problems. *Arabian Journal for Science and Engineering*, 46(9):8953–8967, 2021.

[23] Yong Yu, Xiaosheng Si, Changhua Hu, and Jianxun Zhang. A review of recurrent neural networks: Lstm cells and network architectures. *Neural computation*, 31(7):1235–1270, 2019.

[24] Nikunj K Mangukiya and Ashutosh Sharma. Deep learning-based approach for enhancing streamflow prediction in watersheds with aggregated and intermittent observations. *Water Resources Research*, 61(1):e2024WR037331, 2025.

[25] Ichwana Ramli, Hairul Basri, Ashfa Achmad, RGAP Basuki, and Moch Abdilah Nafis. Linear regression analysis using log transformation model for rainfall data in water resources management krueng pase, aceh, indonesia. *Int. J. Des. Nat. Ecodynamics*, 17(1):79–86, 2022.

[26] Abdul Rahman and Sreeja Pekkat. Identifying and ranking of cmip6-global climate models for projected changes in temperature over indian subcontinent. *Scientific Reports*, 14(1):3076, 2024.

[27] Prabha Kushwaha, Vivek Kumar Pandey, Prashant Kumar, and Divya Sardana. Cmip6 model evaluation for mean and extreme precipitation over india. *Pure and Applied Geophysics*, 181(2):655–678, 2024.

[28] Dilip Kumar Gautam and Raju Dhar Pradhananga. Verification and bias correction of rainfall and temperature forecasts over the babai river basin of nepal. *Journal of Hydrology and Meteorology*, 12(1):1–10, 2024.

[29] Hari Prasad Dhital, Madhav Joshi, and Nabin Budhathoki. Impacts of climate change on temperature and precipitation in nepal: Projections and bias correction. *Journal of Sustainability and Environmental Management*, 2(4):203–212, 2023.

[30] Vikram S Chandel and Subimal Ghosh. Components of himalayan river flows in a changing climate. *Water Resources Research*, 57(2):e2020WR027589, 2021.

Plagiarism Detection Summary

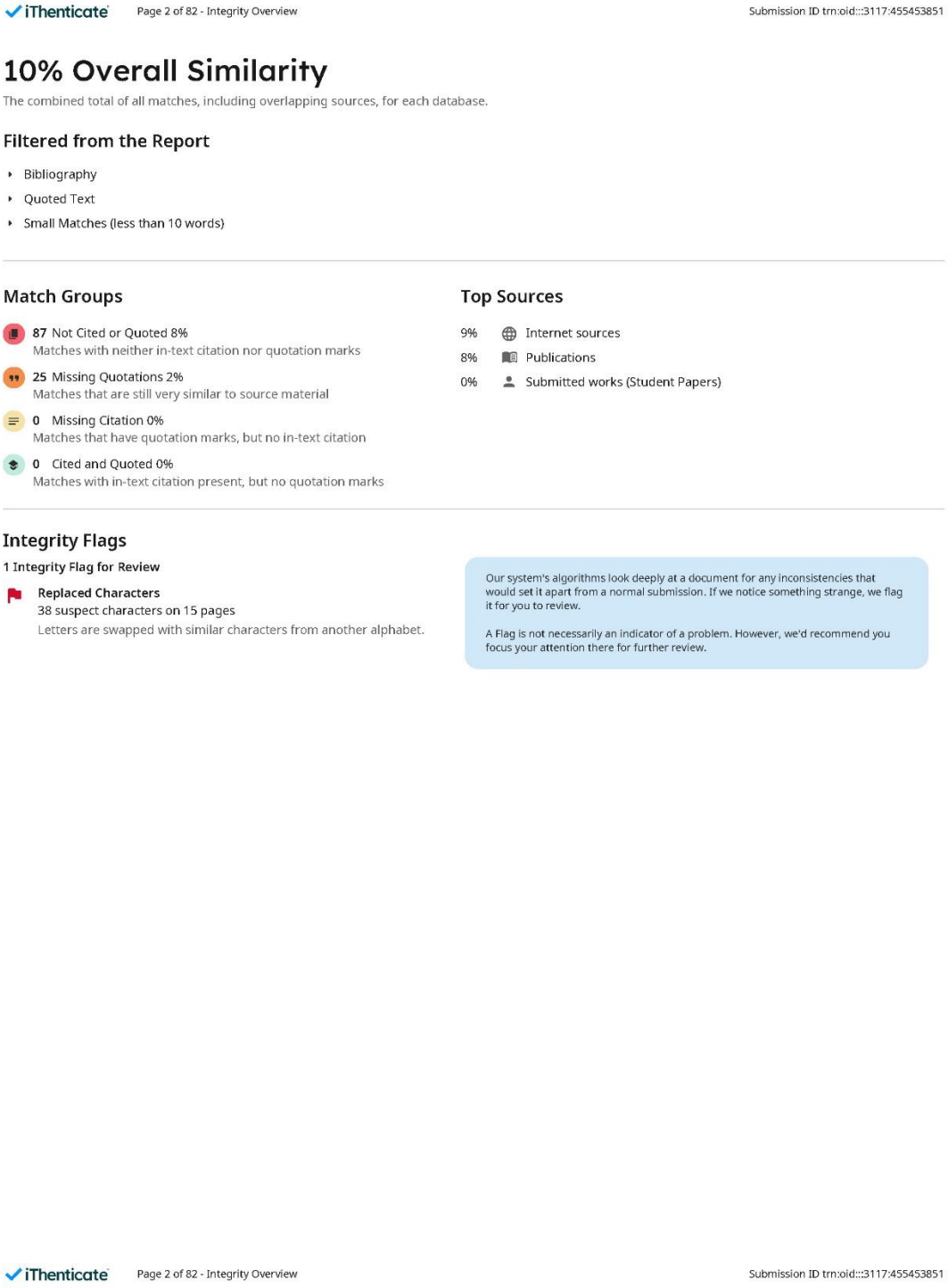

iThenticate Page 2 of 82 - Integrity Overview Submission ID trn:oid:::3117:455453851

10% Overall Similarity

The combined total of all matches, including overlapping sources, for each database.

Filtered from the Report

- Bibliography
- Quoted Text
- Small Matches (less than 10 words)

Match Groups

87 Not Cited or Quoted 8%
Matches with neither in-text citation nor quotation marks

25 Missing Quotations 2%
Matches that are still very similar to source material

0 Missing Citation 0%
Matches that have quotation marks, but no in-text citation

0 Cited and Quoted 0%
Matches with in-text citation present, but no quotation marks

Top Sources

9% Internet sources
8% Publications
0% Submitted works (Student Papers)

Integrity Flags

1 Integrity Flag for Review

Replaced Characters
38 suspect characters on 15 pages
Letters are swapped with similar characters from another alphabet.

Our system's algorithms look deeply at a document for any inconsistencies that would set it apart from a normal submission. If we notice something strange, we flag it for you to review.

A Flag is not necessarily an indicator of a problem. However, we'd recommend you focus your attention there for further review.

iThenticate Page 2 of 82 - Integrity Overview Submission ID trn:oid:::3117:455453851

Match Groups

- 87 Not Cited or Quoted 8%
  Matches with neither in-text citation nor quotation marks
- 25 Missing Quotations 2%
  Matches that are still very similar to source material
- 0 Missing Citation 0%
  Matches that have quotation marks, but no in-text citation
- 0 Cited and Quoted 0%
  Matches with in-text citation present, but no quotation marks

Top Sources

9% Internet sources
8% Publications
0% Submitted works (Student Papers)

Top Sources

The sources with the highest number of matches within the submission. Overlapping sources will not be displayed.

1	Internet	
www.mdpi.com		1%
2	Internet	
iwaponline.com		<1%
3	Internet	
assets-eu.researchsquare.com		<1%
4	Internet	
www.nature.com		<1%
5	Internet	
www.frontiersin.org		<1%
6	Internet	
pastel.archives-ouvertes.fr		<1%
7	Internet	
www.tandfonline.com		<1%
8	Internet	
repository.library.noaa.gov		<1%
9	Internet	
ebin.pub		<1%
10	Internet	
link.springer.com		<1%

iThenticate Page 3 of 82 - Integrity Overview Submission ID trn:oid:::3117:455453851